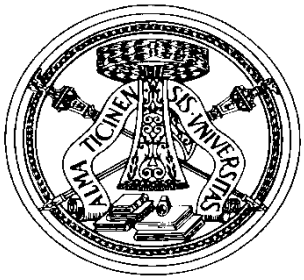

UNIVERSITY OF PAVIA

PhD IN BIOMEDICAL SCIENCES

DEPARTMENT OF BRAIN AND BEHAVIORAL SCIENCES

SECTION OF NEUROPHYSIOLOGY

DISTINCT ROLES OF *EPS8* GENE IN THE MATURATION OF COCHLEAR AND VESTIBULAR HAIR CELLS

PhD Tutor: Prof. Ivo Prigioni

PhD Supervisor: Prof. Egidio Ugo D'Angelo

PhD dissertation of

Marco Manca

2016-2017

Contents

Introduction

Inner ear genetic disease

Deficits in the inner ear end organs, i.e. cochlea or vestibule, or in their neural innervation can lead to hearing loss, vestibular dysfunction, or both.
Hearing loss related to peripheral injury most commonly is characterized by the elevated hearing thresholds at particular frequencies, which sometimes may be accompanied by altered otoacoustic emissions. Instead vestibular deficits may be revealed in many ways, such as abnormal posturing and imbalance, nystagmus (rhythmic eye movements), abnormal vestibulo-ocular reflexes (VOR), abnormal vestibulo-collic reflexes (VCR) and/or reports of disorientation, altered subjective vertical, spinning sensations, dizziness, nausea and blurred vision.
Hearing impairment is an age-related disease, but 0.1-0.3% of children at birth are affected by severe to profound hearing impairment. A significant part of age related hearing loss, almost 30%, is thought to have a genetic cause. In 2004 about 400 syndromes have been demonstrated to carry to hearing loss. Moreover, about 100 chromosomal loci have been identified for nonsyndromic hearing loss with genes identified for over 40 forms (Van Camp and Smith, Hereditary Hearing Loss Homepage: http://hereditaryhearingloss.org).
While we know so much about the genetics of hearing loss, we know relatively little about the role of genes in vestibular impairment. It has been estimated that from 30 to 90% among children with hearing impairment of various causes and 34% among children with hereditary hearing impairment present vestibular dysfunction.
Not all genetic mutations produce both cochlear and vestibular abnormalities, for example in Usher syndrome there is a wide heterogeneity. In this disease, retinal degeneration and auditory impairment are common, but vestibular function depends on the different genes involved. Usher Type I syndrome, due to mutations in a variety of genes including *MYO7A* (myosin 7A), *USH1C* (harmonin), *CDH23* (cadherin 23), or *PCDH15* (protocadherin 15), has profound inner ear vestibular deficits. Curiously Usher Type II syndrome, due to *USH2A* (usherin) mutations, does not produce vestibular deficits and finally Usher Type III syndrome, due to mutations in *CLRN1* (Clarin 1), shows variable vestibular dysfunction.
DFNA9, one form of nonsyndromic hereditary hearing loss, caused by mutations in the *COCH* gene, has also been reported to cause variable inner ear vestibular dysfunction. Therefore, depending upon the gene and the protein encoded by that gene, along with other factors, vestibular dysfunction may accompany peripheral cochlear impairment and hearing loss or it may not.
Here, I have investigated the role of *EPS8* gene in vestibular and cochlear functions.

Ear anatomy

The ear consists of three part: outer ear, middle ear and inner ear (Fig.1). The structure and function of each part will be described below.

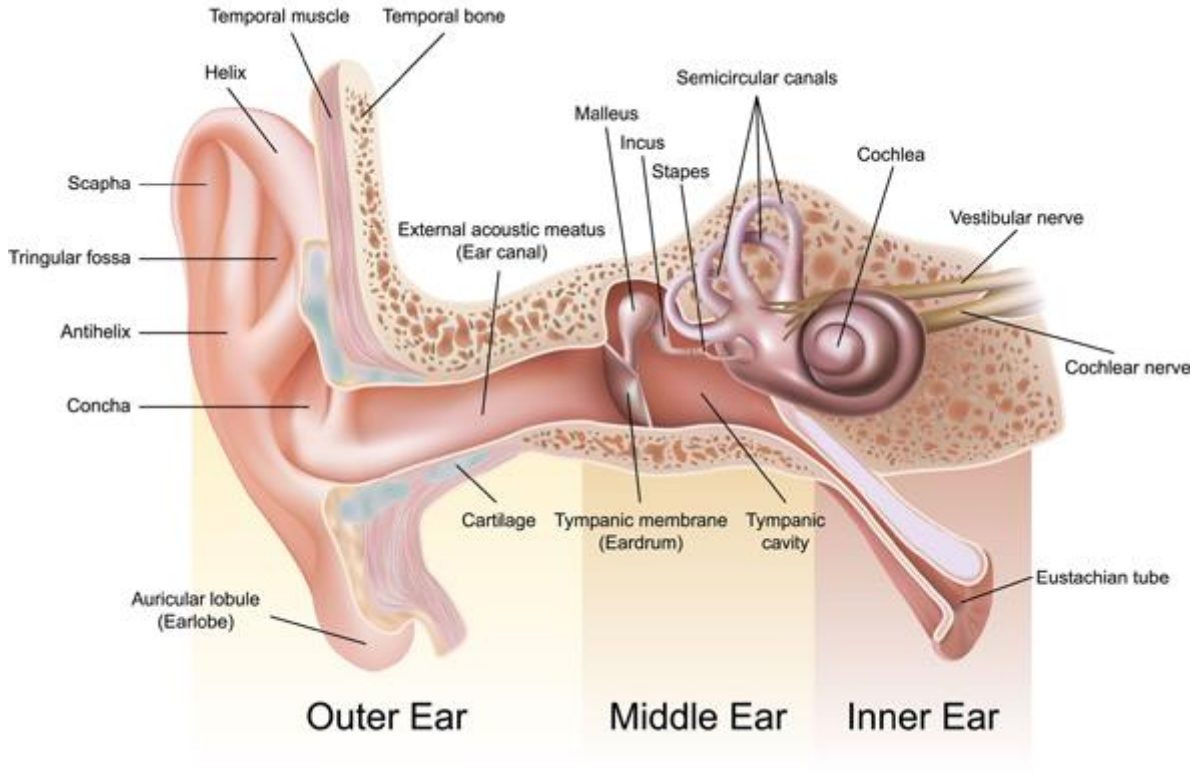

Fig. 1. Schematic representation of the anatomy of the human ear.
The outer and the middle ear are dedicated to the hearing system, whereas the inner ear houses the organs of hearing and of the peripheral vestibular system (Copyright © Peter Junaidy).

Outer ear

The outer ear (Fig. 1) is the external portion of the ear and is made up of the auricle, the concha and the auditory meatus (included the outer surface of the eardrum or tympanic membrane).

The auricle is the visible cartilaginous flange that sits on the external surface of the head and it consists of the helix and the antihelix. They are the outer and inner curved rim of the auricle, respectively, and they are separated by a depression called scapha.

Helix and antihelix open into the auditory meatus, which is partially obscured by the tragus protrudes and the facing antitragus. The hollow region in front of the auditory meatus is the concha, which works as resonance cavity.

The role of auricle and concha is to collect and amplify incoming sound waves and direct them down the auditory meatus *(Pickles, 2008; Purves et al., 2007*). The auricle and the concha are also

able to selectively filter incoming sound waves depending on their direction to give cues about the location of the source of the sound (*Pickles, 2008; Purves et al., 2007*).

The auditory meatus or ear canal is the cylindrical structure, which connects the auricle to the tympanic membrane (length ~2.5 cm). The ear canal is composed by cartilage in the first part (near the auricle) and by bone in the second part (near the tympanic membrane). Once directed down the ear canal, the sound waves cause the tympanic membrane to vibrate.

Middle ear

The middle ear is the portion of ear located between the outer and the inner ear, and it essentially consists of the tympanic cavity. The tympanic membrane or eardrum (Fig. 1) is an oval and thin membrane, which terminates the ear canal and divides the outer and middle ear. The eardrum has a cone-shaped structure, with the apex pointed inward, composed by three membrane layers. The tympanic membrane is continuous with skin on the outside and with mucus on the inside, whereas between the two, there is a layer of radial and circular fibers that give the membrane its tension and stiffness. As mentioned before, the sound waves cause the tympanic membrane to vibrate and the stimulus goes to the middle ear through the umbo, which is a point on the inner surface of the tympanic membrane connected to the handle of malleus.

The tympanic cavity is an air-filled cavity, which contains: the three ossicles: (malleus or hammer, incus or anvil and stapes or stirrup), their stabilizing ligaments, the auditory tube (Eustachian tube) and the round and oval windows. The chain of three small bones acts as a piston and its function is to amplify and transmit the sound from the tympanic membrane to the oval window, a membrane covered opening, separating the middle and inner ear. The vibration of the tympanic membrane causes through the umbo the movement of the malleus, which connects to the incus, which in turn connects to the stapes. The stapes is attached to the flexible oval window of the cochlea and causes this to vibrate, introducing pressure waves in the inner ear. Because the majority of sound waves traveling through the air are reflected from the fluid, the aim of the middle ear is to reduce this reflection. It is provided in two different ways. First, the oval window is 20 (twenty) times smaller than the tympanic membrane, hence the same pressure applied to the tympanic membrane results in a 20 times bigger pressure at the oval window. The second mechanism is provided by the lever action of the ossicles, which double the pressure on the oval window. The synergy of these two mechanisms amplifies the pressure soundwave about 40 (forty) fold and it allows the cochlea to detect the sounds (*Pickles, 2008; Purves et al., 2007*).

The function of the Eustachian tube, which joins the tympanic cavity with the nasal cavity (nasopharynx), is to equalize the pressure between the middle ear and throat. The slitlike ending of this tube in the nasopharynx is normally closed, but muscle movements open the entire passage during for example: yawning, swallowing or sneezing. The difference in pressure between outside the ear and in the middle ear can excessively stretch the tympanic membrane and cause pain.

Finally, the function of the round window is to allow the fluid within the inner ear to move. As the stapes pushes the secondary tympanic membrane (oval window), the fluid in the inner ear moves through the cochlea and pushes the membrane of the round window out by a corresponding amount into the middle ear.

Inner ear

The inner ear is (Fig. 1) the innermost part of the vertebrate ear and it is located within the temporal bone in a complex cavity called the bony labyrinth. The bony labyrinth is filled with a fluid, called perilymph, in which is situated the membranous labyrinth (Fig. 2). The perilymph is an extracellular fluid rich in Na^+ (140 mM) and low in K^+ (4–5 mM) (*Bernard et al., 1986*).

The membranous labyrinth is fixed to the bony labyrinth by connective tissue trabeculae and, differently from the bony labyrinth, it is filled with a peculiar extracellular medium, called endolymph (Fig. 2). The endolymph has a composition similar to the intercellular fluid, in fact it is rich in K^+ (150 mM) and low in Na^+ (1 mM) and Ca^{2+} (20 µM) (*Pickels, 2008*). The difference in composition, between endolymph and perilymph, allows the K^+ transducer current to flow from the endolymphatic compartment to the perilymphatic compartment (*Davis, 1965*). The membranous labyrinth consists of three semicircular canals (SCCs), two otolith organs (utricle and saccule) and the cochlea (Fig. 2).

The inner ear consists of cochlea and vestibule. The cochlea is a snail-shaped structure dedicated to hearing. It converts sound pressure patterns from the outer and middle ear into electrochemical impulses, which are passed on to the brain via the auditory nerve. Instead, the vestibule is the structure dedicated to balancing. It converts movements into electrochemical impulses which are passed on to the brain via the vestibular nerve.

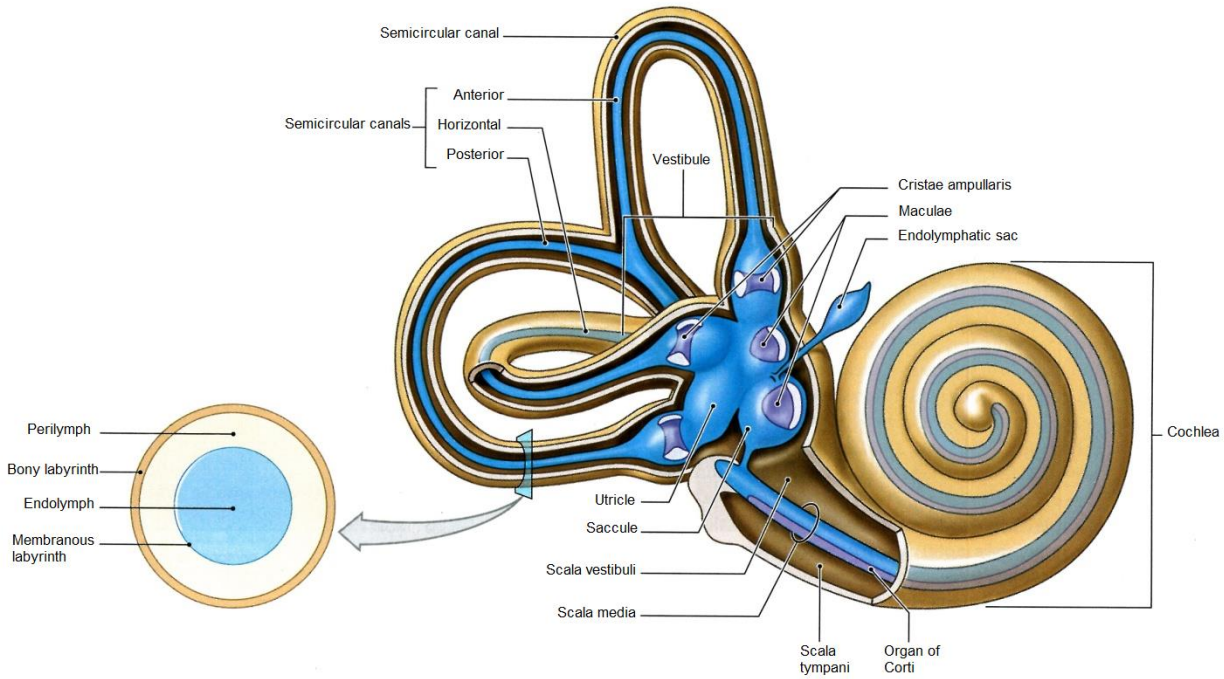

Fig. 2. Drawing of the cochlear and vestibular labyrinth.
The bony labyrinth (brown) is filled with perilymph and it contains the membranous labyrinth (blue), which is filled with endolymph. Inside the membranous labyrinth are located the sensory epithelia of cochlea and vestibule (dark blue).
The inset of the drawing represents the cross-section of the semicircular canal and it shows better how perilymph (light brown) and endolymph (light blue) are organized in the inner ear (Martini et al., 2014).

Cochlea

The cochlea is the spiral shaped organ, which contains the sensory cells for sound detection. The cochlea has three fluid-filled chambers: the scala vestibuli, the scala tympani and the scala media (or cochlear duct) (Fig. 3).

The scala vestibuli is above the scala media and it borders on the oval window, while the scala tympani is below the scala media and it ends at the round window (Fig. 3). The fluid fills the scala vestibuli and scala tympani is rich in Na^+ (140 mM) and low in K^+ (4–5 mM), similar to extracellular fluid, while the fluid in the scala media is rich in K^+ (150 mM) and low in Na^+ (1 mM), similar to the intracellular fluid.

The scala media completely divides lengthwise the cochlea and it is separated from the scala vestibuli by the Reissner's membrane and from the scala tympani by the basilar membrane. On the basilar membrane of the scala media is located the organ of Corti, which contains the sensory receptor cells, known as hair cells (Fig. 3).

When the oval window is depressed by the middle ear bones, it creates waves that travel through the fluid of the cochlea. These waves cause oscillation of the basilar membrane, a ribbon-like collagenous sheet that lies along the cochlea and supports the organ of Corti. The mechanical properties of the basilar membrane make it more sensitive to high-frequency oscillations at the base of the cochlea and to low frequencies at the apex (*Marcotti, 2012*).

The geometry of the organ of Corti and the disposition of another collagenous structure, the tectorial membrane, ensure that when the basilar membrane vibrates it causes deflection of the mechanosensory hair bundles that are the characteristic feature of hair cells (*Petit and Richardson, 2009; Schwander et al. 2010*) (Fig. 3).

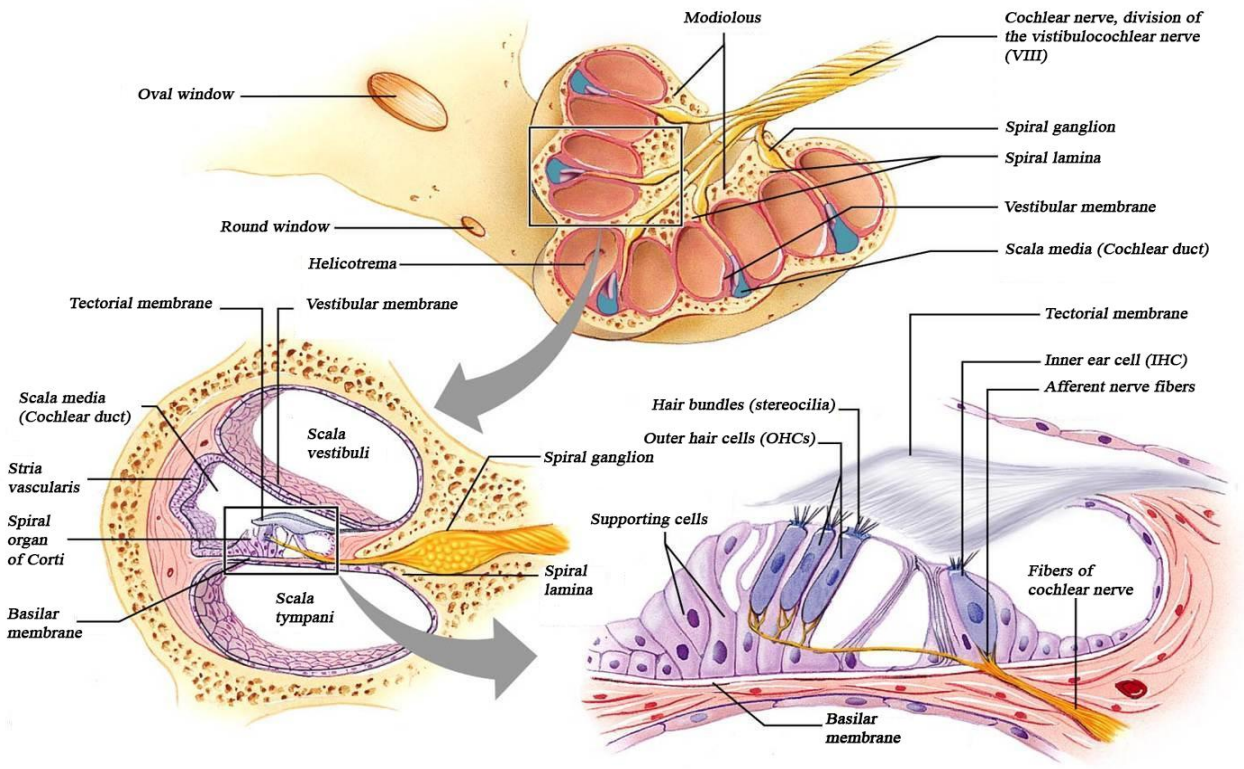

Fig. 3. Internal structure of the cochlea viewed in cross-section.
Top: Cross-section drawing of the entire cochlea with its typical snail-shape. Left Bottom: Cross-section through one spiral of the cochlea, where there are the three different scala: vestibuli, media and tympani. Right Bottom: Cross-section of the organ of Corti made up of the sensory cells and supporting cells with above the tectorial membrane (Marieb, 2001).

Vestibule

The vestibule is the sensory organ that provides the leading contribution to the sense of balance and spatial orientation. The vestibule is composed of large interconnected chambers, which consists of two otolithic organs, the utricle and the saccule, and three semicircular canals (SCCs) (Fig. 2).

The utricle and the saccule provide information about linear accelerations and changes in the head position relative to the forces of gravity (*Goldberg and Fernández, 1975*). Both of these organs contain a sensory epithelium, the macula, which consists of particular sensory cells, the hair cells, and supporting cells. Overlying the hair cells and their hair bundles is a gelatinous layer, and above this is a fibrous structure, the otolithic membrane, where are embedded crystals of calcium carbonate called otoconia. The otolithic membranes of saccule and utricle differ for membrane thickness and size of otoliths (*Lindeman, 1973*) (Fig. 4).

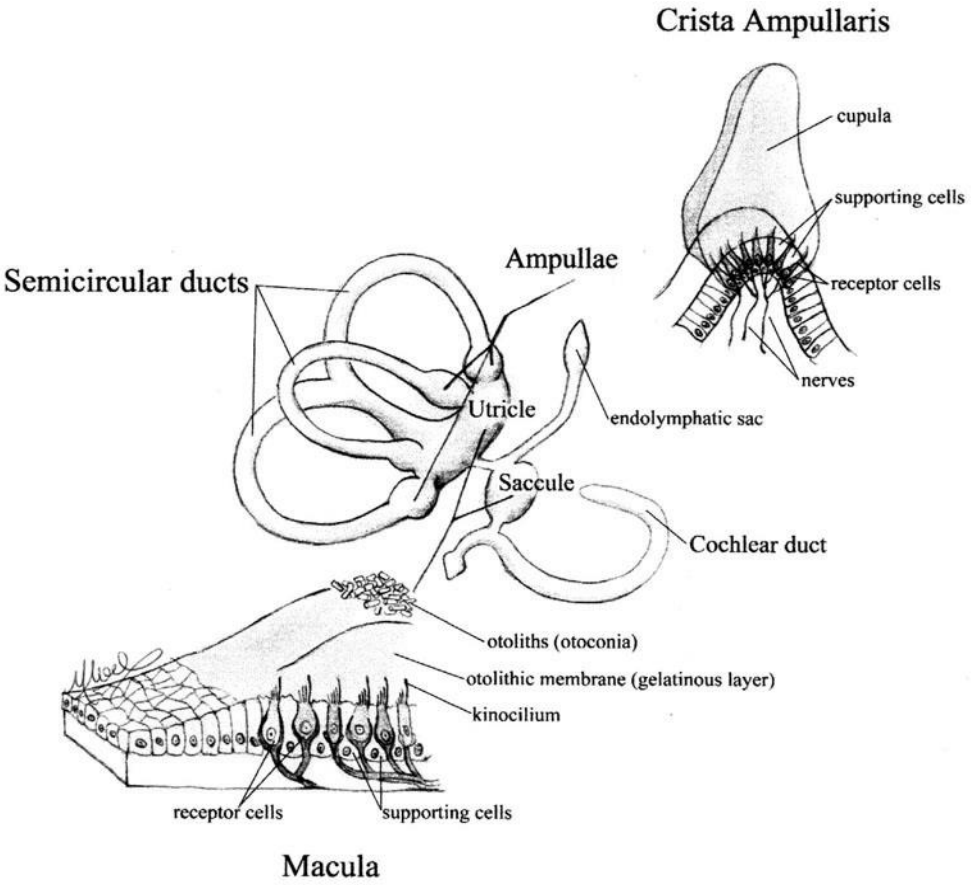

Fig. 4. Different organization of vestibular sensory epithelia.
Middle: Diagram of the vestibular labyrinth with the magnification of the crista ampullaris of the ampulla (top), where hair bundles are embedded into the cupula, and of the macula of the otolithic organs (bottom), where hair bundles are embedded into the otolithic membrane (De Lemos-Chiarandini and Shafland, 2007).

When the head tilts, the shearing motion between the otolithic membrane and the macula displaces the hair bundles and we sense the movement.

In both saccule and utricle, the orientation of the hair cell bundles is organized relative to the striola, which divides the hair cells into two populations with opposing hair bundle polarities (Fig. 5). The saccular *macula* is oriented vertically and the utricular macula horizontally, moreover analysis of the excitatory orientations in the maculae indicates that the utricle responds to movements of the head in the horizontal plane (e.g. sideways head tilts and rapid lateral displacements), whereas the saccule responds to movements in the vertical plane (e.g. up-down and forward-backward movements in the sagittal plane). The saccular and utricular *maculae* on one side of the head are specular of those on the other side, hence a movement to one side has opposite effects on corresponding hair cells of the two utricular *maculae*.

In mice, the length of the utricular *macula* is 0.432 ± 0.006 mm and the length of the saccular *macula* is 0.405 ± 0.043 mm (*Desai et al., 2005b*).

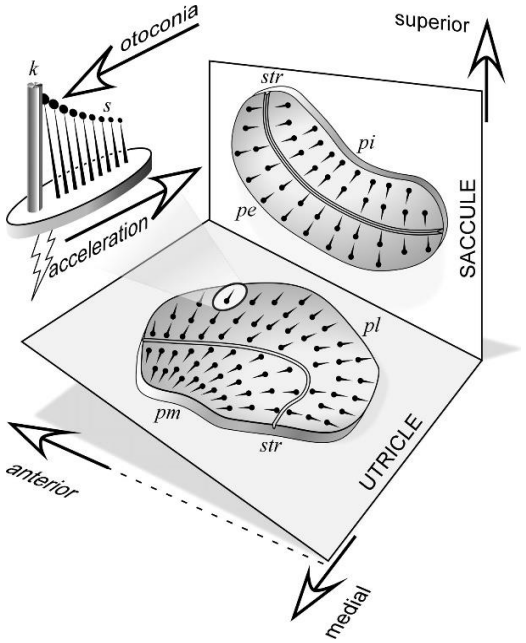

Fig. 5. Orientation of the maculae of the utricle and saccule.
The saccular macula is in a vertical plane whereas the utricular macula is mostly horizontal plane. The alignments of the hair cells on the macula surface are drawn with the kinocilia (k) at the thick end and stereocilia (s) at the thin end. Each hair cell responds positively to acceleration in the direction of its alignment, increasing firing rate when the stereocilia are deflected toward the kinocilium. Thus linear acceleration of the head from kinocilium toward stereocilia will cause an increase in discharge. A striola (str) divides each macula into two regions of reversed hair-cell polarity, so that when all afferents of a macula are excited or inhibited, the net signal will be determined by the relative weighting of each region. In the schematic drawing: pe, pars externa; pi, pars interna; pl, pars lateralis; pm, pars medialis (Fitzpatrick and Day, 2004).

The semicircular canals (SCCs) are curved ducts, connected to the utricle, which sense head rotations arising from self-induced movements or angular accelerations of the head. The three SCCs are situated nearly to 90 degree angles to each other and, depending on the orientation of the three planes and on the plane where they lie, they are distinguished in superior or anterior vertical canal (AC), posterior vertical canal (PC) and horizontal canal (HC).

The superior and posterior canals are aligned in a 45 degree angle to the sagittal plane, and the lateral canals are aligned in a 30 degree angle in the axial plane (*Lee et al., 2011*). The ducts of the two vertical canals join together to form the crus commune.

Each SCCs is characterized by the presence of an enlargement known as *ampulla*, where is located the sensory epithelium, or *crista ampullaris*, that contains the hair cells. The hair bundles extend out of the *crista* into a gelatinous mass, the *cupula*, which spans the *ampulla*, forming a fluid barrier through which endolymph cannot pass (Fig. 4).

As the head rotates in the plane of one of the SCCs, the inertia of the endolymph distorts the *cupula*, distending it away from the direction of head movement and causing a displacement of the hair bundles within the *crista*. In contrast, linear accelerations of the head produce equal forces on the two sides of the *cupula*, so it will not occur distortion of the *cupula* and no displacement of the hair bundles (Fig. 6).

Each SCC works together with a SCC on the other side of the head and it means that SCCs are paired as follows: right superior with left posterior, left superior with right posterior, left horizontal with right horizontal. For this reason each canal is able to detect angular acceleration in its specific plane; this arrangement allows for a 3-dimensional vector representation of rotational acceleration (*Khan and Chang, 2013*).

Finally in each *crista ampullaris*, the hair bundles of the *stereocilia* have the same polarization, hence they are organized with the hair bundles pointing in the same direction. Conversely in the saccular and utricular *maculae*, as seen before, hair bundles reverse orientation at a line of polarity reversal (LPR) running through or next to the striola (*Li et al., 2008*). The striola has sometimes been equated with the LPR. More commonly the striola is a swath of *epithelium*, 10-20% of the *macula* in rodents (*Desai et al., 2005b; Eatock and Songer, 2011*).

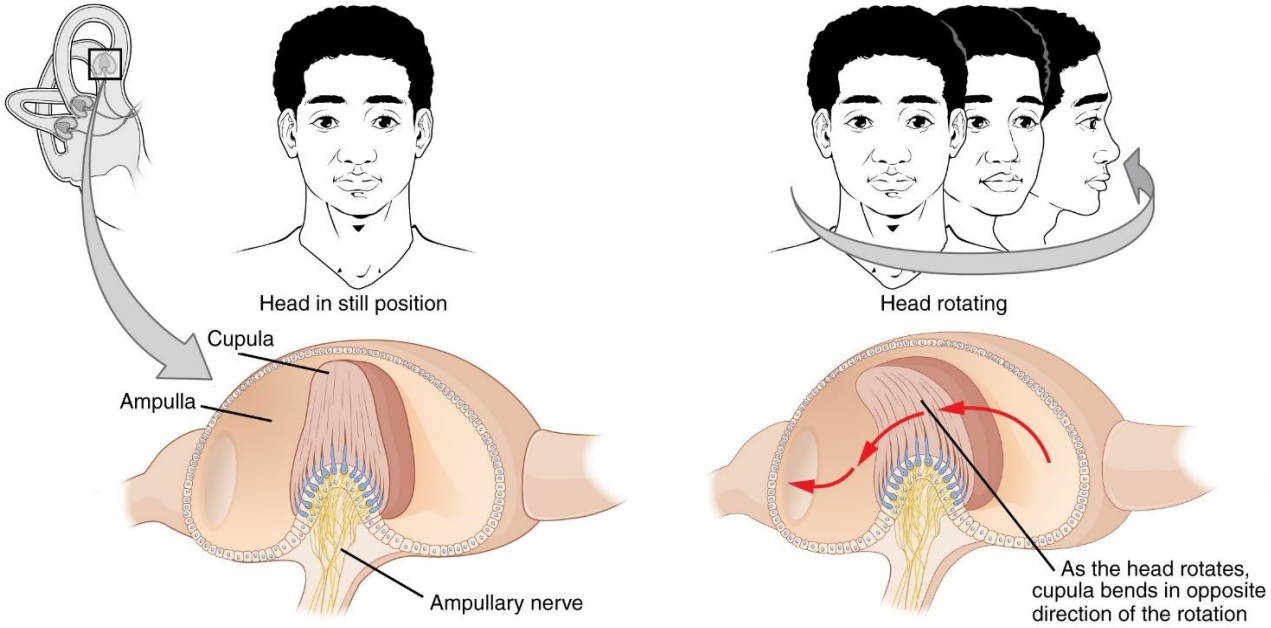

Fig. 6. SCCs have the task of detect rotational movement of the head.
As one of the canals moves in an arc with the head, the endolymph moves in the opposite direction, causing the cupula and stereocilia to bend. The movement of two canals within a plane results in information about the direction in which the head is moving (https://www.boundless.com/).

Hair cells

Hair cells are the sensory receptors, within the inner ear, of the auditory-vestibular system in all vertebrates. The name of these cells derives from the highly specialized hair-like elements, called hair bundle, protruding from the top of each cell. The function of the hair cells is to transduce sound or motion, through mechanical displacement, into electrical signals by the hair bundles.

The hair bundle consists of stereocilia and *kinocilium* organized in a staircase-like structure, where the tallest site of the bundle is the *kinocilium* (*Furness and Hackney, 2006*). Staircase-like structure means that the *stereocilia* within a single row are the same height, whereas stereocilia of different rows are graded in height, and the outermost row is the tallest.

Kinocilium and *stereocilia,* in the single hair bundle, move as a single unit (*Goodyear et al., 2005*) because the structure of the hair bundle is stabilized through several different connections between individual *stereocilia* and *kinocilium* (Fig. 7).

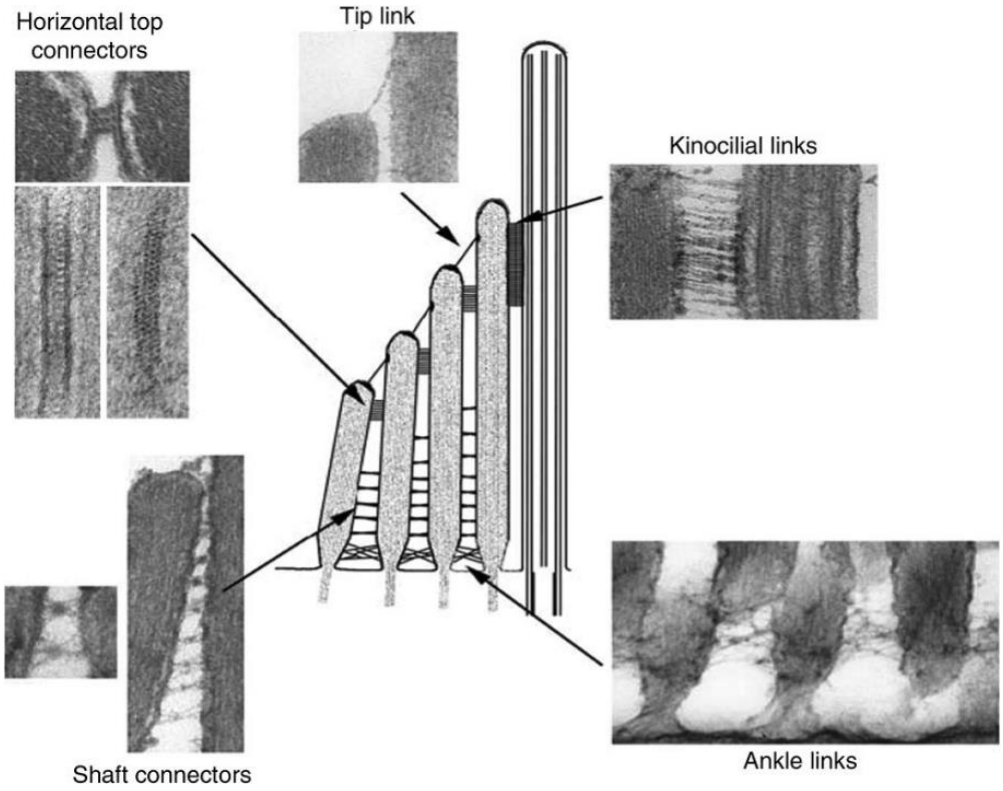

Fig. 7. Stabilizing structures in hair bundles.
The central illustration shows how many connecting structures are present in the hair bundles, such as tip links, lateral links and kinocilial links. These links are not always present, but they appear and fade at different developmental time. Lateral links in turn are distinguished into horizontal top connector links, shaft connector links and ankle links. In fact, lateral links connect stereocilia with each other, either within the same row or across adjacent rows. Electron micrographs illustrate the ultrastructural appearance of each link type. The horizontal top connector electron micrograph section planes are parallel (top image) and orthogonal (lower images) to the hair cell's apical surface; the lower right image shows a section of stereocilium. All other electron micrographs show section planes orthogonal to the hair cell's apical surface (Nayak et al., 2007; Goodyear and Richardson, 1992; 2003).

The precise distribution of these filaments varies between hair cells of different types, but there are two main categories, tip links and lateral links, which vary during the different stages of the development (*Goodyear et al., 2005; Hackney and Furness, 2013)* (Fig. 7).

The lateral links are horizontal filaments, which connect the rows of stereocilia, either along a row either between rows. In the mouse, they are classified corresponding to their localization along the stereocilia in ankle links (inferior connectors), shaft links (medial connectors) and top links (apical connectors).

Only the top links persist in the mature hair bundle of cochlear and vestibular hair cells, whereas ankle links disappear in the mature cochlea (*Goodyear et al., 2005; Michalski N et al., 2007*).

The molecular structure of the lateral links is still uncertain but there are few candidates and more might yet be discovered. In particular, the top connectors stains with antibodies against stereocilin

and, in a stereocilin-KO mouse, the hair bundle morphology is normal until postnatal day 9 (P9), after that it progressively deteriorates (*Verpy et al., 2011*).

The shaft links seem to be characterized by the protein tyrosine phosphatase receptor type Q (PTPRQ), which is essential for the develop and extension of the lateral links (*Nayak et al., 2011*).

Finally, the ankle links are composed by G-protein-coupled receptor (VLGR1), the transmembrane proteins usherin and vezatin, and the submembrane protein whirlin (*Hackney et al., 2013*). These proteins might be targeted to ankle links by myosin VIIa during the development of hair cells (*Michalski N et al., 2007*). Interestingly, adult vestibular hair cells maintain ankle links and they express usherin (*Adato et al., 2005*).

Cadherin-23 (CDH23) and Protocadherin-15 (PCD15) are also part of the lateral link but they will be discussed extensively later.

The *kinocilium* is connected to the tallest *stereocilia* through the kinocilial link (*Michel et al., 2005*) (Fig. 7). This arrangement permits the mechanotransduction, through the changes of tension in the tip links, which trigger the opening and closing of mechanotransduction channel (described later).

The *stereocilia* are projections that protrude from the apical surface of the hair cell. Their cytoskeleton is composed by dense arrangement of parallel oriented actin filaments, not tubulin like true cilia, that are cross-bridged by different proteins such as including plastin-1 and fascin-2, the two most abundant (*Shin et al., 2010*), and espin (*Zheng et al., 2000*). Usually, a mature *stereocilium* is composed by around 2000 actin filaments (*Revenu et al., 2004; Schneider et al., 2002*) and it is continuously remodeled by the addition of actin monomers to the *stereocilium* tip, in fact the entire core of each *stereocilium* is renewed every 48 hours (*Schneider et al. 2002*). Before elongating to reach the mature levels, actin filaments in to the basal region of the *stereocilia* extend down, forming a root, into the apical region of the hair cell or cuticular plate. The cuticular plate is a horizontal network of actin filaments, which also contains myosin, α-actinin, fimbrin, tropomyosin, fodrin and calcium-binding proteins (*Pack and Slepecky, 1995; DeRosier and Tilney, 1989*).

The basal region of the *stereocilia*, which connects to the cuticular plate is called the rootlet and it is thinner than the rest of the *stereocilia*. In fact, the number of actin filaments is reduced from a few hundred to about a dozen. This conical shape is essential for the pivoting of the hair bundle.

The number of *stereocilia* changes depending on the inner ear organ, however, the diameter of cochlear and vestibular hair cell *stereocilia* is about 0.1-0.2 mm. Also the length of the stereocilia varies through the different organs, but it is remarkable that vestibular hair cell *stereocilia* can be as much as 40 μm.

The *kinocilium* is a true ciliary structure which, along with the stereocilia, comprises the hair bundle of vestibular and cochlear hair cells in mammals. It consists of a thin bundle of fibrils made up of

two central fibrils surrounded by nine double fibrils. The fibrils of the *kinocilium* end in the apical part of the hair cell in a bud-like swelling, called the basal corpuscle (*Marcotti and Masetto, 2010*). The *kinocilium*, as mentioned before, is the tallest site of the hair bundle but, differently from the *stereocilia*, it is formed from the basal body of the hair cell and not anchored to the cuticular plate. The function of the *kinocilium* is still unclear, moreover it has been demonstrated that in mammalian cochlea it disappears shortly after birth and the reason is still unknown (*El-Amraoui and Petit, 2005; Tilney et al., 1992*).

The tip-links are extracellular fine elements, which are thought to gate the mechanotransducer channel of the sensory hair cell by deflecting the hair cell bundle towards the taller row (*Ahmed et al., 2006*). Tip links are formed by two Ca^{2+}-dependent transmembrane proteins positioned in series, which are cadherin-23 (CDH23), in contact with the taller *stereocilium*, and protocadherin-15 (PCD15), in contact with the shorter *stereocilium* (*Schwander et al., 2010*) (Fig. 8). These proteins interact through their N-termini in a Ca^{2+}-dependent manner and the concentration of Ca^{2+} affect the length, and hence, the tension of tip-links.

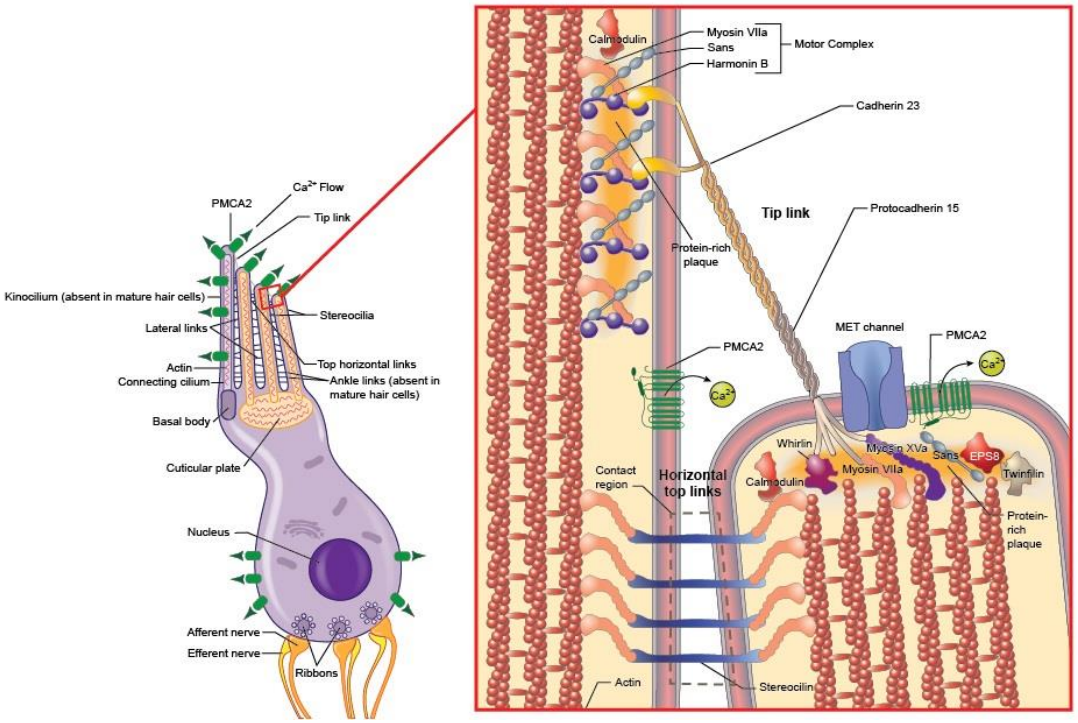

Fig. 8. Structure of tip-links.

The inner hair cells' hair bundle is composed of numerous stereocilia that have a core of parallel actin filaments anchored in the cuticular plate. Lateral to the tallest stereocilium is the kinocilium, which is formed from the basal body. The synaptic junction between the hair cell and afferent and efferent neurons is located at the base of the cell and contains ribbons.

The inset shows the molecular components of the cross-link complexes of the inner ear hair cell. In the tip-link, cadherin23 interacts with protocadherin15, harmonin, Myo7a, Myo1c, calmodulin, and Sans to help maintain the structure and function of the inner ear hair cell (https://mutagenetix.utsouthwestern.edu/phenotypic/phenotypic_rec.cfm?pk=1299).

Cochlear hair cells

In mammals, auditory hair cells are located along the spiral structure of the cochlea and transduce acoustic stimuli into an electrical response, that is relayed to the brain, enabling us to perceive sound (*Marcotti and Masetto, 2010*).

In the cochlea there are two types of hair cells: the inner hair cells (IHCs) and the outer hair cells (OHCs). These cells can be recognized by their shape and their location in the organ of Corti.

IHCs are pear shaped cells with a round centrally located nucleus, while OHCs have a regular cylindric and elongated shape with a round nucleus located in the basal portion of the cell.

In the organ of Corti cochlear hair cells are arranged in four rows. A single row is constituted by the IHCs (Fig. 9) which are joined by tight junction, near the apical surface, and by an adherens junction. The IHCs' function is to relay acoustic information to the central nervous system via afferent auditory nerve fibers (*Raphael and Altschuler, 2003*). The other three rows are constituted by the OHCs (Fig. 9), whose function is to augment the sensitivity and frequency selectivity along the cochlea by active mechanical amplification. OHCs differ along the cochlea, in fact at the basal turn they are shorter than those located in the apical turn. The junctional complexes connecting OHCs to their neighboring cells are similar to those found in inner hair cells, in particular the most apical complex, the tight junction, forms a mixed complex with the adherens junction, so that they alternate along an extensive length (*Raphael and Altschuler, 2003*).

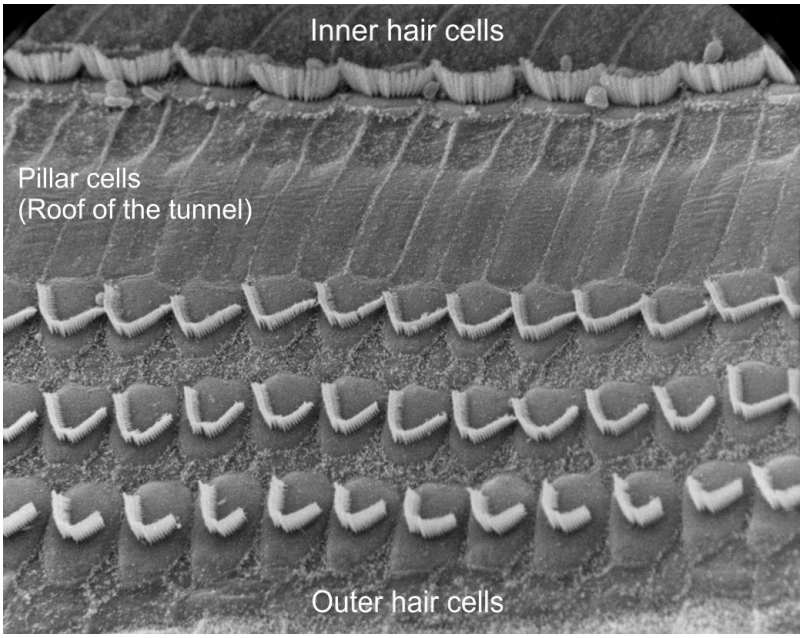

Fig. 9. Surface view of mid-turn of the cochlea.
One row of inner hair cells (IHCs) and three rows of outer hair cells (OHCs) are visible, along with the supporting cells that are positioned between the sensory cells (Copyright © 1999-2014 The Hospital for Sick Children (SickKids)).

IHCs and OHCs are separated by outer pillar cells, which form an arch called tunnel of Corti. IHCs are supported and enclosed by additional supporting cells called inner phalangeal cells, while OHCs are mainly supported by the Deiter's cells (*Marcotti and Masetto, 2010*).

About three curved rows of stereocilia constitute the IHC bundle and the tallest stereociliar row faces the inner pillar cells. The OHCs' *stereocilia* are organized in 3–6 rows and they have a V or W architecture, with the smallest stereocilia facing the inner pillar cells (Fig. 9). The angle of the V architecture varies in a gradient along the scala media, with the acutest angle at the apical turn.

The apical portion of the cell (cell surface) along with its *stereocilia* are bathed in endolymph of scala media, whereas the basolateral domain is bathed in perilymph.

Cochlear hair cells are tonotopically organized. It means that cochlear hair cells are positioned, along the cochlear sensory epithelium, according to their best respond frequency. In fact, high-frequency cells are located at the base, whereas low-frequency cells are located at the apex. Moreover, the morphological properties of hair cells change progressively along the cochlea, indeed the longest hair bundles are located at the apex in the low-frequency cells and the shortest are at the base in the high-frequency cells (*Fettiplace and Hackney, 2006*).

The maturation of mouse cochlear hair cells follows a tightly regulated developmental program (*Marcotti, 2012*). Hair cells of cochlea undergo terminal mitosis, which is the last cellular division and the onset of a stable cell population, between embryonic day 12 and 15 (E12 and E15). Hair cell differentiation progresses in a basal to apical direction for several more days and it is completed around postnatal day 20 (P20), around 8 days after the onset of hearing in rodent (P12; *Marcotti and Masetto, 2010*).

Concurrently with the maturation, cochlear hair cells change their specific voltage-dependent channels, hence their biophysical properties, and their synaptic connections. Both changes turn immature hair cells into mature sensory receptors. Hence, these cells are able to conduct their specific functions correlated to the point they are located in the sensory organ (*Masetto et al., 2000; Housley et al., 2006*).

Before the onset of hearing, different central auditory nuclei show spontaneous activity, but this activity is initiated from the developing cochlea. In fact, after several experiments, it was seen that the firing activity of embryonic chick was eliminated following removal of the cochlea or by application of tetrodotoxin (TTX) (*Lippe, 1994*). Moreover, *Jones et al., 2001; 2007* perform some in vivo experiments, which showed similar action potentials between central auditory nuclei and spiral ganglion neurons (SGNs). Later on, it has been discovered that the spontaneous action potentials present in the SGNs are related to Ca^{2+}-mediated neurotransmitter release from IHCs (*Robertson and Paki, 2002; Tritsch and Bergles, 2010*).

Pre-hearing IHCs are capable of firing Ca^{2+}-action potentials, called Ca^{2+} spikes, which have much slower kinetics than conventional Na^{+}-based action potentials (*Wang and Bergles, 2015*). These spikes are mediated primarily by L-type Ca^{2+} channels containing the $Ca_{v1.3}$ subunit, which are activated by small depolarization of the resting membrane potential (*Platzer et al. 2000; Marcotti et al., 2003b*). The rate of the upstroke and the maximum potential of the generated spikes id dependent on the extracellular Ca^{2+} concentration, in fact if it increases also the two parameters do it. Conversely the frequency of the action potentials is modulated by the Na^{+}, in fact higher Na^{+} concentration produces an increase in the action potential frequency (*Marcotti et al., 2003b*).

During every Ca^{2+} spike a big amount of Ca^{2+}, sufficient to trigger Ca^{2+}-mediated glutamate release from immature ribbon synapses, enters in to the cell (*Beutner and Moser, 2001; Glowatzki and Fuchs, 2002; Johnson et al., 2005).* The release of the neurotransmitter evokes action potentials in the afferent fibers, which pass through the SGNs and the eighth nerve to arrive to the auditory brainstem.

Hence, even if the ribbon synapses are immature and there is a low Ca^{2+} efficiency during the exocytosis, IHCs are capable of releasing neurotransmitter several weeks before hearing onset. It is supposed that in the cochlea, like in nervous system, the presence of spontaneous Ca^{2+}-dependent action potential activity in the immature IHCs promotes the maturation of the cells (*Moody and Bosma, 2005*).

On the basolateral membrane, OHCs and IHCs are innervated by specialized afferent and efferent fibers forming a network to and from the brainstem. In particular, IHCs are synaptically connected to a large diameter and myelinated type I spiral ganglion neurons (90–95% of all afferent fibers; Fig. 10 left) forming the radial afferent system going to the cochlear nuclei (CN). The peculiarity of these afferent fibers is that they innervate only one IHC (*Pujol et al., 1998*), but IHCs are able to communicate with different afferent neurons. The activity of individual afferent neurons is driven by the neurotransmitter L-glutamate, released from specialized presynaptic structures named ribbon synapses (*Fuchs, 2005; Sterling and Matthews, 2005*).

The IHCs receive messages from the SNC (lateral part of the efferent olivocochlear system) through neurons developing in the brainstem and ending below IHCs synapsing with the afferent type I dendrites (indirect connection to IHCs; Fig. 10 left). It has been hypotesized that different subtances could modulate the lateral efferent system, such as acetylcholine, gamma-aminobutyric acid (GABA), dopamine, enkephalin and dynorphin (*Oestreicher et al., 2002*).

The OHCs synapse with a few smaller and unmyelinated type II spiral ganglion neurons (5–10%; Fig. 10 right), forming the spiral afferent system. This afferent system connect about ten OHCs,

which are generally in the same row. Like in IHCs, afferent synapse is directly connected with the OHC and the neurotransmitter used to communicate is L-glutamate.

The OHCs are principally connected to efferent fibers, because their role is to modulate the electromechanical amplification of the cochlear partition (*Marcotti and Masetto, 2010*). The efferent system is made by large neurons of the medial efferent system which, originating from the two sides of the medial superior olivary complex (MSO), form axo-somatic synapses with the OHC.

Differently from IHCs, efferent synapse is directly connected with the OHC and the neurotransmitter used are few, such as acetylcholine, GABA and calcitonin gene-related peptide (CGRP) (*Schrott-Fisher et al., 2007*).

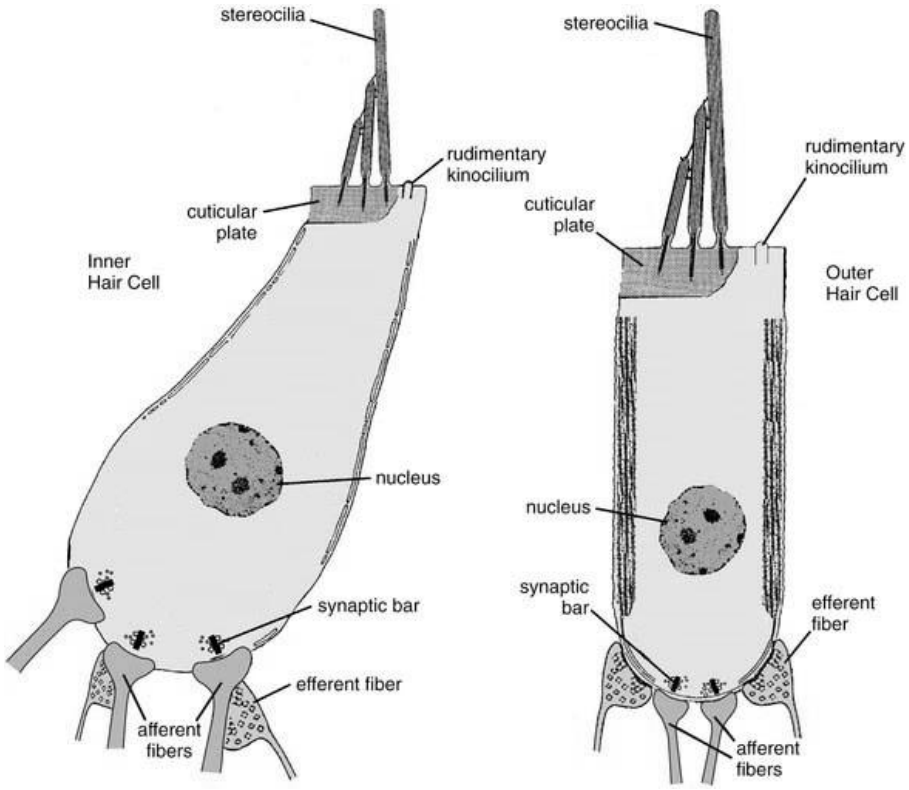

Fig. 10. Schematic depictions of inner and outer hair cells.
Inner hair cells are flask-shaped (left), receive extensive afferent innervation, and receive indirect efferent innervation. Outer hair cells (right) are cylindrical and receive direct afferent and efferent innervation (modified Runge-Samuelson and Friedland, 2010).

Vestibular hair cells

Reptiles, birds and mammals are characterized in their *cristae* and *maculae* of the vestibule by the presence of two types of hair cells, called Type I and Type II (*Jørgensen, 1974; Wersäll and Bagger-Sjöbäck, 1974*). Type I and Type II hair cells are different, indeed they diverge for shape, afferent innervation and ion channel express on the basolateral membrane (*Wersäll, 1956*).

It is interesting how Type I hair cells are only found in mammals, birds and some reptiles, whereas Type II are found in all the species (i.e. amphibians and fish). Type I hair cells are amphora- or flask-shaped, whereas Type II hair cells are cylindrically shaped (Fig. 11). Both Type I and Type II hair cells are surrounded by supporting cells, which have an irregular shape and microvilli protruding from their apical surface (Fig. 11).

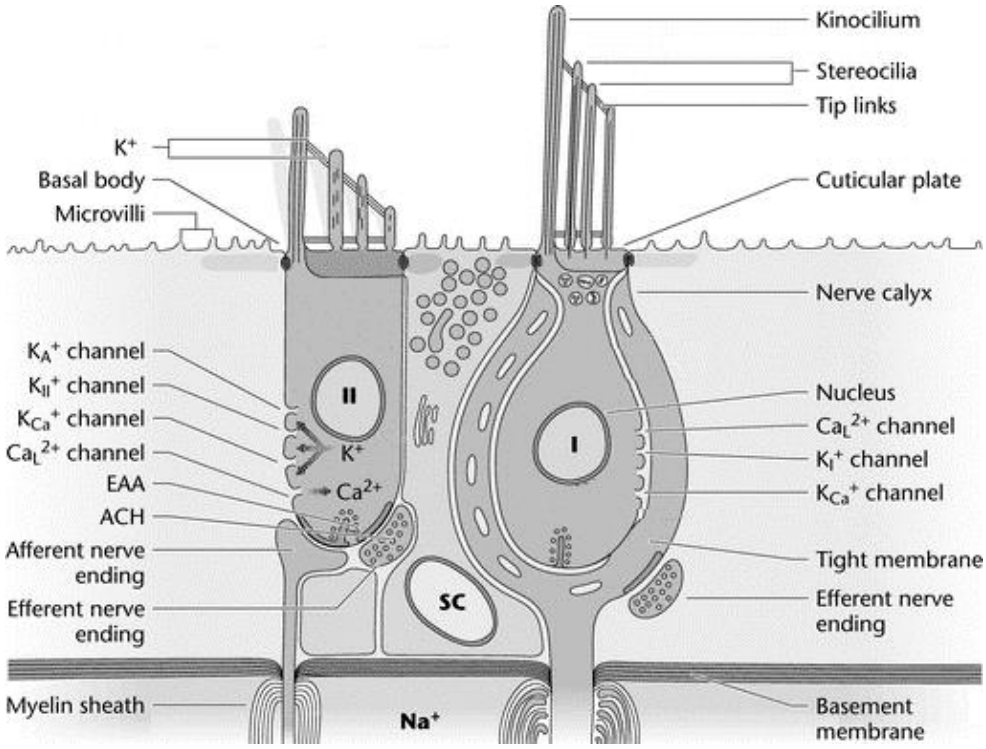

Fig. 11. Schematic diagram of the adult mammalian vestibular neuroepithelium.
Type II hair cell (II, left) is contacted by bouton terminals whereas Type I (I, right) basolateral membrane is enveloped by the calyx terminal. The diagram reports also the different synaptic vesicles containing glutamate (afferent neurotransmitter) or acetylcholine (efferent neurotransmitter). The apical surface of hair cells is characterized by the hair bundle, whereas the body by the presence of different ion channels. Supporting cells (SCs) have short microvilli on their apical surface and they are connected to the upper part of the body of the vestibular hair cells by tight junctions. Below the basement membrane afferent nerve fibers become coated by the myelin sheath.

In the mouse, the number of hair cells changes according to the organ and the type of hair cells considered. Type I hair cells are around 761 ± 57 in each mouse *crista*, 1297 ± 45 in the saccular *macula* and 1789 ± 43 in the utricular *macula*, whereas Type II hair cells are around 653 ± 61 in each mouse *crista* 1180 ± 81 in the saccular *macula* and 1457 ± 62 in the utricular *macula* (*Desai et al. 2005a, Desai et al. 2005b*).

In general, Type I and Type II hair cells are not uniformly located. For example in the *crista ampullaris* Type II hair cells are more present in the peripheral zone and less in the central one. Instead in the *macula* there is a different number of Type I and II hair cells in the striola, where Type I are more numerous than Type II. Only in the extrastriola of the *macula* Type I and II hair cells are almost equally distributed (*Lindeman 1969, Watanuki et al. 1971, Desai et al. 2005b*).

Type I vestibular hair cells are wider and longer than Type II, furthermore they have taller and thicker *stereocilia* and a thicker cuticular plate (*Lapeyre et al. 1992, Morita et al. 1997, Ciuman 2011*). According to the position, the size of the cells and the length of hair bundles change also between the same type of cell, in fact in the central zone of the *crista* the hair cells are larger but the hair bundles are shorter.

Vestibular hair cells, like cochlear hair cells, are innervated by afferent and efferent innervations that inform the brain about the head motion (*Fernández et al., 1988*). In contrast to the cochlea, each vestibular afferent innervation receives input from multiple ribbon synapses and connect to one or more hair cells (*Goldberg, 2000*).

Type I hair cells are characterized by their basolateral membrane being enveloped in a single large afferent nerve terminal, named calyx, which is different from the calyces of Held and of the superior cervical ganglia (*Bao et al., 2003*) because the latters are presynaptic rather than postsynaptic. The calyx receives synaptic inputs on their inner side from Type I hair cells and on the outer side by the efferent synapses (*Lysakowski and Goldberg, 2008*) (Fig. 11). Conversely, Type II hair cells are connected by bouton-type afferents synapse.

Cristae and *maculae* receive innervation originating in the brain stem (*Gacek, 1960*), the efferents fibers end as boutons and appear vesiculated (*Engström, 1958*). Efferent nerve terminals directly contact Type II hair cells or, as mentioned before, the calyx of Type I hair cells (*Iurato et al., 1972; Lysakowski and Goldberg, 1997*).

The hair cell afferent neurotransmitter is glutamate, which binds to the postsynaptic AMPA (a-amino-3-hydroxyl-5-methyl-4-isoxazole-propionate) receptors on the afferent nerve terminal (*Glowatzki et al., 2008*). While the efferent neurotransmitter is the acetylcholine, which is principally responsible for the inhibitory responses. It can bind to metabotropic or ionotropic cholinergic receptors present located on the outer side of the calyx (Type I) or on the hair cell's

basolateral membrane (Type II; Fig. 11), where it increases the background afferent discharge and decreases afferent sensitivity to rotational stimuli (*Poppi et al., 2017*). Unfortunately, the cellular mechanisms at the base of these effects is still unknown.

Supporting cells are bipolar cells, which are located in the sensory *epithelium* between Type I and Type II hair cells (Fig. 11). These cells are characterized by the presence of short microvilli and large secretory granules in the apical region and by the nucleus in the basal region. The supporting cells, like the vestibular hair cells, differ in number according to the organ considered. They are around 1858 ± 220 in each mouse *crista*, 2073 ± 18 in saccular *macula* and 2754 ± 50 in utricular *macula* (*Desai et al., 2005a; Desai et al., 2005b*).

It has been hypothesized that the supporting cells are involved in several important functions, such as mediators of development, death and phagocytosis of the hair cells (*Bird et al., 2010; Monzack and Cunningham, 2013*). Moreover, supporting hair cells could be crucial for the synthesis and maintenance of the *cupula* and to mediate glutamate clearance at synapses in order to prevent excitotoxicity (*Pujol and Peul, 1999; Gale and Jagger, 2010*).

Finally, supporting cells are involved in removing damaged or dead hair cells from the sensory *epithelium* (*Monzack and Cunningham, 2013*). This process is realized by the extrusion of hair cell or sub-liminal phagocytosis with the littlest damage to the function and structure of the surrounding tissues (*Li et al., 1995; Seoane and Llorens, 2005*).

During sub-liminal phagocytosis the whole hair cell, under the epithelial surface, is separated from the *stereocilia* and destroyed. Using a time-lapse confocal imaging in the living chick utricle (*Bird et al., 2010*), it has been demonstrated that phagosomes are created from supporting cells. This phagosomes are phagocytic structure composed of multiple cells, which cover the remaining bundleless hair cell under the luminal surface and then eliminate it completing the phagocytic process. Once the empty space is formed, the supporting cells occupy it and start the healing procedure, forming a scar in the area previously occupied by hair cells (*Raphael and Altschuler, 1991; Meiteles and Raphael, 1994*).

The supporting cells can also regenerate hairs cell via mitotic replacement and direct transdifferentiation. In the former process supporting cells split to generate new hair cells, whereas in the latter supporting cells turn into an hair cell without dividing. As mentioned before, it is important to remember that in some mammals, frogs, newts and birds the supporting cells can be progenitors of the hair cells after damage (*Matsui et al., 2000; Monzack and Cunningham, 2013*).

Mechano-electrical transduction in hair cells

Hair cells are the sensory receptors in the inner ear that detect sound and head motion to begin the processes of hearing and balance control. The biophysical process, where the incoming mechanical stimulus is converted into the electrical signal is called mechano-electrical transduction. The mechano-electrical transduction (MET) takes place in the hair bundle of both cochlear and vestibular hair cells.

The hair bundle is a precise structure, whose aim is to detect even small mechanical stimuli. In fact, hair bundle deflections of few nanometers are sufficient to trigger the mechano-electrical transduction (~0.1 μm in the cochlea, *Fettiplace and Ricci, 2003*; ~1.5 μm in the vestibular cells *Géléoc et al., 1997; Holt et al., 1997*).

As mentioned before, the stereocilia and the kinocilium in the hair bundle are horizontally linked together by filaments called tip links, which play a central role in mechano-electrical transduction ensuring a unified movement of the hair bundle (*Goodyear et al. 2005*).

The mechanical displacement of the hair bundle towards its taller *stereocilia*, called excitatory deflection (Fig. 12 left), leads to stretch the tip links (*Pickles, 2008*). This stretching results in an increased open probability of the mechano-electrical transduction (MET) channels located at the tip of the stereocilia and the flow of a cation current (especially K^+ and Ca^{2+}; *Jaramillo and Hudspeth, 1991*).

The flow of small cations from the endolymph into the cell is defined transduction inward current and it causes depolarization of the hair cell membrane (receptor potential) (*LeMasurier and Gillespie, 2005*) (Fig. 12 left). In contrast, deflection of the stereocilia towards the shorter stereocilia, called inhibitory deflection, closes these channels and hyperpolarizes the hair cell membrane (Fig. 12 right).

When the hair cell is not stimulated around the 15% of the MET channels are open, whereas when there is a stereociliary deflection, in the opposite plan of the excitatory or the inhibitory deflections, it has little or no effect.

The biophysical and morphological properties of the mechano-electrical transduction channels have been largely investigated (*Fettiplace and Hackney, 2006; Furness and Hackney, 2006*) but unfortunately the molecular identity of the channel is still unclear. The MET channel does not show or has a very little homology with other known ion channels (*Strassmaier and Gillespie, 2002*).

As mentioned before (chapter “Hair cells”), mature tip links are formed by PCD15 and CDH23 molecules. There are evidence that, at the lower end of the tip link, PCD15 could be connected to transmembrane channel-like protein 1 and 2 (respectively, TMC1 and TMC2), which contribute to

the subunits forming the MET channel (*Maeda R et al., 2014*). It is also possible that TMC1 and TMC2 could interact with additional subunits, such as LHFPL5 and TMIE, which are essential for the MET complex (*Kawashima Y et al., 2011; Xiong W et al., 2012; Zhao B et al., 2014*). Moreover, some of these proteins could have Ca^{2+}-binding elements to account for the multiple Ca^{2+} effects on the MET current, but the molecular identity of these components is still unknown *(Giese APJ et al., 2017).*

A characteristic of the transducer currents is that they can adapt, when there is maintained bundle. It happens thanks to two different mechanisms in combination, both triggered by the Ca^{2+} influx into the cell that reset the range of bundle displacements.

The first is the slow adaptation, which takes few tens of millisecond and it involves a change in the attachment point of the element connected to the MET channels. During the excitatory deflection the increased tension in the tip link causes its upper attachment point to slip down the side of the stereocilium. It results in a reduction of the tension in the elastic element and adaptation. At the end of the stimulus, the tension is reduced and the attachment point of the tip link is pulled back up the stereocilium by a motor ascending along the actin backbone of the stereocilium to re-tension the tip link (*Fettiplace, 2017*). In nonmammals the motor is the myosin IC (*Gillespie and Cyr, 2004*), whereas in mammals two it could be the myosin VIIa (*Kros et al., 2002*) or myosin VI (*Marcotti W et al., 2014*).

The second is the fast adaptation, it takes less than a millisecond in mammals and it is mediated by the direct action of Ca^{2+} by blocking the transducer channel itself (*Fettiplace R and Kim KX, 2014*). The adaptation is an important mechanism to always keep the transducer channel within its most sensitive range and avoid saturation even after a sustained bundle displacement stimuli.

After the excitatory deflection of the hair bundle, due to depolarization, it occurs the opening of voltage-dependent calcium (Cav) channels allowing Ca^{2+} entry, which stimulates the fusion of synaptic vesicles to the cell membrane. The presynaptic Ca^{2+} channels are close to the Ca^{2+} sensor responsible of the exocytosis (10–40 nm), hence the variation of Ca^{2+} concentration within microseconds to high micromolar range favors a precise temporal resolution of the signal (*Moser et al., 2006*).

The synaptic vesicles are organized around synaptic ribbons, which are electron-dense structures adjacent to the hair cell membrane and opposite to afferent terminals (*Eatock and Songer, 2011*). The synaptic vesicles fuse with the presynaptic element and release of the excitatory neurotransmitter, glutamate, into the synaptic cleft (*Glowatzki et al., 2008*).

The excitatory neurotransmitter opens the glutamate-receptor (GluR) channels in the post-synaptic element and the cations (excitatory postsynaptic current or EPSC) depolarize it evoking excitatory

postsynaptic potential or EPSP. EPSPs activate voltage-gated Na^+ (Na_V) channels in the afferent fiber, which generate action potentials (spikes). Then, spikes propagate down the myelinated afferent process and along the central afferent process toward secondary neurons in the brain stem and the cerebellum (*Eatock and Songer, 2011*).

In summary, the excitatory mechano-electrical transduction process may be resume into six steps:

1) deflection of hair-bundle, which results in the opening of MET channels. They carry a depolarizing transducer current;
2) depolarization of the hair cell leads to the opening of K^+ and Ca^{2+} channels in the basolateral membrane of the hair cell;
3) increment of cytosolic Ca^{2+} concentration, which stimulates the glutamate release from the vesicles in the presynaptic element;
4) glutamate diffusion in the synaptic cleft and then into the post-synaptic receptors;
5) depolarization of the post-synaptic terminal;
6) generation of a train of action potentials, which is transmitted to the brain.

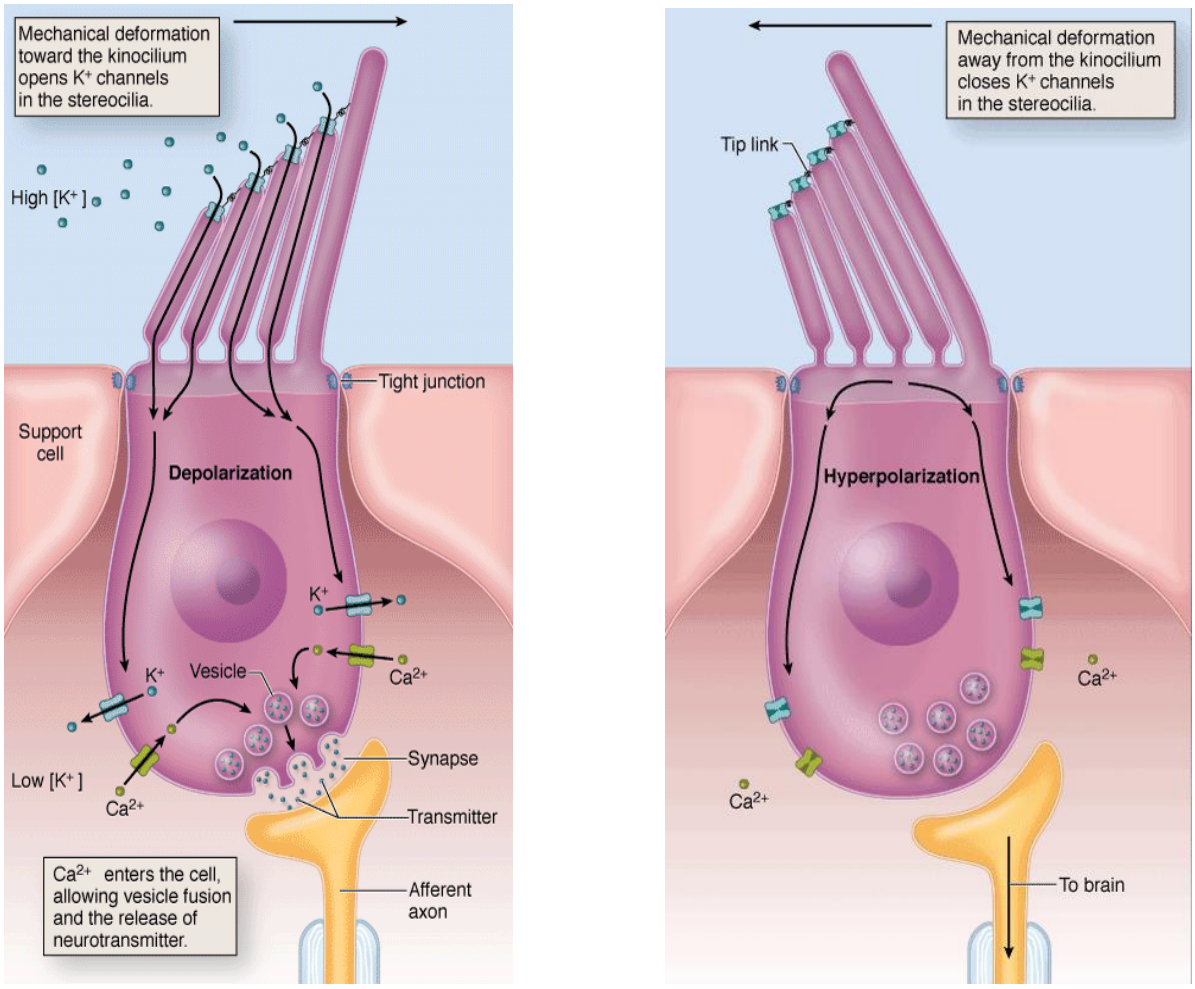

Fig. 12. Schematic diagram of mechanotransduction in hair cells.

On the left is shown the consequence of an excitatory deflection, whereas on the right is shown the consequence of an inhibitory deflection.

In particular, deflection toward the kinocilium (left) results in the opening of MET channels, which carry a depolarizing transducer current. Depolarization carries to the opening of K^+ and Ca^{2+} channels in the basolateral membrane with the consequent receptor potentials depolarization and the release of vesicles containing the neurotransmitter (glutamate). Glutamate diffuses in the synaptic cleft and then entries in the post-synaptic (afferent) element, depolarizing it. Depolarization is converted to action potentials.

Otherwise deflection toward the smallest stereocilium results in the closing of all MET channels. (Mescher, 2011).

Hair cell voltage-dependent channels

The ion channels expressed by the cochlear and vestibular hair cells, positioned in different regions of the sensory epithelia, change significantly. It is due to the distinct functions they have to conduct and to better react to the different stimuli. Ion channels are involved in establishing the resting membrane potential, setting the hair cell's input impedance and thus determining its speed and sensitivity, filtering the membrane potential response, initiating the process of afferent fibers excitation (i.e. neurotransmitter release) (*Marcotti and Masetto, 2010*). Ion channels for these reasons have an important role and their malfunction can lead to both hearing and vestibular dysfunction (*Dumont and Gillespie, 2003; Rüttiger et al., 2004; Wangemann et al., 2004*).

The hair cells' receptor potential produced by the resting depolarizing inward transducer current (described before) shaped to several types of voltage- and time-dependent ion channels present in the basolateral region (*Eatock and Hurley, 2003a; b; Housley et al., 2006*). The hair cells are characterized principally by the presence of slow and fast outward K^+ currents and in a less percentage by Ca^{2+} and Na^+ currents.

Ion channels in cochlear hair cells

Around embryonic day 14.5 (E14.5) IHCs begin to express an outwardly rectifying K^+ channel. These channels have a very low open probability around the resting membrane potential (~ -50 mV) and when opened by membrane depolarization, a small and slowly activating delayed-rectifier K^+ current, known as $I_{K,emb}$, can be recorded (*Marcotti et al., 2003a*).

After four embryonic days the radial afferent endings concentrate around the base of the IHCs and there is the formation of the first synaptic-like contacts (*Pujol et al., 1998*). During the same period IHCs begin to express new additional currents, such as the inward rectifier K^+ currents ($I_{K1;}$ *Marcotti et al., 2003a*) and the small-conductance K^+ currents Ca^{2+}-activated (I_{SK2}; *Marcotti et al., 2004b*). Moreover, there are Ca^{2+} current (I_{Ca}, carried by $Ca_v1.3$ voltage-gated Ca^{2+} channels; *Dou et al., 2004*) and TTX-sensitive Na^+ current (I_{Na}, probably carried by $Na_v1.7$ channels; *Marcotti et al., 2003b*).

I_{K1} is an inward rectifier K^+ current, which has a very fast kinetics, is K^+-selective, and is blocked by Ba^{2+}. This current is transiently expressed in cochlear hair cells before the onset of hearing, in fact g_{K1} increases in size until the onset of hearing (P12) after which it rapidly decreases to a small current (*Marcotti et al., 1999*) (Fig. 13).

I_{K1} has faster activation kinetics than $I_{K,emb}$ and it is the major contributor to the resting conductance of these immature cells. The simultaneous presence of a wide variety of voltage-gated inward and outward currents, during the late embryonic development, causes IHCs to elicit slow and repetitive spontaneous action potentials. Probably, embryonic IHCs can communicate information to the developing neuronal connections within the cochlear neuroepithelium.

After birth, all currents increase in size and change the cells' voltage responses. $I_{K,emb}$ develops in a 4-AP insensitive outward K^+ current, known as $I_{K,neo}$ (Fig. 13). The depolarized activation range of the outward current and the small size of the developing inward rectifier I_{K1} make the 'resting potential' relatively more positive.

Neonatal IHCs can generate rapid spontaneous Ca^{2+} action potentials up to about P6–P7 in the mouse, because, although immature IHCs express both Ca^{2+} and Na^+ currents, only the former is required for the generation of action potentials since they are reversibly abolished during superfusion of a Ca^{2+}-free solution but not by TTX *(Marcotti et al., 2003a; b*). After the birth and until the onset of hearing (P10–P12; *Marcotti et al., 2003a; b*), the endolymphatic Ca^{2+} concentration (0.3 mM) in the immature cochlea continues to increase the open probability of the MET channels causing action potential (*Johnson et al., 2012*).

In addition to I_{Ca}, other immature currents are involved in modulating the shape and frequency of action potentials. While I_{Ca} together with the delayed rectifier $I_{K,neo}$ determines the rate of rise and fall and the amplitude of the spike, I_{Na} reduces the inter-spike interval by speeding up the time required for the membrane potential to reach spike threshold (*Marcotti et al., 2003b*). The function of this spiking behavior is crucial for the establishment of precise tonotopy, the major organizing principle of central auditory pathways (*Clause et al., 2014*).

After the onset of hearing, IHCs reduce their excitability because of the changes in the biophysical properties such as loss of I_{Na}, reduction of I_{Ca} and I_{K1} and the increment of a new outward rectifying K^+ currents, which hyperpolarize the resting membrane potential. These new outward K^+ currents in mature IHCs are $I_{K,n}$, a linopiridine-sensitive K^+ current, $I_{K,f}$, a fast calcium-activated K^+ current, I_{BK} and $I_{K,s}$, a slower delayed rectifier with a component that is sensitive to block by 4-aminopyridine.

$I_{K,n}$ was originally described in OHCs (*Housley and Ashmore, 1992*), and it is expressed differently in the mouse cochlea. Indeed, its size in IHCs is about 45% of that in the OHCs.

$I_{K,f}$ is a large current (about 10 nA at 0 mV) and shows rapid activation kinetics. Moreover, it activates around -85 mV and it is directly modulated by the voltage-dependent release of Ca^{2+} from intracellular Ca^{2+} stores (*Marcotti et al., 2004a*).

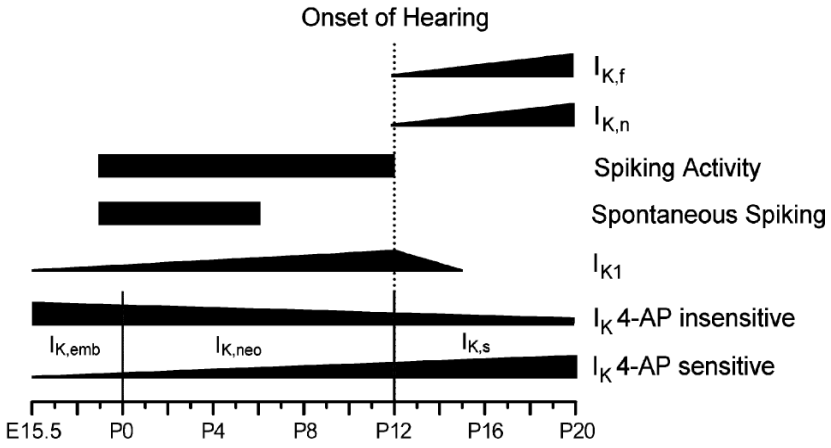

Fig. 13. Schematic representation of changes in K^+ current expression during development in mouse IHCs.

The change in width of the horizontal bars gives an indication of developmental changes in the size of the currents. I_{K1}, an anomalous inward potassium rectifying, and I_{KS}, which is an apamine sensitive calcium-activated K^+ current, are conductances present since the birth while during the development, precisely after the onset of hearing, other two conductances such as $I_{K,n}$ and $I_{K,f}$ are acquired by the IHCs (Marcotti et al., 2003a).

Immature OHCs express currents similar to those present in immature IHCs, which include outward ($I_{K,emb}$ and $I_{K,neo}$) and inward (I_{K1}) K^+ currents , a Ca^{2+} current and a Na^+ current.

In OHCs profound modifications in the properties of the outward K^+ conductance can be detected from P8, indicating an earlier functional maturation compared to IHCs. Mature OHCs have at least two type of K^+ channels (*Housley and Ashmore, 1992*): a big conductance calcium activated K^+ current (BK) and a big K^+ current ($I_{K,n}$).

Concurrently with the functional maturation, OHCs at P8 start showing the electromotility, which is a process responsible for the cochlear amplification, where OHCs shape alternates from ovoid to cylindrical. This process is voltage driven and powered by prestin, a member of the SLC26A family of membrane antiporters that transfer anionic molecules across the cell membrane (*Dallos, 2008*).

Moreover, OHCs start expressing the apamin-sensitive small conductance (SK2) Ca^{2+}-activated K^+ current called I_{SK2} (*Oliver et al., 2000*), being innervated by the cholinergic efferent fibers (*Shnerson et al., 1982*) and having $I_{K,n}$.

As seen before in IHCs, $I_{K,n}$ is the more conspicuous fraction of the total outwardly rectifying conductance in OHCs, it is activated at very negative potentials and it is crucial to maintain the OHCs resting potential hyperpolarized. The channel through which flows $I_{K,n}$ current is made up of four KCNQ subunits, which belong to six transmembrane domain.

All the cochlear hair cells express type L calcium channel and through these channels ($Ca_v1.3$) Ca^{2+} entries into the cells, where it regulates the neurotransmitter release.

Ion channels in vestibular hair cells

Despite the similar onset of differentiation among hair cells (E15), the maturation of mouse vestibular hair cells is completed before that of the cochlear hair cells. In fact, vestibular hair cells maturate around birth (~P4) whereas the cochlear hair cells at P12 (onset of hearing).

In mice, between birth and P4 immature vestibular Type I and Type II hair cells can sometimes be distinguished by their morphology (i.e. presence of calyx) but not by their basolateral membrane currents. Both Type I and Type II hair cells present essentially a delayed K^+ rectifier ($I_{DR,N}$ for neonatal), a rapidly activating and partially inactivating K^+-selective inward rectifier current (I_{K1}), a mixed cation inward rectifier current (I_h), a Ca^{2+} current and a large Na^+ current (*Eatock and Fay, 2006*).

A small outwardly rectifying delayed rectifier K^+ current (I_{DR}) is present in vestibular hair cells at embryonic day 14 and it increased in amplitude during the next several days (*Géléoc et al., 2004*). This current, soon after birth, constituted the main current in vestibular hair cells of mouse (*Géléoc et al., 2004; Li et al., 2010*) and it was demonstrated that it is blocked by 4-aminopyridine (4-AP) or Ba^{2+} (*Meredith and Rennie, 2016*).

Ca^{2+} currents (I_{Ca}) in association with Na^+ (I_{Na}) evokes action potentials in both hair cell during development (*Géléoc et al., 2004*). After few postnatal days I_{Ca} and I_{Na} decline, at a certain point I_{Na} completely disappears, hence mature vestibular hair cells no longer fire action potentials, similar to mature auditory hair cells (*Meredith and Rennie, 2016*).

The expression of different channels (K^+, Ca^{2+} and Na^+) make immature vestibular hair cells similar to immature cochlear hair cells, but in contrast to cochlear hair cells minor K^+ currents, such as I_{K1}, persist on maturation (always in Type II and sometimes in Type I) (*Meredith and Rennie, 2016*).

After maturation, Type I hair cells are characterized by the presence of K^+ channels almost fully activated at -60 mV. The current that flows through these channels was initially termed $I_{K,I}$ (*Correia and Lang, 1990*), but later it has been called $I_{K,L}$ (*Rüsh and Eatock, 1996*) where "L" is for low voltage activated. The kinetic of the channel is characterized by a slow and sometimes sigmoidal activation and a low or none inactivation.

$I_{K,L}$ is responsible for the low input resistance of these cells. Moreover, $I_{K,L}$ is functionally analogous to $I_{K,n}$ in cochlear hair cells (*Wong et al., 1994*), where its acquisition reduces the input resistance of IHCs from 140 MΩ to 40 MΩ (*Raybould et al., 2001*).

The ion channels identity responsible for the $I_{K,L}$ is unknown yet, notwithstanding it is supposed to belong to KCNQ and *erg* channel family, the same channels generate M-currents (*Selyanko et al.,*

2002). In particular, the M-current is a slowly activating and deactivating current, which controls the excitability in sympathetic and central neurons and KCNQ2 and KCNQ3 potassium channel genes encode subunits that co-assemble to form heteromeric channels, which underlie the M-current (*Pan et al., 2001*).

The correspondence, between $I_{K,L}$ and M currents, seems to support the hypothesis that $I_{K,L}$ may be modulated by second messengers (*Behrend et al., 1997; Chen and Eatock, 2000*).

$I_{K,Ca}$ is a minor contributor to the macroscopic K^+ conductance of the vestibular Type I HC. In fact, in a minority of cells may be present small conductance calcium-activated K^+ current (SK) and large conductance calcium-activated K^+ current (BK) components (*Rennie and Correa, 1994; Schweizer et al., 2009*).

In Type II vestibular hair cells, after the maturation, it appears an A-type outward potassium current ($I_{K,A}$), which is prominent around the resting membrane potential and it is characterized by a fast activating and moderately fast inactivating current. Moreover, it has been described in mature vestibular Type II hair cells an outward delayed rectifier current (I_{DR}) with a relatively slow activation and inactivation kinetics (*Meredith and Rennie, 2016*). After maturation it is generated a fast current by a "BK-type" calcium-activated potassium channel that *Schweizer et al*. (2009) found in a minority of hair cells in rat vestibular epithelia and demonstrated that its expression declined with age.

In mature vestibular Type II hair cells only two inward currents have been identified, I_{K1} and I_h. The former is a fast activating and partially inactivating K^+-selective current, which is present since birth and it is blocked by external Ba^{2+} and Cs^+ (*Levin and Holt, 2012*).

The latter is an inward rectifying K^+ current, which appears significantly around P4 and is a sign of the maturation of both Type I and Type II hair cells. Upon maturation, I_h is mainly expressed in Type II and rarely in Type I hair cells.

As shown in the electrophysiological experiments of *Horwitz et al.* (*2011)*, I_h is a slowly activating and sustained mixed cation inward current that in vestibular hair cells is carried by HCN1 channels. In fact, there is a complete loss of I_h in *Hcn1*-KO mice and a normal I_h in *Hcn2*-KO mice, which suggests that HCN1 is necessary and sufficient to form the channels that carry I_h in vestibular hair cells.

In vestibular hair cells the Ca^{2+} current is carried by $Ca_v1.3$ L-type channels. These channels activate near –55 mV and their role is to regulate the neurotransmitter release (*Bao et al., 2003*).

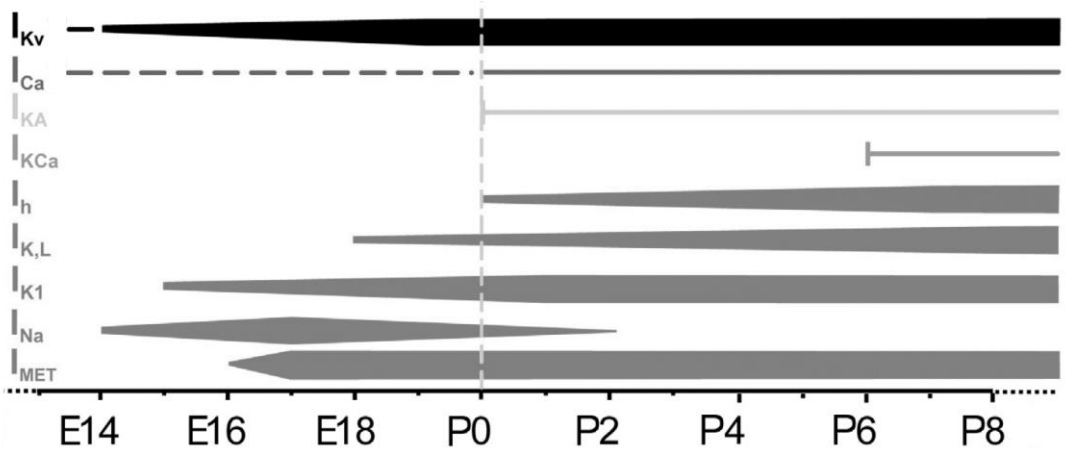

Fig. 14. Schematic representation of changes in current expression during development in mouse vestibular hair cells.
The change in width of the horizontal bars gives an indication of developmental changes in the size of the currents. I_{Kv}, I_{K1} and I_{Na} appear at around E15, whereas $I_{K,L}$ is first detected at around E18. I_{KA} and I_h are expressed from neonatal stages. The expression of I_{Ca} has not been investigated before P4 in mice, but in rats is since birth. Finally, I_{KA} is expressed only in type II hair cells (Corns et al., 2014).

Role of *EPS8* gene in hair cells

EPS8 is the acronym for "Epidermal growth factor receptor Pathway Substrate 8", which is an enzyme that in humans is encoded by the *EPS8* gene.

Eps8 was originally isolated by an expression cloning strategy, designed to isolate intracellular substrates for the kinase activity of the EGFR (*Fazioli et al., 1993*). A more recent study demonstrated that Eps8 is not only an efficiently tyrosine phosphorylated by a variety of tyrosine kinase receptors (RTKs) (*Fazioli et al., 1993*), but also a Src tyrosine kinase (*Maa et al., 1999*).

EPS8 gene has been mapped to human chromosome 12p13.2 via fluorescence *in situ* hybridization (FISH) (*Ion et al., 2000*) and then its localization was confirmed by a computer search of a genomic DNA database utilizing human *EPS8* cDNA sequence (GeneBank accession number U12535). Similarly, the murine *Eps8* genomic DNA sequences have been defined on chromosome 6G1.

EPS8 is ubiquitously expressed in human but *Eps8* homologues are found also in *Drosophila* and in the nematode *C. elegans* (*Wong et al., 1994*). It means that probably this protein had an important role conserved in the evolution and that *Eps8* could have a role in pathways common to very distant species. In mammals it has been hypothesized that exist at least three other *Eps8*-related genes, which show collinear topology and high degree of similarity to *Eps8* (*Mongiovi et al., 1999*).

Recent studies reported that proteins with molecular weights of 97 kDa and 68 kDa were recognized by EPS8 antibodies and these two EPS8 isoforms have been called $p97^{Eps8}$ and $p68^{Eps8}$ (*Tocchetti et al., 2003; Maa et al., 2013*). The precise structure and function of the isoform $p68^{Eps8}$

are still unknown, but by contrast the isoform $p97^{Eps8}$ has been well characterized and moreover it was found in different cells involved in human cancer.

Different studies of the EPS8 molecular structure determined that it is an 822 amino acids protein in human (821 in mice), which contains 3 principal domains:

- N-terminal pleckstrin homology (PH) domain. It is involved in protein-protein and protein-phospholipid interaction, thus contributing to the process of membrane anchorage, which is important in signal transduction (*Di Fiore and Scita, 2002*).
- Src Homology 3 (SH3) domain. It is centrally located in the EPS8 protein and is essential for the formation of complexes with ABI1, RN-TRE and IRSP53 (*Matòsková et al., 1996; Biesova et al., 1997; Funato et al., 2004*).
- C-terminal domain. It is essential for the actin barbed-end-capping domain activity. Moreover, the C-terminal region has significant sequence homology with the sterile-motif (SAM) domains (*Disanza et al., 2004*).

Interestingly, each domain is spaced out by several proline rich-regions, which can enhance the association with other proteins such as IRSP53.

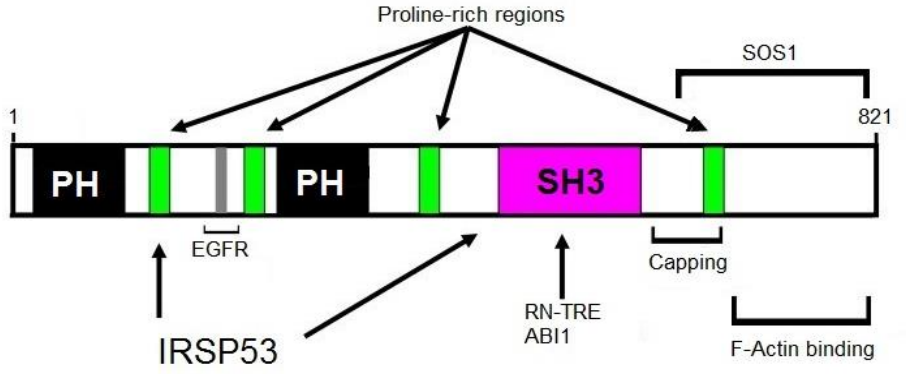

Fig. 15. Structural organization of murine Eps8 protein.
The N-terminal contains PH domain (PH), which is important for Eps8 membrane recruitment. Green boxes indicate proline-rich regions, whereas gray box indicates the potential nuclear localization signal. SH3 domain is essential for Eps8 interactions with other proteins such as RN-TRE and ABI1. Finally the C domain allows the protein for the barbed-end capping activity (Maa and Leu, 2013).

EPS8 plays different roles. It can directly control actin dynamics, such as rate of polymerization and depolymerization, and architecture of actin based structures by capping barbed ends and cross-linking actin filaments, respectively (*Croce et al., 2004; Disanza et al., 2006*).

The capping barbed end activity prevents actin monomers, which are the single unit of the actin filaments, to be linked together and hence EPS8 stops the further elongation of the actin filaments.

This process happens with an affinity in the nanomolar range if the C-terminal domain is isolated, but this activity is auto-inhibited in case of full-length EPS8. The interaction with the ABI1 protein relieves this inhibition (see below for more information; *Disanza et al., 2004*).

The bundling activity enables full-length EPS8 protein to actin cross-link and hence to organize the actin filaments into higher order structures, such as microvilli and stereocilia (*Hertzog et al., 2010*).

Furthermore, EPS8 directly interact with the epidermal growth factor receptor (EGFR) and, when it is overexpressed, EPS8 enhances the EGF-mediated mitogenesis but the underlying mechanisms are not known yet (*Fazioli et al., 1993*). EPS8 interacts with EGFR through its specific interaction regions, aa298–aa362 whereas EPS8-binding region in EGFR is the juxtamembrane region, aa648-aa688 (*Castagnino et al., 1995*). EGFR-binding region in EPS8 is characterized by a high presence of basic amino acids, whereas multiple glutamic acid residues are found in the juxtamembrane region of EGFR.

EPS8 can regulate different processes depending on its association with other proteins such as ABI1, RN-TRE etc. Here I will describe some of them.

SRC is a non-receptor tyrosine kinase, which tyrosyl phosphorylates EPS8 protein. In this way SRC enhances EPS8 expression and it is essential for the cell proliferation (*Maa et al., 1999*).

EPS8 can also interact with GTPase of Rho and Rab family. Among the Rho GTPases, Rac is necessary for RTK-dependent modulation/polymerization of actin (*Di Fiore and Scita, 2002*). Rac is the last step of the cascade, in fact it all start from Ras and RTK which activate phosphatidylinositol 3 kinase (PI3K). PI3K is an enzyme that converts phosphatidylinositol-4,5-biphosphate (PIP_2) to phosphatidylinositol-3,4,5-triphosphate (PIP_3). Meanwhile EPS8, SOS1 and ABI1 form a trimeric complex, which in association with PIP3 enhance Rac-specific Guanine Exchange Factors (GEF) leads to the activation of Rac and subsequently actin polymerization.

Through its SH3 domain, EPS8 interacts with RN-TRE (Related to the N-terminal of *tre*) which is a RAB5 GTPase-activating protein (GAP), whose activity is to regulate the EGFR internalization. By entering in a complex with EPS8, RN-TRE acts on RAB5 and inhibits internalization of the EGFR. Furthermore the association between RN-TRE and EPS8, diverts EPS8 from its Rac-activating function (no complex with ABI1 and SOS1), resulting in the attenuation of RAC signaling (*Lanzetti et al., 2000*).

The barbed-end capping activity of EPS8, which resides in its conserved C-terminal effector domain, is tightly down-regulated within the context of the single protein (*Menna et al., 2009*). It means that EPS8 binds the adaptor protein ABI1 through its SH3 domain, releasing autoinhibitory binding within EPS8 and promoting actin capping (*Disanza et al., 2004*). In conclusion, EPS8 displays barbed-end actin capping activity only when associated with ABI1 (*Disanza et al., 2004*).

EPS8 must associate with IRSP53 (insulin receptor tyrosine kinases substrate of 53 kDa, also known as brain-specific angiogenesis inhibitor 1-associated protein 2 or BAIAP2) to efficiently cross-link actin filaments (*Oda et al., 1999*). This complex enhances BAIAP2-dependent membrane extensions and promoting filopodial protrusions. In contrast, it is phosphorylated by the brain derived neurotrophic factor (BDNF) leading to inhibition of its actin-capping activity and stimulation of filopodia formation.

Moreover, at stereocilia tips EPS8 is required, in complex with whirlin (WHRN) and myosin-15A (MYO15A), for elongation of the stereocilia actin core. EPS8 is indirectly involved in cell cycle progression and its degradation following ubiquitination is required during G2 phase to promote cell shape changes (*Disanza et al., 2006*). Finally, EPS8 regulates the migration of dendritic cells (*Frittoli et al., 2011*) and the morphogenesis of intestinal cells and microvilli (*Croce et al., 2004; Zwaenepoel et al., 2012*).

EPS8 expression is also increased in several different cancer types, such as cervical cancer (*Wang et al., 2009*), pancreatic cancer and oral squamous cell carcinoma (*Chu et al., 2012; Welsch et al., 2007*). The 97 kDa isoform of EPS8 has been variously linked to proliferation, migration and oncogenic transformation (*Maa and Leu, 2013*), implying that *Eps8* role in cancer cell phenotypes is complex and might be dependent on context.

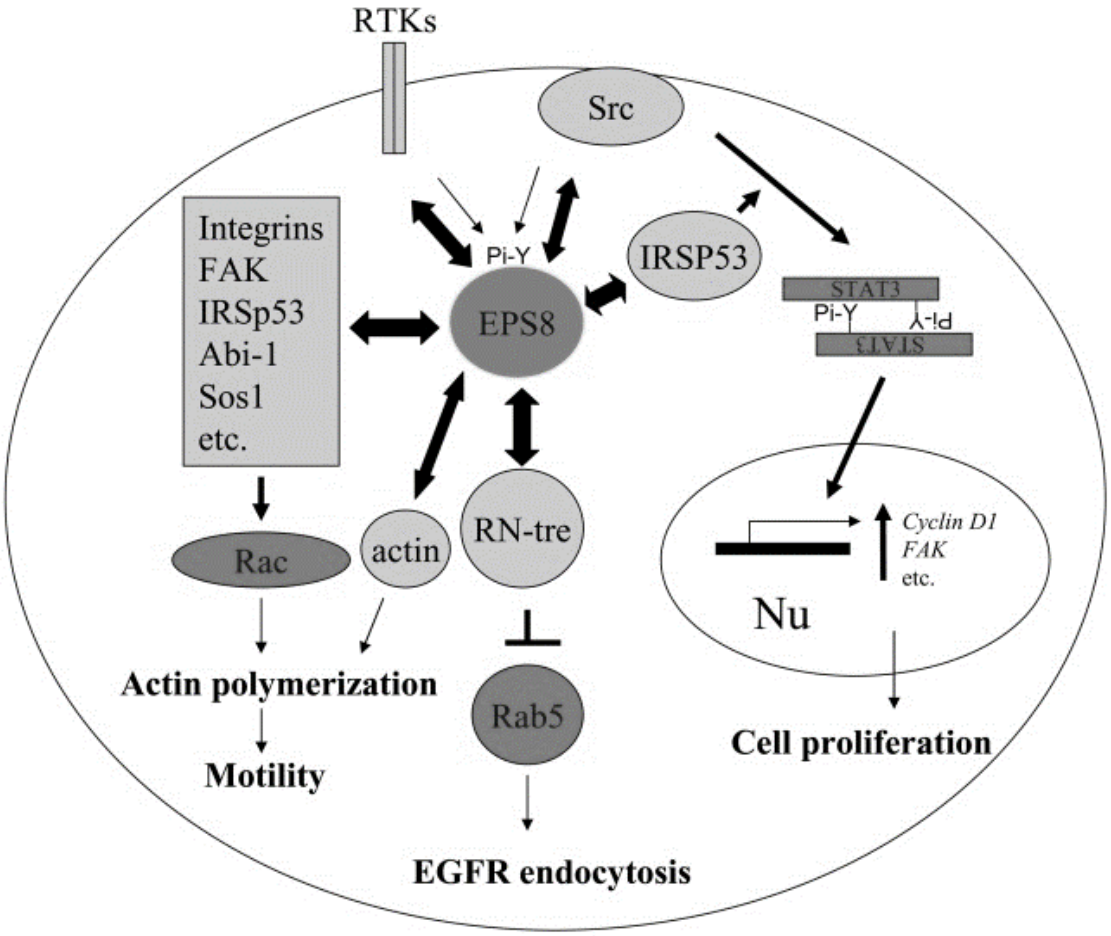

Fig. 16. The signals transmitted by EPS8 protein.
Activated EGFR of the family RTK and SRC phosphorylate EPS8, which in turn induces EPS8-IRSp53 interaction that facilitates SRC-mediated STAT3 Pi-Y705 and dimerization, resulting in the increased transcription of Cyclin D1 and FAK and in cell cycle progression. By binding to RN-tre, EPS8 reduces Rab5 activity and hinders EGFR endocytosis. In addition to its actin-capping activity, EPS8 interacts with proteins listed in the square box, activates Rac, promotes membrane actin polymerization, and increases motility. Nu: nucleus (Maa and Leu, 2013).

Eps8-KO mice

Offenhauser et al. (*2004)* reported that *Eps8*-null mice (*Eps8*$^{-/-}$ or *Eps8*-KO) are healthy, fertile and devoid of any obvious defect.

However, *Eps8*-KO mouse embryonic fibroblasts fail to form membrane ruffles in response to growth factor stimulation. *Offenhauser et al.* (*2004*) found that the expression of human EPS8L1 or EPS8L2, but not EPS8L3, restored EGF-induced membrane ruffles in *Eps8*-KO fibroblasts, suggesting redundancy of function.

Eps8-KO mice were resistant to some acute intoxicating effects of ethanol and showed increased ethanol consumption (*Offenhauser et al., 2006*). EPS8 was localized to postsynaptic structures and was part of the NMDA receptor complex, a major target of ethanol, in wild-type (WT) adult mouse

cerebellum. In *Eps8*-KO mice, NMDA receptor currents and their sensitivity to inhibition by ethanol were altered, in fact *Eps8*-KO neurons were resistant to the actin-remodeling activities of NMDA and ethanol. For this reason it was proposed that proper regulation of the actin cytoskeleton is a key determinant of cellular and behavioral responses to ethanol.

A recent paper showed that Eps8 is localized predominantly at the tip of the hair cells' stereocilia and it is essential for their normal elongation and function (*Zampini et al., 2011*). *Eps8*-KO mice show increased rows of stereocilia and reduced length of predominantly tall stereocilia in both inner and outer hair cells.

Moreover, *Eps8*-KO mice were found to be profoundly deaf and IHCs fail to mature into fully functional sensory receptors. It has been proposed that Eps8 directly regulates stereocilia growth in hair cells and also plays a crucial role in the physiological maturation of mammalian cochlear IHCs exerting a critical role in coordinating the development and functionality of mammalian auditory hair cells (*Manor et al., 2011; Zampini et al., 2011*).

The expression of *Eps8* was recently discovered also in mammalian vestibular hair cells. Similarly to IHCs, it is localized at the tip of stereocilia, but nothing is known about its role (*Manor et al., 2011*).

The role of *EPS8*, in stereocilia function, is supported by the description of a rare human germinal *EPS8* mutation leading to hearing impairment (*Behlouli et al., 2014*). Two Algerian brothers, born from consanguineous parents, show an autosomal recessive deafness-102 (DFNB102), where there is a homozygous truncating mutation in the *EPS8* gene (Q30X). The mutation was found performing whole-exone sequencing. Moreover, the researchers noted that the *EPS8* gene is expressed in the hair bundle and in the sensory antenna of the auditory sensory cells of the cochlea, where it operate mechano-electrical transduction necessary for hearing.

Experimental investigation

Introduction

The auditory and vestibular systems, in all vertebrates, are characterized by the presence of sensory receptors, called hair cells. These hair cells are endowed with *stereocilia* of different lengths that are organized in a staircase-like structure and the number of which depends on the given inner ear organ. The sound or head motion deflect the hair bundle, inducing an excitatory or inhibitory action by modulating the open probability of mechano-electrical transducer channels localized at the tips of the *stereocilia* (*Beurg et al., 2009*). Cell voltage responses, initiated by the transduction current, are then shaped by different types of voltage-dependent ion channels, among which Ca^{2+} channels are coupled to neurotransmitter (glutamate) exocytosis.

The development and/or function of cochlear hair cells is affected by several genetic mutations, which cause deafness in mice and humans (see Hereditary Hearing Loss Homepage http://hereditaryhearingloss.org). The common embryonic origin of the auditory and vestibular hair cells suggests that single gene mutations known to cause hearing loss would also lead to vestibular dysfunction. Instead, vestibular function is often preserved even in the case of profound deafness (Jones and Jones, 2014). One possible explanation is that deficits in vestibular hair cells have sometimes gone undetected because of compensation or adaptation by the central nervous system.

Recent studies have demonstrated the importance of epidermal growth factor receptor pathway substrate 8 (*Eps8*), which is a gene involved in actin remodeling (*Di Fiore and Scita, 2002*), hampers normal *stereocilia* growth (*Manor et al., 2011; Zampini et al., 2011*) and ion channel expression in mouse cochlear inner hair cells (IHCs) (*Zampini et al., 2011*).

Despite the similar expression profile of *Eps8* in cochlear and vestibular hair cells (*Manor et al., 2011; Zampini et al., 2011*), *Eps8*-KO mice are deaf, but they do not show evident vestibular deficits. In addition, *Behlouli et al.* (*2014*) showed how a biallelic nonsense mutation of human *EPS8*, where the protein is probably truncated or not present (like the *Eps8*-KO mouse), results in deafness but no clear balance defects.

In the present study, I investigated the role of *Eps8* gene in the hair bundle morphology and in the biophysical properties of vestibular hair cells. These properties were then compared with those of cochlear hair cells. To achieve this objective, I first evaluated the morphology of *Eps8*-KO and WT mice measuring the length of the *stereocilia*. Then, using the technique of whole-cell patch-clamp in voltage-clamp and current-clamp mode, I investigated the expression of K^+ currents and the voltage responses of hair cells in *Eps8*-KO mouse and compare them to those of WT mouse.

I found that *Eps8* deletion alters the growth of vestibular hair cells *stereocilia* as in cochlear hair cells. I also found that, different from IHCs, the receptor potential of vestibular hair cells was not

affected by *Eps8* deletion. The above findings could explain why Eps8 loss, and presumably *EPS8* mutation, primarily affects the auditory function.

Materials and Methods

Animal procedures were performed under the protocols approved by the Ministero della Salute (Rome, Italy).

Experiments were performed on both male and female mice. *Eps8*-KO mice were obtained by subsequently crossing heterozygous mice. To increase the number of controls, in particular for the hair cells dissociation protocol (see below), wild-type (WT) mice (C57BL/6J and Swiss CD1) were also obtained from Harlan Italy (Italy). C57BL/6J and Swiss CD1 mice show no differences in hair cells' morphological and electrophysiological properties, as it was already reported by *Contini et al.* (*2012*).

DNA genotyping

All animals were genotyped both at around P7 or after death, in the way that I describe below.

Murine genomic DNA was extracted after the collection of distal tail tissue (tail biopsy). Little pieces of tail (~0.5 cm) were lysed using PureLink™ Genomic DNA Mini Kit (Invitrogen, USA) with the addition of 2 mg/ml Proteinase K (Invitrogen, USA). Following the procedure indicated by Invitrogen, it was possible to extract DNA which was stored at 4 ºC for short-term or –20°C for long-term storage.

The genotype of mice was determined by PCR, using three oligonucleotides (Carlo Erba Reagents SRL, Italy). The oligonucleotides are: F069 (neo) with the following sequence 5′-CAGCGCATCGCCTTCTATCGC-3′, F02595 with the following sequence 5′-GCCCAGAACCCAAGTTACCTG-3′ and finally F02597 with the following sequence 5′-AAGTAAAAGTTGACCAGTGCGTGG-3′.

The PCR was performed using a solution with the final volume of 25 µl, which contains: 5 µl Buffer 5x (Promega, USA), 0.5 µl dNTPs (10 mM), 0.5 µl F069 (neo) (10 µM), 1 µl F02595 (10 µM), 0.5 µl F02597 (10µM), 0.2 µl GoTaq G2 Polymerase (Promega, USA), 1 µl DNA and 16.3 µl H_2O.

The PCR consists of three step. The first is the initialization at 94 °C for 5 minutes, then there are 30 repeated cycles of denaturation (at 94 °C for 1 minute), annealing (at 65 °C for 2 minutes) and elongation (at 72 °C for 1 minute) and finally there is the final elongation at 72 °C for 10 minutes.

The amplified DNA was analyzed through a gel electrophoresis, using a matrix of 2% Agarose (Sigma Aldrich, Italy). The size of DNA samples was determined loading in the first well of the gel,

the molecular weight marker VIII (Roche Diagnostic, USA). WT mice are characterized by one amplification product that corresponds to 200 base pair (bp) stripe, whereas *Eps8*-KO mice by one amplification product of 500 bp stripe. Finally, heterozygous mice are characterized by two stripes of 200 bp and 500 bp (Fig.17).

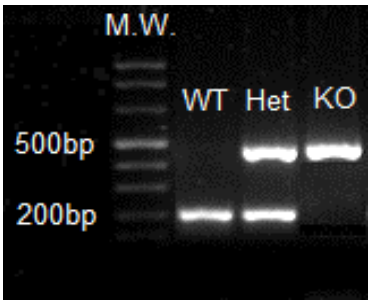

Fig. 17. Agarose gel electrophoresis of PCR products.
From left to right. In the first well there is the standard reference, which is the Molecular Weight Marker VIII (M.W.). The following wells were dedicated to amplified DNA samples. Each well was loaded with DNA of one mouse. The second well presents one fragment of 200 bp that corresponds to WT mouse (WT). The third well presents two fragments of 200 bp and 500 bp that correspond to heterozygous mouse (Het). Finally the fourth well presents one fragment of 500 bp that corresponds to Eps8-KO mouse (KO).

Morphology of *crista* hair cell bundles

Kinocilia and stereocilia measurements were performed using enzymatically and mechanically dissociated hair cells from the semicircular canal *cristae*. Following brief anesthesia with 2-bromo-2-chloro-1,1,1-trifluoroethane (Sigma Aldrich, Italy), mice were killed by cervical dislocation and immediately decapitated.

Using stout and pointed scissors the head was bisected along the mid-sagittal plane and the two sections were quickly transferred to a Petri dish containing chilled (4 °C) extracellular solution to preserve the tissue. The following solution was used (Extra_std, in mM): 135 NaCl, 5.8 KCl, 1.3 $CaCl_2$, 0.9 $MgCl_2$, 0.7 NaH_2PO_4, 5.6 D-glucose, 10 Hepes-NaOH, 2 sodium pyruvate, vitamins (MEM 100x GIBCO Invitrogen, 10 ml/L) and aminoacids (MEM 50x GIBCO Invitrogen, 20 ml/L) (pH 7.48; osmolality 310 mOsm/kg). Salts and other compounds were purchased from Sigma-Aldrich (Italy) unless otherwise noted.

In each skull-half, to gain access to the semicircular canals (SCCs), the brain and the otic capsule were removed. A portion of the bony labyrinth was gently popped up, the *ampullae* of the SCCs were visualized and gradually excised with fine forceps. A micro-dissecting spoon, filled with ice-cold extracellular solution, was used to move carefully the isolated *ampullae* from one Petri dish to

another. The use of this micro-dissecting spoon was essential to avoid any deformation of the *ampullae* by surface tension forces. The harvest *ampullae* were gently handled and the lumen space was opened to expose the *crista ampullaris* (sensory *epithelium*). This is a critical point because the delicate *ampullaris* membranes tend to stick together. Special care and minute forceps were absolutely necessary to lift off the *cupula*, overlying the *crista*, and to avoid any damage to the sensory *epithelium*.

After the sensory *epithelium* has been exposed, the thin *crista* was positioned in a recording chamber containing Extra_std solution. Then, the *crista* was held under a weighted nylon mesh. During the immobilizing phase, precautions were taken to minimize any stretching or strain on the tissue by touching the apical surface of the *epithelium.*

Once the sensory *crista epithelium* was exposed it could be used both for recording or for the morphological experiments. The latter was performed after an enzymatic treatment, during which the preparation was first placed in a Petri dish containing the following extracellular solution, for 7 min at room temperature (RT, 22–25 °C) (Extra_D, in mM): 138 NaCl, 0.1 $CaCl_2$, 5.8 KCl, 0.9 $MgCl_2$, 10 HEPES, 15 glucose, 0.7 NaH_2PO_4, 2 Na-pyruvate, vitamins (MEM 100x GIBCO Invitrogen, 10 ml/L) and aminoacids (MEM 50x GIBCO Invitrogen, 20 ml/L) (pH 7.4 with NaOH). Protease VIII (Sigma Aldrich; 0.05 mg/ml) was added to the above solution for 10 min at room temperature (RT: 22-24 °C). It essentially differs for the low Ca^{2+} concentration because it has demonstrated that it favoured the hair cells dissociation, probably by rupturing the bivalent bridges in the cysteine of the intercellular junctional proteins and the links between hair bundles and the remaining *cupula*.

Then, the *cristae* were incubated with crude papain (Calbiochem-Nova Biochem Corporation, USA; 0.5 mg/ml) plus L-cysteine (Sigma Aldrich; 0.3 mg/ml), dissolved in Extra_D, for 23 min at 37 °C. Finally, the *ampullae* were transferred to a Petri dish containing Extra_D plus bovine albumin serum (Sigma Aldrich; 1 mg/ml) for 40 min at RT to stop the enzymatic activity. Afterward, the *cristae* were transferred to the recording chamber filled with Extra_D.

Finally, to mechanically dissociate the hair cells from the *epithelium*, each *crista ampullaris* was gently scraped with an eyelash and smeared onto the glass-bottom of the recording chamber to dislodge the hair cells. Hair cells were allowed to settle for 20 min and then visualized by an upright microscope (Olympus BX51WI, Japan), equipped with Nomarski optics and a 60x water immersion objective (Olympus LUMPlan FI, Tokyo, Japan).

Images were acquired by a digital camera (ORCA-05G, Hamamatsu Photonics, Hamamatsu City, Japan) and digitally stored with cellSens Dimension software (version 1.6, Olympus, Japan); this software was also used for all measurements, calibration = 107.5 nm/pixel. Only hair cells with

well-preserved hair bundles were considered. These were a small minority of the dissociated hair cells because hair bundles are closely embedded in the *cupula*, which is easily stressed during dissection. Since the morphology of hair cells can change following their dissociation (*Zenner et al., 1990*), we compared hair bundles without subdividing hair cells in Type I and Type II.
The morphological experiments were performed on *Eps8*-KO mice from postnatal day (P) 37 to P65 and on WT mice from P32 to P61, where the day of birth is P0.

Recordings from vestibular and cochlear hair cells

For patch-clamp experiments, the organ of Corti or the whole *cristae* were dissected as previously described (see also *Contini et al., 2012; Johnson et al., 2013*). Whole-cell recordings were obtained *in situ* from inner hair cells (IHCs) of the apical coil of the cochlea and Type I and Type II hair cells, in voltage-clamp (VC) and current-clamp (CC) mode.
Patch-clamp data were obtained from 18 WT IHCs, 13 *Eps8*-KO IHCs, 33 WT vestibular Type I hair cells, 17 *Eps8*-KO Type I hair cells, 26 WT vestibular Type II hair cells and 14 *Eps8*-KO Type II hair cells, P6 to P29.
The tissue and microelectrode were viewed using differential interference contrast optics employing an upright microscope (Olympus BX51WI, Japan) equipped with 60x water immersion objective and positioned on an optical anti-vibration isolation table (Newport VH 3036W-OPT, USA) to perform a complete isolation from mechanical vibration. A Faraday cage, provided with a frontal latch, covers all the instrumentation to isolate it from electrical interferences.
Patch-clamp recording pipettes were made from soda glass capillaries (outer diameter = 1.7 mm, inner diameter = 1.2 mm; Hilgenberg, Germany) and pulled to tip diameters of about 2 µm. Then they were fire-polished, using a micro-forge (MF-830 Narishige, Japan), and partially coated with Sylgard (Dow Corning 184, USA) to minimize the fast patch pipette capacitance transient.
Pipettes were moved near the preparation using two micromanipulators. One manipulator (PS7000, Scientifica, UK) was for the recording patch pipette, whereas the second (PCS-5000, Burleigh, USA) was for the cleaning pipette. Cleaning pipettes are glass pipette, filled with Extra_std solution, used to simplify the approach of the patch-pipette to the hair cells.
All recordings were obtained at room temperature. Voltage- and current-clamp recordings were obtained using the following intra-pipette solution (in mM): 131 KCl, 3 $MgCl_2$, 1 EGTA-KOH, 5 Na_2ATP, 5 HEPES-KOH (pH 7.2; 293 mOsm/kg).
Electrophysiological recordings were made using an Axopatch 200B amplifier (Molecular Devices, Sunnyvale, USA). Data acquisition was controlled by pClamp software using a Digidata 1322A

board (Molecular Devices, USA). The amplifier's filter bandwidth was set at 2–5 kHz. Digital sampling frequency of voltage- and current-clamp protocols was at least three times the analog bandwidth of the signal recorded. Recordings were stored on computer for off-line analysis (Origin, OriginLab, USA).

When filled with the intra-pipette solution, micropipettes had a resistance in the bath of 2–5 MΩ. Pipette capacitance and resistance were compensated in cell-attached configuration. The pipette resistance was kept as low as possible, despite the greater difficulty in obtaining a gigaseal, to minimize the series resistance (R_s). On-line R_s compensation in Type I hair cells may lead to substantial errors because no voltage range without active ion currents can be found in these cells. The low pipette resistance and good access to the whole-cell configuration gave acceptably low R_s (<10 MΩ). This was confirmed in Type II hair cells, where R_s and cell membrane capacitance (C_m) were monitored during trains of 5 mV hyperpolarizing voltage steps delivered from the cell membrane holding potential of –63 mV. Current traces were not corrected for cell membrane capacitive transients; in a few traces however, as noted in the figure legends, they were partially blanked. Voltages in voltage-clamp experiments and cell membrane resting potential (V_{rest}) in current-clamp recordings were corrected *a posteriori* for the liquid junction potentials of intra-pipette solutions *vs.* extracellular solution (3 mV negative inside the pipette).

Statistical comparisons of means were made by Student's two-tailed t test. In the text, mean values are quoted ± standard deviation (S.D.), where $P<0.05$ indicates statistical significance. In Figs. 22 and 23, data points refer to mean ± standard error (S.E.).

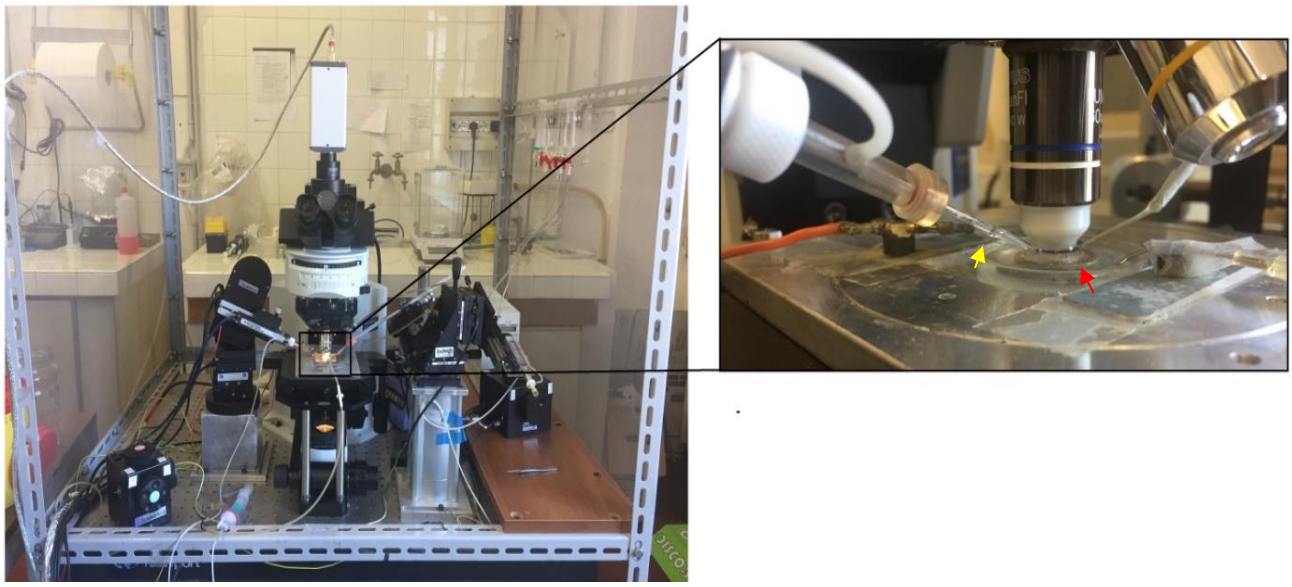

Fig. 18. Picture of the set-up.
On the left is visible how the microscope is located in the Faraday cage on an anti-vibration table. The inset on the right is the magnification of the stage. It is visible the Petri dish containing the crista held under a weighted nylon mesh (red arrow) and the patch pipette (yellow arrow).

Results

Morphological features of *Eps8*-KO vestibular hair cells

Vestibular and cochlear hair cells express EPS8 at the tips of *stereocilia* (*Manor et al., 2011*). In 2011, *Zampini et al.* reported that *Eps8*-KO mice are characterized by IHCs that show shorter hair bundles than WT. This mutation is particularly pronounced at the tallest row of *stereocilia.* Since no data are available on *Eps8*-KO vestibular hair bundles, I decided to first investigate this aspect. Experiments performed in mammalian WT and *Eps8*-KO (Fig. 19 left and right, respectively) hair bundles from different *cristae ampullaris* showed similar compactness at their base, but in the upper part (above the dashed line in Fig. 19 right) *Eps8*-KO hair bundles seemed to be less packed.

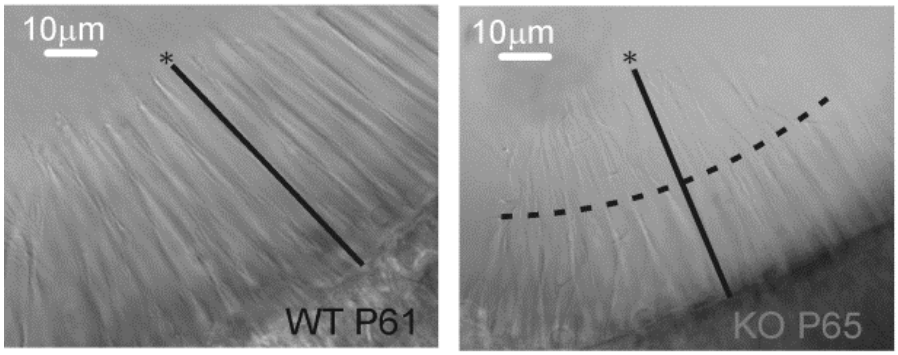

Fig. 19. Representative photomicrographs of a small portion of the vestibular crista intermediate region.
Hair bundles from a P61 WT (left) and a P65 Eps8-KO (right) mouse. Vestibular hair bundle shows a similar compactness at the base, but it seems reduced in the upper part of the Eps8-KO preparation (above the dashed line). The continuous line indicates the maximal length of the hair bundle, which is dictated by the kinocilium (asterisks).

To investigate closer this aspect, I isolated the vestibular hair cells in order to have a clear view of the morphology of the single hair bundles. For a correct analysis of the results it is important to remember that vestibular hair cells keep the *kinocilium* throughout their life, whereas cochlear hair cells lose it during maturation (at P10, *Leibovici et al., 2005*).

I found that vestibular WT and *Eps8*-KO hair bundles had a normal staircase organization with an easy discernible, central and long *kinocilium* (Fig. 20 left and right). When I analyzed the *stereocilia,* I found that in *Eps8*-KO mice only the longest row was significantly shorter in length (about 50%; $P<0.0001$) than the WT (Fig. 21A, B, C).

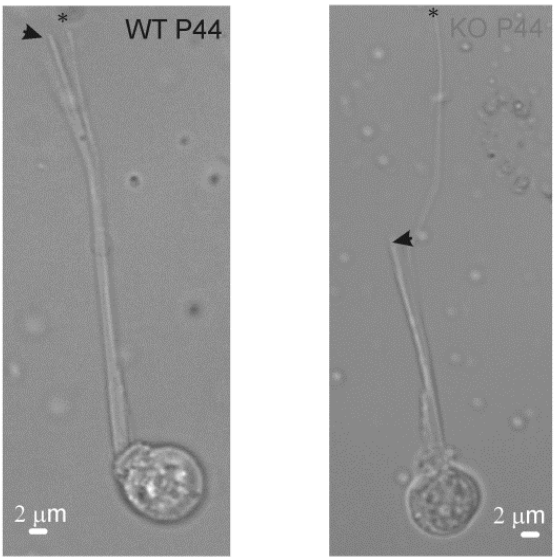

Fig. 20. Photomicrographs of isolated hair cells.
Isolated vestibular hair cells from a P44 WT (left) and a P44 Eps8-KO (right) mouse, show a similar kinocilia (asterisks), but different stereocilia. The arrowheads point at the longest stereocilium in the hair bundle. Note that the staircase organization of the hair bundle is maintained in both mice.

Further analysis showed no statistically difference in the hair cell size between *Eps8*-KO and WT mice, indicating that in the vestibule the absence of *Eps8* was not affecting the growth of the cell body.

Table 1. Morphological characteristics of WT and Eps8-KO isolated vestibular hair cells. *All the measure are written in µm, as mean ± S.D.*

	Kinocilium	***Longest stereocilium***	***Hair cell body***
WT, n=14 *P32-44*	53.53 ± 5.14	48.92 ± 4.66	8.16 ± 1.28
Eps8-KO, n=10 *P37-57*	52.58 ± 5.21	22.32 ± 3.36	7.97 ± 0.79
t-test P value	0.66	2.96E−13	0.68

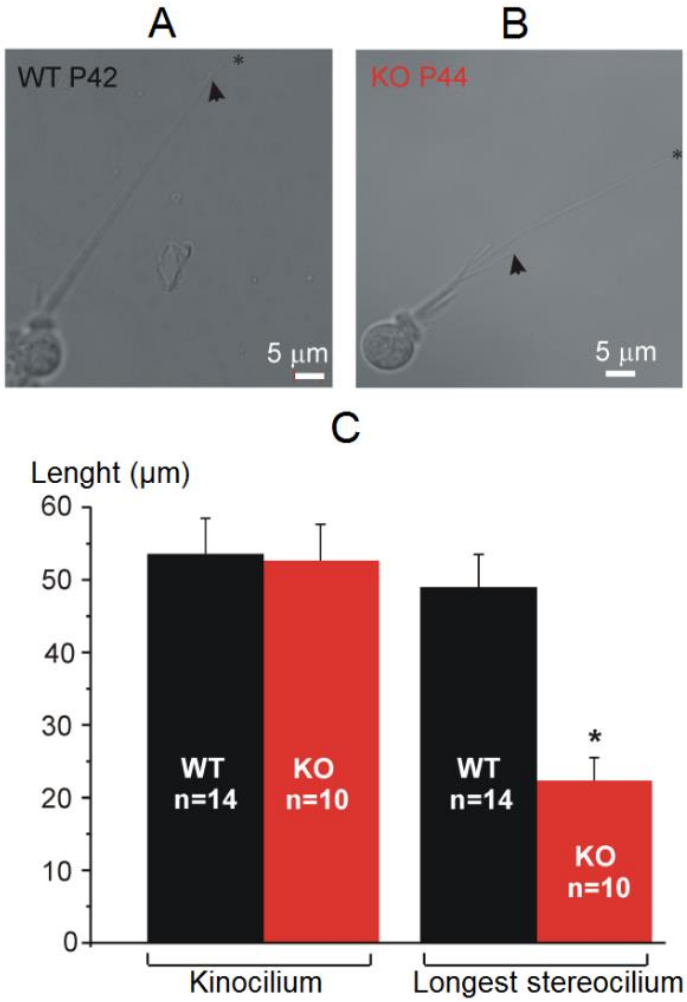

Fig. 21. Photomicrographs of isolated hair cells and histogram showing the average length of the kinocilia and the first stereociliary row.
(A and B) P42 WT and P44 Eps8-KO isolated vestibular hair cells mouse. Note that these are representative photomicrographs. The kinocilium (asterisks) has the same length in the two cells, whereas the longest stereocilium (arrowheads) is shorter in the Eps8-KO hair cell.
(C) Histogram which reports the average length, in WT and Eps8-KO mice, of the kinocilia and of the longest stereocilium. A statistically significant difference was found only for the stereocilia.

Electrophysiological properties from vestibular hair cells of WT and *Eps8*-KO mice

Mammalian vestibular Type I and Type II hair cells can be distinguished by the expression of K^+ channels (*Rennie and Correia, 1994; Eatock et al., 1998; Eatock and Songer, 2011*).

In Fig. 22A, B I have reported whole-cell current recordings from vestibular Type II hair cells (P23) of WT and *Eps8*-KO mice. In both WT and *Eps8*-KO Type II hair cells, an hyperpolarization of the cell membrane, from the holding potential –63 mV, evoked an anomalous rectifying K^+ current ($I_{K,1}$). During hyperpolarization, an additional small slow inward rectifying cationic current, called

I_h, is evoked sometimes from both WT (Fig. 22A; see also *Contini et al., 2012*) and *Eps8*-KO (not shown) hair cells. In both WT (Fig. 22A; see also *Contini et al., 2012*) and KO cells (Fig. 22B) a depolarization of the cell membrane activates two outward rectifying K^+ current. The first is a rapid and transient current ($I_{K,A}$), while the second is a delayed and sustained current ($I_{K,v}$).

In Fig. 22C, D I have showed the mean peak and steady-state current-voltage (I-V) relations of the macroscopic inward and outward rectifying K^+ currents in WT and *Eps8*-KO Type II hair cells. The amplitude of the inward and outward rectifying K^+ currents in KO cells was not significantly different from that measured in WT cells.

These results indicate that the loss of *Eps8* does not affect the K^+ current properties in vestibular Type II hair cells. Similarly, no significant differences were observed in the mean membrane input resistance (R_m), calculated between –63 mV and –53 mV, which was 721.07 ± 359.72 MΩ in WT cells (n=5) and 978.18 ± 396.73 MΩ in KO cells (n=7). The resting membrane potential (V_{rest}) of Type II hair cells was slightly different (P=0.029), in fact WT hair cells (–67.38 ± 5.74 mV, n=26) were more hyperpolarized than KO hair cells (–63.64 ± 3.05 mV, n=14).

The more depolarized V_{rest} in *Eps8*-KO cells was due to unknown reasons related to the hair cell sampling because the mean peak and steady-state current-voltage (I-V) relations of the macroscopic K^+ currents' amplitude were not significantly different. Moreover, *Eps8*-KO and WT vestibular Type II hair cells sometimes expressed I_h, a mixed Na^+/K^+ current, which is expected to depolarize the V_{rest}. Obviously, the more or less V_{rest} depolarization is based on the relative contribution of I_h and the different K^+ currents in the voltage range close to –60 mV.

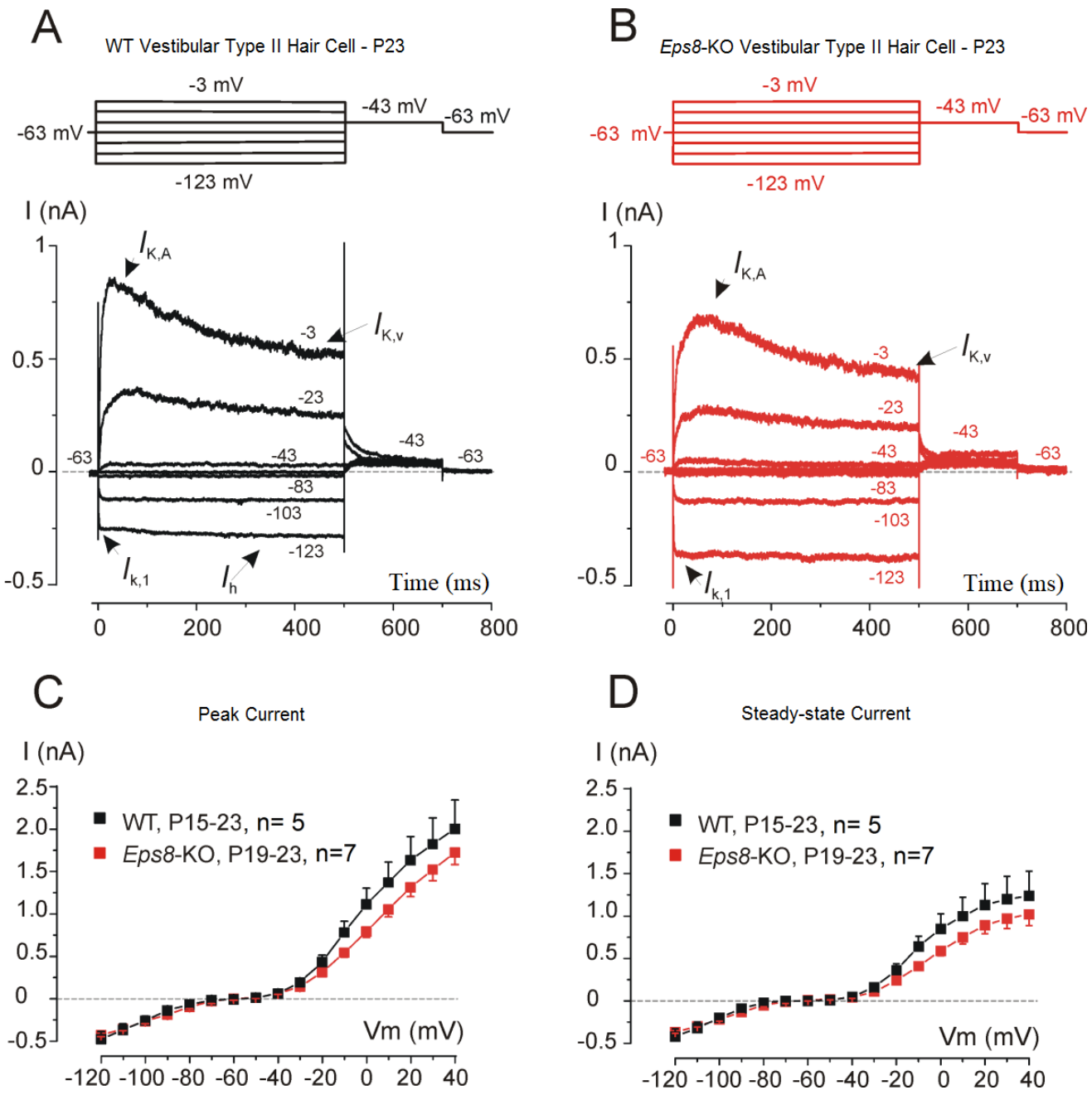

Fig. 22. Similar macroscopic currents in WT and Eps8-KO mouse vestibular Type II hair cells.
(A and B) Type II hair cell representative macroscopic currents from WT and Eps8-KO mice (P23), respectively. Currents were elicited by hyperpolarizing and depolarizing voltage steps from the holding potential of –63 mV to the various test potentials shown next to each trace (from –123 mV to –3 mV). Residual transient capacitive artifacts have been partially erased.
Hyperpolarizing steps elicited inward (anomalous) rectifying K^+ currents ($I_{K,1}$) and, in some cells both WT and Eps8-KO, an additional small cationic current (I_h) was elicited. Depolarizing steps evoked large transient outward K^+ currents ($I_{K,A}$) and a slow sustained K^+ current ($I_{K,v}$). No differences were found in the macroscopic currents between control and Eps8-KO mice. C and D: mean peak (± S.E.) and steady-state current-voltage (I-V) relations obtained from adult WT (P15–23, n=5) and Eps8-KO (P19–23, n=7) Type II hair cells, respectively. In this and the following figures, voltage commands (V_m) are shown as nominal values.

In Fig. 23A, B I have reported the whole-cell currents recorded from vestibular Type I hair cells of WT (P18) and *Eps8*-KO (P16) mouse, respectively. Both cells were characterized by the low-voltage outward rectifying K^+ current ($I_{K,L}$), which is almost fully active at –60 mV, and by the slow outward rectifying K^+ current ($I_{K,v}$), which activates for depolarization above –40 mV (*Rennie and Correia, 1994; Rüsch and Eatock, 1996; Contini et al., 2012*).

Since *Hurley et al.* (*2006*) reported that the K^+ channel subunits forming $I_{K,L}$ channel change during the first three postnatal weeks, I analyzed if there were any differences in WT and *Eps8*-KO cells during that period. P7–9 mean peak and steady-state I-V relations are represented in Fig. 23C, D, whereas P16–23 mean peak and steady-state I-V relations are represented in Fig. 23E, F. The size of the K^+ currents, in WT and *Eps8*-KO Type I hair cells, was not significantly different at both age ranges. The R_m, calculated between –63 mV and –53 mV, was not significantly different in either the younger (36.02 ± 11.95 MΩ, n=4 in P7–9 WT cells and 32.61 ± 11.57 MΩ, n=8 in P7–12 KO cells) or older hair cells (20.39 ± 8.43 MΩ, n=7 in P16-23 WT cells and 16.50 ± 3.28 MΩ, n=7 in P16–19 KO cells). Finally also the V_{rest} was not found to be significantly different (P=0.055) between WT (–70.24 mV ± 5.42; n=33) and *Eps8*-KO (–66.70 ± 6.47 mV; n=17) Type I hair cells, even if WT cells were slightly more hyperpolarized than the KO.

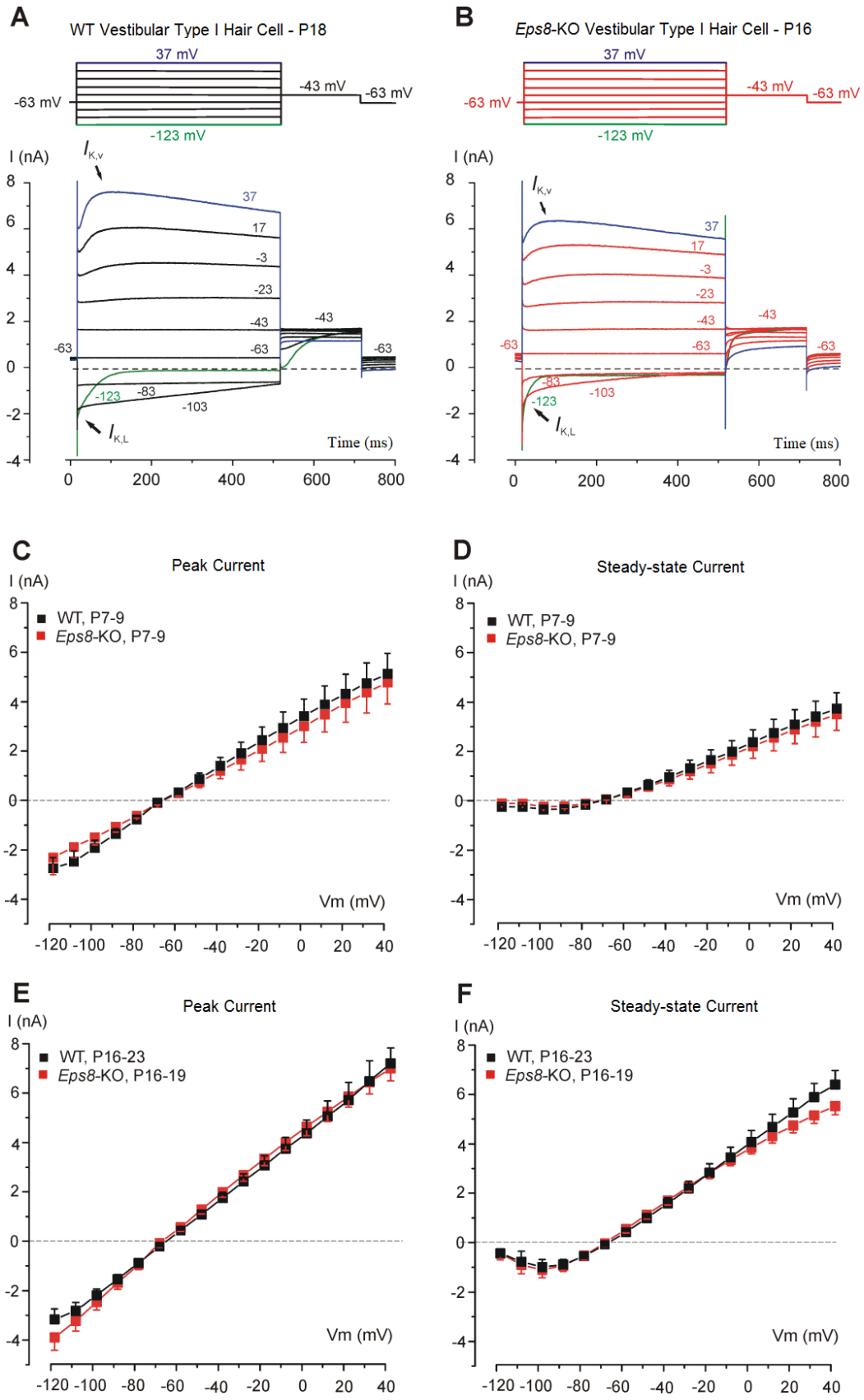

Fig. 23. Similar macroscopic currents in WT and Eps8-KO mouse vestibular Type I hair cells. *(A and B) Type I hair cell representative macroscopic currents from WT (P18) and Eps8-KO (P16) mice. Current were elicited as described in Fig. 22. At the holding potential (–63 mV) is clearly visible the presence of an outward current, known as $I_{K,L}$. Conversely, hyperpolarizing steps*

deactivate $I_{K,L}$ and depolarizing steps evoke, from –43 mV, an additional outward rectifying K^+ current ($I_{K,v}$).
(C, D) Mean peak (± S.E.) and steady-state I–V relations obtained from WT (P7–9, n=4) and Eps8-KO (P7–9, n=4). This group represents Type I hair cells during early stages of developmental.
(E, F) Mean peak (± S.E.) and steady-state I–V relations obtained from older WT (P16–23, n=7) and Eps8-KO (P16–19, n=7). This group represents developed Type I hair cells.

Electrophysiological properties from cochlear inner hair cells (IHCs) of WT and *Eps8*-KO mice

During the development (P0–12), IHCs express $I_{K,neo}$, a K^+ current showing a 4-aminopyridine (4-AP)-sensitive and a TEA-sensitive component (*Marcotti et al., 2003a*), I_{SK2}, an apamin-sensitive Ca^{2+}-activated K^+ current (*Marcotti et al., 2004b*), $I_{K,1}$, an anomalous rectifying K^+ current (*Marcotti et al., 1999*) and a Na^+ and a Ca^{2+} current (I_{Na} and I_{Ca}; *Marcotti et al., 2003b*). At around P12, IHCs acquire $I_{K,n,}$ a low voltage-activated K^+ current (*Oliver et al., 2003; Marcotti et al., 2003a*), and $I_{K,f}$, a fast-activating Ca^{2+}-dependent K^+ current (*Kros et al., 1998*), while I_{SK2}, $I_{K,1}$ and I_{Na} are down-regulated. *Zampini et al.* (*2011*) showed that, after P12, *Eps8*-KO IHCs don't express both $I_{K,n}$ and $I_{K,f}$. I decided then to compare IHCs and vestibular hair cells to better understand the underlying voltage response (see next section) of these cells. Hence, I performed some voltage-clamp recordings from IHCs at different developmental ages (Fig. 24) and then compare them to those obtained in the vestibular hair cells (Figs. 22 and 23).

Remarkable, the current behavior of *Eps8*-KO P12 IHCs (Fig. 24C: onset of cell maturation) was similar to that obtained by the immature WT cells at P8 (Fig. 24A). The immature-type current profile of *Eps8*-KO IHCs generated a negative slope in the I-V relation (Fig. 25C), which was not evident in age-matched WT IHCs cells (Fig. 25B). This leads to a net inward Na^+/Ca^{2+} current at voltages around –30 mV (*Marcotti et al., 2003a*). The negative slope conductance near the action potential (AP) threshold (see *Benson and Adams, 1987*) determines the persistence of AP-like activity in adult *Eps8*-KO IHCs (compare Fig. 25E, F) (*Zampini et al., 2011*). To characterize the consequences of *Eps8* deletion upon the receptor potential, we recorded voltage responses from vestibular and cochlear hair cells during sinusoidal current stimuli.

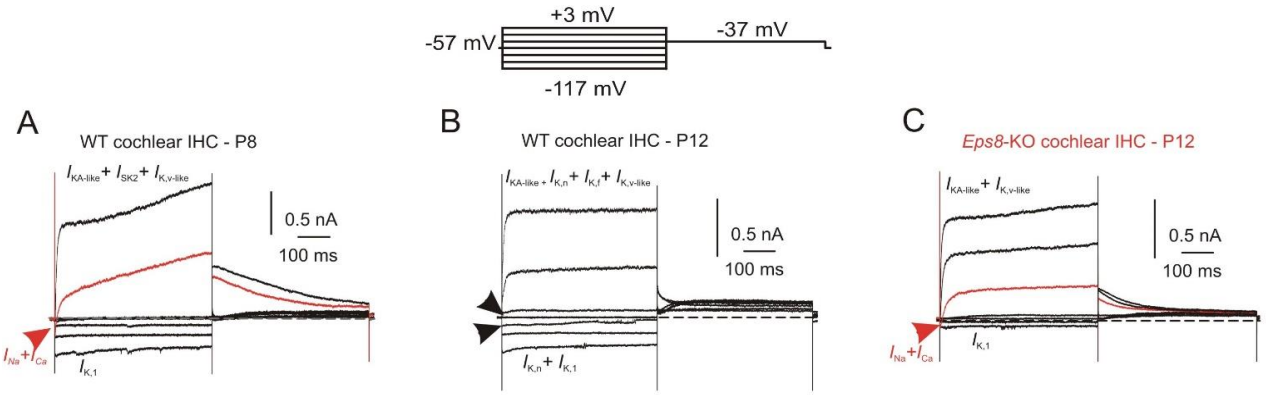

Fig. 24. Voltage-clamp responses from WT and Eps8-KO IHCs.
(A) Cochlear P8 WT IHC representative macroscopic ionic currents recorded in response to the voltage-clamp protocol shown on the top panel (the same voltage-clamp protocol was used for B and C). Hyperpolarizing steps from the holding potential of –63 mV elicited an inward rectifying K^+ current, called $I_{K,1}$. While depolarizing steps elicited a fast inward current, presumably consisting of I_{Na} and I_{Ca}, and a slow outward rectifying K^+ current, most likely carried out by I_{SK2}, $I_{K,v}$-like and I_{KA}-like (Marcotti et al., 2003a).
(B) Cochlear P12 WT IHC representative macroscopic ionic currents recorded in response to the voltage-clamp protocol. Note that during the conditioning steps we had the presence of $I_{K,n}$ (arrowheads), which is expressed in the mature-type cells, and $I_{K,1}$, which is normally down-regulated at about P16.
(C) Cochlear P12 Eps8-KO IHC representative macroscopic ionic currents recorded in response to the voltage-clamp protocol. Hyperpolarizing steps from the holding potential of –63 mV elicited $I_{K,1}$, while depolarizing steps elicited a small transient inward current (red trace), presumably consisting of I_{Ca} and I_{Na}, followed by a slow-activating outward rectifying K^+ current clearly resembling the macroscopic current of a younger WT IHC (compare with the trace A on the left).
In WT IHCs, at all ages, is present a Ca^{2+} current which is not detectable because $I_{K,f}$ and $I_{K,n}$ in adult animals are several times bigger and faster (Marcotti et al., 2003b).

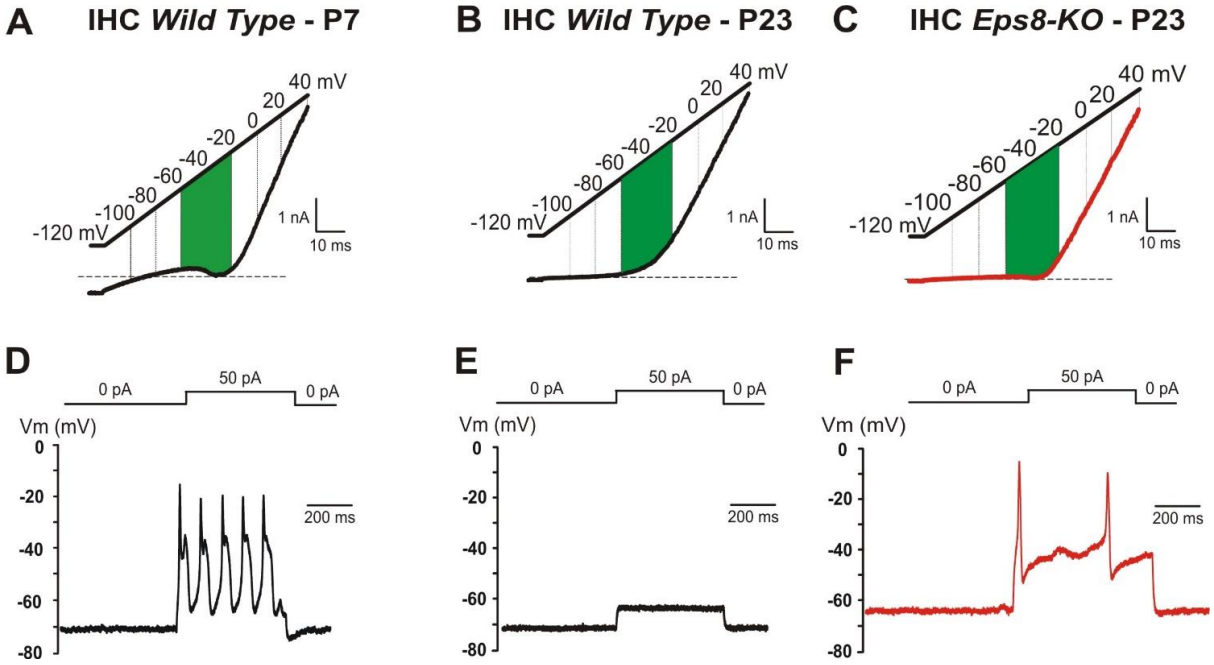

Fig. 25. WT and Eps8-KO IHCs voltage- and current-clamp responses.
(A - C) Representative currents elicited by a voltage ramp from –120 mV to 40 mV. The green areas indicate the presumed voltage range of the hair cell receptor potential (from –60 mV to –20 mV), when considering that afferent neurotransmitter release occurs at rest, and I_{Ca} peaks at around –20

mV. Immature WT (A) and mature Eps8-KO (C) IHCs have a negative slope in the receptor range, which is a required characteristic to evoke action potentials (Benson and Adams, 1987).
(D - F) Representative current-clamp responses evoked by a depolarizing current step of 50 pA delivered from the cell resting (0 pA) membrane potential (V_m; same cells as above). Immature WT (D) and mature Eps8-KO IHCs (F) are able to evoke AP or AP-like activity, whereas mature WT IHCs (E) follow almost faithfully the stimulus.

Voltage responses of vestibular and cochlear hair cells to sinusoidal currents

Figure 26 shows representative voltage responses to an injected sinusoidal current, which was used to mimic the motion stimulation (0.2 Hz; 200 pA peak-to-peak; assuming a resting open probability of the MET channels of 10%; see Figure legend).

Mature Type I and Type II vestibular hair cells from WT mice (P9: Fig. 26A, C, respectively) showed a similar voltage responses to sinusoidal *stimuli* to those obtained from aged-matched *Eps8*-KO mice (Fig. 26B, D). It is important to note that the amount of membrane depolarization in Type I hair cells (the "voltage gain" $\Delta V/\Delta I$) was much smaller than that observed in Type II hair cells, because a much lower R_m was produced by $I_{K,L}$ in Type I hair cells. Moreover, the shape of the voltage response in Type I hair cells, conversely to those of Type II hair cells, overlaid to that of the stimulus (i.e. the voltage gain varies linearly with the amplitude of the MET current). This overlap was also due to the presence of $I_{K,L}$ since, which is almost fully activated at V_{rest} and it produces an ohmic or linear change of the cell membrane voltage in response to the sinusoidal current stimulus.

Type II hair cells' voltage response cannot follow faithfully the sinusoidal stimulus because $I_{K,A}$ and $I_{K,v}$ start activating close to V_{rest}. Hence the recordings show that the voltage gain is initially very large but, as the outward rectifying K^+ currents activate, it decreases and the voltage response flattens.

For my experiments, I selected a stimulus with a frequency of 0.2 Hz because it is in the vestibular frequency domain, i.e. below the cochlear frequency range (approximately 4–75 kHz in the mouse; *Nyby, 2001*). However, since fast depolarization in IHCs from *Eps8*-KO mice elicited Ca^{2+} dependent APs (see Fig. 25F), the slow depolarizing sinusoidal *stimuli* allowed to characterize the ''analog" time course (direct current (d.c.) component) of the receptor potential. At immature developmental stages (P8), both the WT and *Eps8*-KO IHCs showed an intense firing activity (Fig. 26E, F; see also *Zampini et al., 2011*). After the onset of hearing at P12, IHCs from WT mice stop firing APs and instead showed a voltage response that faithfully follows the sinusoidal *stimulus* (P22, Fig. 26G). In adult *Eps8*-KO IHCs (P23), APs could still be elicited and the shape of the voltage response did not match that of the stimulus (Fig. 26F), but resembled the responses

observed in Type II hair cells (Fig. 26C, D). These observations indicate that *Eps8*-KO IHCs fail to acquire the basolateral membrane property of mature graded receptors. Lack of expression of $I_{K,n}$ in IHCs from *Eps8*-KO mice caused their R_m to be significantly larger (718.19 ± 490.61 MΩ, n=5, P23–29; P<0.05) than that measured in WT IHCs (66.00 ± 23.09 MΩ, n=4, P15–28). Therefore, an additional indirect effect of *Eps8* deletion is that the IHC membrane time constant is one order of magnitude greater than that in WT IHCs, which would preclude *Eps8*-KO IHCs to follow *stimuli* in the kHz (acoustic) range.

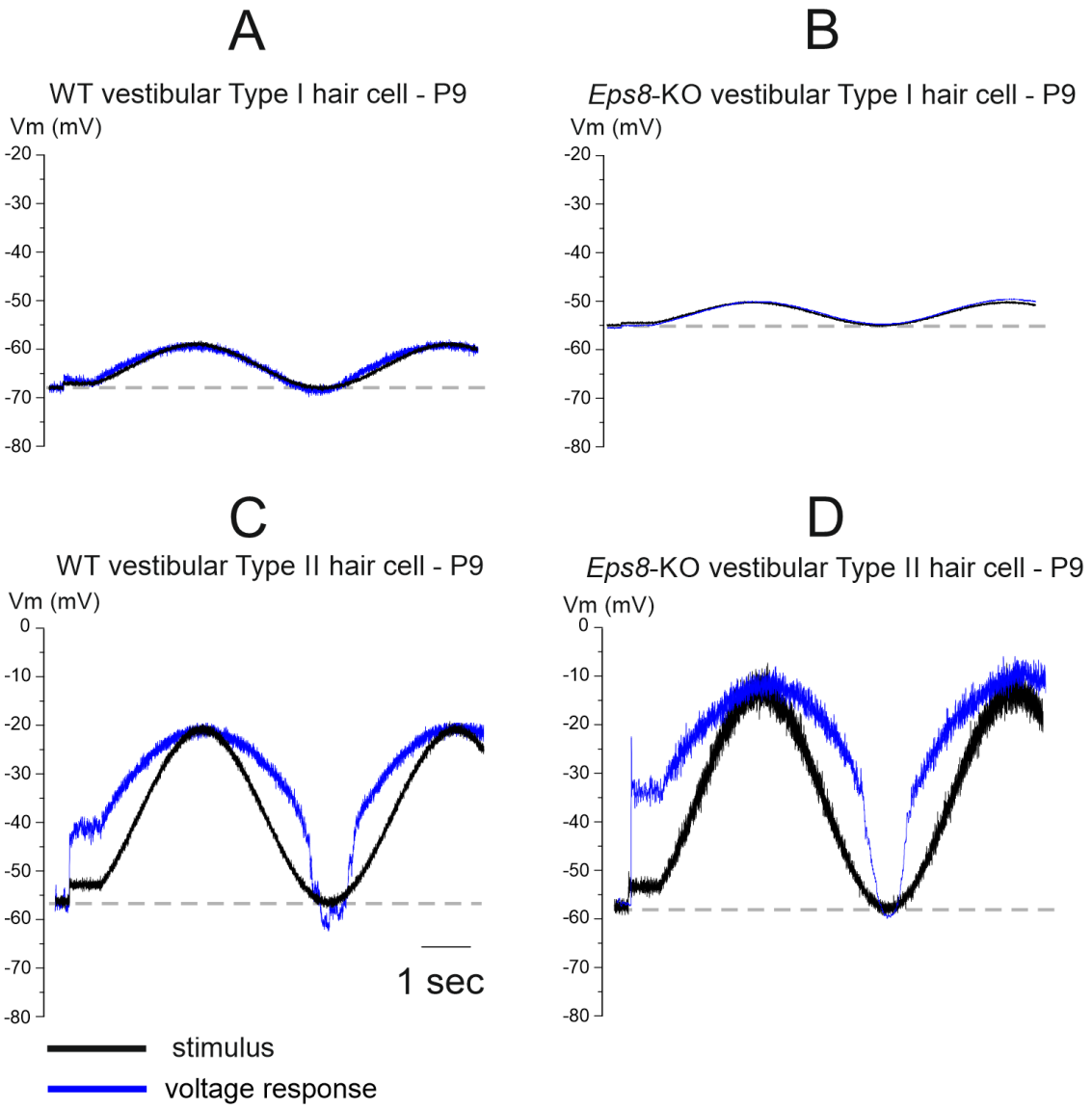

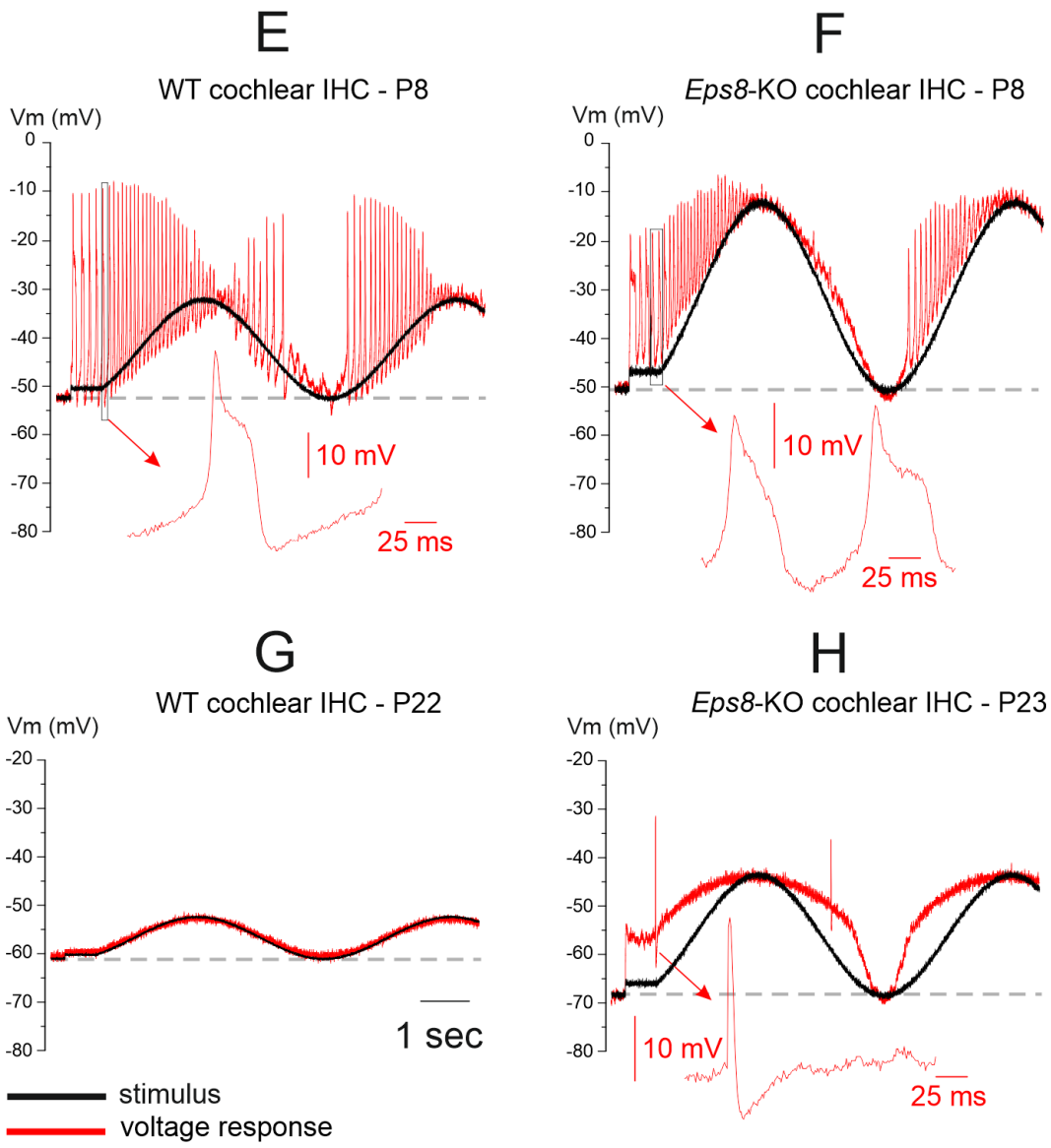

Fig. 26. Vestibular and cochlear hair cells voltage responses to sinusoidal injected currents.
(A) Representative WT vestibular Type I hair cell (P9) voltage response to a sinusoidal stimulus. The stimulus frequency and amplitude were 0.2 Hz and 200 pA peak-to-peak (it applies to all panels). Three cycles were delivered, but here only the first and half cycle of the sinusoidal stimulus/response are shown. Starting from the cell resting (zero-current) membrane potential, it was delivered a current step of 20 pA in amplitude for 1 s to simulate the resting open MET current (Johnson et al., 2012), before starting the sine-wave. The cell membrane voltage response (Vm) is shown in blue.
The current stimulus, that is the true current delivered by the patch-clamp amplifier to the hair cells, is shown in black (also in the successive panels). Note that it can be scaled in amplitude to maximize overlapping with the voltage response. Finally, the zero current level is indicated by the gray dashed horizontal line (also in the successive panels).
(C) Representative WT vestibular Type II hair cell (P9) voltage response. When compared to Type I (panel A) hair cell, Type II has a different shape and range of voltage response. The horizontal calibration bar in C (1 s) refers to all panels.
(B, D) Representative EPS8-KO vestibular Type I and II hair cells (P9) voltage response. When compared to WT Type I and II (A, C) hair cells, they have an overlapping shape and range of voltage response.
(E, F) Representative voltage responses (red trace) of a P8 WT and a P8 Eps8-KO immature cochlear IHC, respectively. Voltage response from the WT and KO IHCs overlaps with the stimulus and APs were present.

(G, H) Representative voltage responses (red trace) of a P22 WT and a P23 Eps8-KO cochlear IHC, respectively. Voltage response from the WT IHC overlaps with the stimulus and APs were absent, whereas that from the adult KO IHC was completely different. The voltage response chosen for Fig. 26H had few APs in order to better show the d.c. component.

Discussion

The present study demonstrated that the absence of *Eps8* affects the normal growth of the stereociliary bundle in vestibular hair cells. These data are consistent with previous studies on cochlear hair cells (*Manor et al., 2011; Zampini et al., 2011*). However, *Eps8*-KO mice are deaf but do not show any obvious vestibular deficiency (*Manor et al., 2011; Zampini et al., 2011*). A possible reason for this difference, between cochlear and vestibular hair cells, could be due to the preservation of the *kinocilium* and the presence of longer *stereocilia* in vestibular hair cells (Fig. 27). Moreover, the hair bundle of vestibular hair cells is enveloped into accessory structures (i.e. the *cupula* in semicircular canal) which supply an efficient coupling between the stimulus and the hair bundle displacement, even if the hair bundles of *Eps8*-KO mice are shorter.

Conversely in the cochlea, the reduced size of the *Eps8*-KO IHC *stereocilia* compromises the normal deflection of the hair bundle during the sound stimulation.

Furthermore, adult cochlear *Eps8*-KO IHCs show an anomalous expression of basolateral membrane ion channels, whereas *Eps8*-KO vestibular hair cells have a normal expression of basolateral membrane ion channels. Consistent with this, the receptor potential in response to an injected sinusoidal “MET” current was normal in vestibular hair cells, but substantially altered in IHCs. Therefore, even if the MET current could be elicited in *Esp8*-KO IHCs, the resulting receptor potential would be inadequate to signal the stimulus intensity and phase.

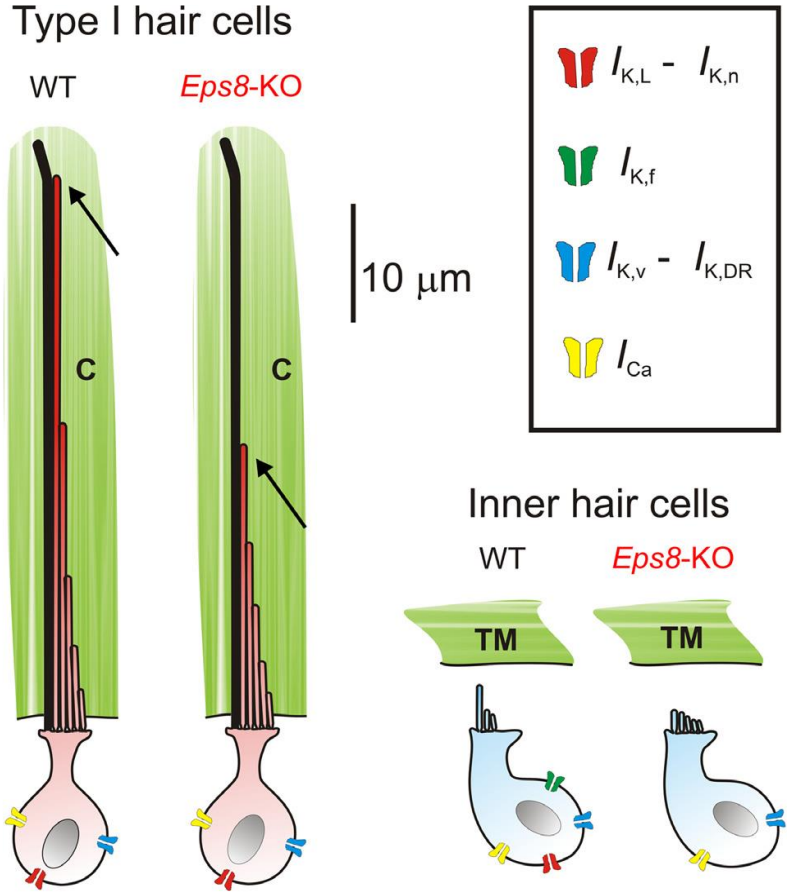

Fig. 27. Schematic drawing showing the effect of Eps8 deletion upon vestibular and cochlear hair cells.

From left to right. Two Type I hair cells are shown as representative of vestibular hair cells, since similar results were obtained for Type II hair cells. Remarkable, the difference in stereocilia height between WT and Eps8-KO vestibular (present thesis) and cochlear (Zampini et al., 2011) hair cells. Arrows indicate the longest stereocilia row of the vestibular hair bundle, which was significantly reduced in size in Eps8-KO mice (Figs. 20 and 21). The height of the shorter stereocilia has been scaled down to mimic the possible overall effect of the mutation, as seen in cochlear hair cells. The hair bundle of semicircular canal hair cells is almost completely enclosed in the cupula (C), a gelatinous structure that bridges the width of the ampulla, forming a fluid barrier through which endolymph cannot circulate. It is the diaphragm-like displacement of the cupula that gives rise to hair bundle displacement during head rotation. At difference, IHCs stereocilia are freely standing and behave like hydrodynamic sensors which respond directly to endolymph motion in the space below the tectorial membrane (TM). Ion channel expression is the same in WT and Eps8-KO vestibular hair cells, whereas Eps8-KO IHCs lack $I_{K,n}$ and $I_{K,f}$. $I_{K,DR}$ represents the delayed outward rectifying K^+ current including $I_{K,neo}$-4AP-sensitive and $I_{K,neo}$-4AP-insensitive.

Eps8 regulates stereocilia growth in cochlear and vestibular sensory cells

The correct development and maintenance of the stereociliary bundle in mammalian cochlear hair cells are regulated by several proteins and two of them are members of the Eps8-like protein family, respectively by Eps8 (*Manor et al., 2011; Zampini et al., 2011*) and Eps8L2 (*Furness et al., 2013*). *Eps8* is highly expressed at the tips of the tallest stereocilia and its deletion leads to shorter and immature hair bundles.

The role of Eps8 is to bind the barbed end of actin filaments (fast-growing ends) at stereocilia tips (*Schneider et al., 2002*), favoring the action of proteins promoting the acting filament elongation, such as espin (*Rzadzinska et al., 2005*) and disadvantaging the interaction with proteins inhibiting it (*Manor et al., 2011*).

In my study, I demonstrate that *Eps8* has an important role also in vestibular hair bundle, in fact the tallest row of *stereocilia i*s about half in length of that in WT vestibular hair cells. On the other hand, the staircase-like organization is unaltered (*Manor et al., 2011; Zampini et al., 2011*).

The development of the hair bundle staircase-like structure is carefully orchestrated mainly during early stages of hair cell postnatal development (*Frolenkov et al., 2004*). Initially, a single and centrally located *kinocilium* is surrounded by numerous short microvilli of uniform height. The microvilli appear on the apical surface of newly differentiated hair cells, at E13.5 in the vestibule and at E15.5 in the cochlea. During the following days, the *kinocilium* moves to the cell periphery surface and the nearest microvilli start elongating, followed by those that are further and further away. This process generates the typical staircase-like organization with the different rows of stereocilia graded in height. Stereociliary elongation in the shortest rows stops at around postnatal day 5 (P5) and that in the tallest row at about P15 (*Manor and Kachar, 2008*).

The present study indicates that the final length of the hair bundle is not related to the development of the *kinocilium,* since in *Eps8*-KO vestibular hair cells the *kinocilium* size was not affected by the mutation but the first row of stereocilia was about 50% shorter than normal. This result supports previous studies showing that the growth of the tallest *stereocilia* row is not affected when the kinocilium either lacks its axonemal part (*Jones et al., 2008*) or it is entirely disconnected from the *stereocilia* (*Lefèvre et al., 2008*). It is probable that the *kinocilium* establishes the hair bundle polarity, orientation and possibly the initial hair bundle growth in the developing vestibular system (*Jones et al., 2008*), but the staircase-like structure of the hair bundle is due to the expression of the other proteins regulating actin polymerization.

In fact, *Peng et al.* (*2009*) showed that an in vitro overexpression of twinfilin 2, a protein localized to the tips of the shorter stereocilia of IHCs and OHCs, causes a significant decrease of IHCs' stereocilia length. Like Eps8, twifilin 2 is an actin-binding protein, which inhibits actin polymerization presumably by sequestering G-actin monomers. It is therefore possible that while EPS8 allows for the first stereociliary row to elongate by precluding the action of other capping proteins, twifilin 2 limits the elongation of the shorter stereocilia to produce the mature staircase architecture of cochlear hair bundles (*Peng et al., 2009*). What causes the differential expression of actin-binding proteins by distinct stereocilia rows remains to be elucidated.

Eps8 and ion channel expression

Eps8-KO IHCs, but not OHCs, fail to acquire their mature array of basolateral membrane channels (*Zampini et al., 2011*). Similar to cochlear OHCs, vestibular *Eps8*-KO Type I and Type II hair cells showed a normal expression of ion channels on the basolateral membrane. From my research, I can speculate that *Eps8* is able to control only the ion channel expression on the IHCs, but why and how it happens, is not clear.

The persistence of $I_{K,1}$ in mature *Eps8*-KO IHCs and the lacking expression of $I_{K,n}$ and $I_{K,f}$, indicate that Eps8 could control the ion channel expression through multiple processes, collaborating with extracellular (BDNF-receptors; *Menna et al., 2009*) and intracellular (e.g. IRSp53 and Abi-1) partners (*Vaggi et al., 2011*).

Otherwise, Eps8 could indirectly determine the expression of voltage-gated ion channels, such as a secondary effect due to the altered MET apparatus observed in *Eps8*-KO mice. The stereocilia of IHCs are free-standing and behave as hydrodynamic sensors (*Guinan, 2012*). In *Eps8*-KO mice, IHCs have short and additional rows of stereocilia (*Zampini et al., 2011*), which could impact on the resting MET current, the role of which is crucial for the maintenance of the normal spontaneous APs in developing IHCs (*Johnson et al., 2012*). Alteration of this electrical activity in pre-hearing IHCs has been associated with defects in the synaptic machinery, basolateral membrane ion channels and formation of tonotopic maps in the brainstem (*Roux et al., 2009; Johnson et al., 2013; Clause et al., 2014*).

The normal pattern of basolateral membrane ion channels found in mature vestibular hair cells from *Eps8*-KO mice suggests that, different from cochlear IHCs, their shorter stereociliary bundle is unlikely to play any developmental role. However, the hair bundle of semicircular canal hair cells is almost completely embedded in the cupula, which might compensate for the shorter stereocilia present in *Eps8*-KO mice, which would result in a normal transducer current.

Eps8 deletion affects auditory but not vestibular function

My thesis project has provided some proofs clarifying why *Eps8*-KO mice show deafness but not vestibular deficits.

First, the shorter hair bundles of *Eps8*-KO IHCs cannot be stimulated by the endolymph movements produced by the acoustic stimuli. Secondly, even if some MET current is elicited, the altered pattern of basolateral membrane ion channels preclude converting the stimulus intensity into the gradual receptor potential. In fact *Eps8*-KO IHCs, when stimulated with a sinusoidal current, evoked a mixed digital/analog response with APs surmounting a d.c. depolarization (Fig. 26H).

It is important because although neurotransmitter release could still occur in *Eps8*-KO IHCs, their ability to inform the brain about the timing of the natural stimulus (*Palmer and Russell, 1986; Trussell, 2002; Magistretti et al., 2015*) would be lost.

Finally, few gene mutation studies have been performed on the vestibule, whereas many studies have been carried out on the cochlea. This is probably due to fact that gene mutations in the cochlea and in the vestibule can have two different phenotypes. In fact gene mutations in the cochlea usually affect the growth and maintenance of stereocilia in IHCs and they produce deafness (*Hilgert et al., 2009; Petit and Richardson, 2009*), whereas the same mutations also altered vestibular hair bundles but there is an absence of vestibular dysfunction, e.g. abnormal posturing, imbalance, nystagmus, etc. (*Jones and Jones, 2014*). This might be due to different roles of particular genes in cochlear and vestibular end organs or by a partially compensation of the central nervous system for mild vestibular deficits. For those reasons specific vestibular tests should be performed to detect mild dysfunction, such as evoked potentials (see e.g. *Street et al., 2008; Goodyear et al., 2012*).

References

Adato A, Lefèvre G, Delprat B, Michel V, Michalski N, Chardenoux S, Weil D, El-Amraoui A and Petit C (2005). *Usherin, the defective protein in Usher syndrome type IIA, is likely to be a component of interstereocilia ankle links in the inner ear sensory cells.* Hum. Mol. Genet. 14:3921-3932.

Ahmed ZM, Goodyear R, Riazuddin S, Lagziel A, Legan PK, Behra M, Burgess SM, Lilley KS, Wilcox ER, Riazuddin S, Griffith AJ, Frolenkov GI, Belyantseva IA, Richardson GP and Friedman TB (2006). *The tip-link antigen, a protein associated with the transduction complex of sensory hair cells, is protocadherin-15.* J. Neurosci. 26:7022-7034.

Bao H, Wong WH, Goldberg JM and Eatock RA (2003). *Voltage-Gated Calcium Channel Currents in Type I and Type II Hair Cells Isolated From the Rat Crista.* J Neurophysiol 90:155-164.

Behlouli A, Bonnet C, Abdi S, Bouaita A, Lelli A, Hardelin JP, Schietroma C, Rous Y, Louha M, Cheknane A, Lebdi H, Boudjelida K, Makrelouf M, Zenati A and Petit C (2014). *EPS8, encoding an actin-binding protein of cochlear hair cell stereocilia, is a new causal gene for autosomal recessive profound deafness.* Orphanet journal of rare diseases. 9:55–65.

Behrend O, Schwark C, Kunihiro T and Strupp M (1997). *Cyclic GMP inhibits and shifts the activation curve of the delayed-rectifier (I_{K1}) of type I mammalian vestibular hair cells.* Neuroreport, 8:2687–2690.

Benson JA and Adams WB (1987). *Significance of the steady-state current voltage relationship*. In: Kaczmarek LK, Levitan IB, editors. Neuromodulation: the biochemical control of neuronal excitability. New York: Oxford University Press. p. 105.106.

Bernard C, Ferrary E and Sterkers O (1986). *Production of endolymph in the semicircular canal of the frog Rana esculenta.* Physiol 371:17–28.

Beurg M, Fettiplace R, Nam JH and Ricci AJ (2009). *Localization of inner hair cell mechanotransducer channels using high-speed calcium imaging.* Nat Neurosci. 12(5):553–558.

Beutner D and Moser T (2001). *The presynaptic function ofmouse cochlear inner hair cells during development of hearing.* J Neurosci 21:4593-4599.

Biesova Z, Piccoli C and Wong WT (1997). *Isolation and characterization of e3B1, an eps8 binding protein that regulates cell growth.* Oncogene 14:233–241.

Bird JE, Daudet N, Warchol ME and Gale JE (2010). *Supporting cells eliminate dying sensory hair cells to maintain epithelial integrity in the avian inner ear.* J Neurosci 30(37):12545–12556.

Castagnino P, Biesova Z, Wong WT, Fazioli F, Gill GN and Di Fiore PP (1995). *Direct binding of eps8 to the juxtamembrane domain of EGFR is phosphotyrosine- and SH2-independent.* Oncogene. 10(4):723–729.

Chen JW and Eatock RA (2000). *Major potassium conductance in type I hair cells from rat semicircular canals: characterization and modulation by nitric oxide.* Journal of Neurophysiology, 84:139–151.

Chu PY, Liou JH, Lin YM, Chen CJ, Chen MK, Lin SH, Yeh CM, Wang HK, Maa MC, Leu TH, Chang NW, Hsu NC and Yeh KT (2012). *Expression of Eps8 correlates with poor survival in oral squamous cell carcinoma.* Asia Pac J Clin Oncol. 8(4):77–81.

Ciuman RR (2011). *Auditory and vestibular hair cell stereocilia: relationship between functionality and inner ear disease.* J Laryngol Otol, 125(10):991–1003.

Clause A, Kim G, Sonntag M, Weisz CJ, Vetter DE, Rübsamen R and Kandler K (2014). *The precise temporal pattern of prehearing spontaneous activity is necessary for tonotopic map refinement.* Neuron, 82:822–835.

Contini D, Zampini V, Tavazzani E, Magistretti J, Russo G, Prigioni I and Masetto S (2012). *Intercellular K^+ accumulation depolarizes Type I vestibular hair cells and their associated afferent nerve calyx.* Neuroscience, 227:232–246.

Corns LF, Bardhan T, Houston O, Olt J, Holley MC, Masetto S, Johnson SL and Marcotti W (2014). *Functional development of hair cells in the mammalian inner ear.* In: Romand R and Varela-Nieto I (eds) Development of the Auditory and Vestibular Systems, 4th Edition, San Diego: Academic Press. 155–188.

Correia MJ and Lang DG (1990). *An electrophysiological comparison of solitary type I and type II vestibular hair cells.* Neuroscience Letters, 116:106–111.

Croce A, Cassata G, Disanza A, Gagliani MC, Tacchetti C, Malabarba MG, Carlier MF, Scita G, Baumeister R and Di Fiore PP (2004). *A novel actin barbed-end-capping activity in EPS-8 regulates apical morphogenesis in intestinal cells of Caenorhabditis elegans.* Nat Cell Biol, 6:1173–1179.

Dallos P (2008). *Cochlear amplification, outer hair cells and prestin.* Curr Opin Neurobiol, 18(4): 370–376.

Davis H (1965). *A model for transducer action in the cochlea.* Cold Spring Harb Symp Quant Biol, 30:181–190.

De Lemos-Chiarandini C and Shafland J (2007). *Special sensory receptors. Eye and ear.* NY University.

DeRosier DJ and Tilney LG (1989). *The structure of the cuticular plate, an in vivo actin gel.* J Cell Biol, 109:2853–2867.

Desai S, Ali H and Lysakowski A (2005a). *Comparative morphology of rodent vestibular periphery. II. Cristae Ampullares.* J Neurophysiol, 93(1):267–280.

Desai S, Zeh C and Lysakowski A (2005b). *Comparative morphology of rodent vestibular periphery. I. Saccular and utricular maculae.* J Neurophysiol, 93(1):251–266.

Di Fiore PP and Scita G. (2002) *Eps8 in the midst of GTPases.* Int J Biochem Cell Biol, 34:1178–1183.

Disanza A, Carlier MF, Stradal TE, Didry D, Frittoli E, Confalonieri S, Croce A, Wehland J, Di Fiore PP and Scita G (2004). *Eps8 controls actin-based motility by capping the barbed ends of actin filaments.* Nat Cell Biol, 6:1180–1188.

Disanza A, Mantoani S, Hertzog M, Gerboth S, Frittoli E, Steffen A, Berhoerster K, Kreienkamp HJ, Milanesi F, Di Fiore PP, Ciliberto A, Stradal TE and Scita G (2006). *Regulation of cell shape by Cdc42 is mediated by the synergic actin-bundling activity of the Eps8-IRSp53 complex.* Nat Cell Biol, 8(12):1337–1347.

Dou H, Vazquez AE, Namkung Y, Chu H, Cardell EL, Nie L, Parson S, Shin HS and Yamoah EN (2004). *Null mutation of alpha1D Ca^{2+} channel gene results in deafness but no vestibular defect in mice.* J. Assoc. Res. Otolaryngol, 5:215–226

Dumont RA and Gillespie PG (2003). *Hearing aid.* Nature, 424:28–29.

Eatock RA, Rüsch A, Lysakowski A and Saeki M (1998). *Hair cells in mammalian utricles.* Otolaryngol Head Neck Surg, 119:172–181.

Eatock RA and Hurley KM (2003a). *Functional development of hair cells.* Current Topics in Developmental Biology, 57:389–448.

Eatock RA and Hurley KM (2003b). *Functional development of hair cells.* In: Romand R and Varela-Nieto I (eds). Development of the Auditory and Vestibular Systems, 348–442. San Diego: Academic Press.

Eatock R and Fay RR (2006). *Vertebrate Hair Cells*. Springer.

Eatock RA and Songer JE (2011). *Vestibular hair cells and afferents: two channels for head motion signals*. Annu Rev Neurosci, 34:501–534.

El-Amraoui A and Petit C (2005). *Usher I syndrome: unravelling the mechanisms that underlie the cohesion of the growing hair bundle in inner ear sensory cells.* J Cell Sci, 118:4593–4603.

Engström H (1958). *On the double innervation of the sensory epithelia of the inner ear.* Acta Otolaryngol, 49(2):109–118.

Fazioli F, Minichiello L, Matoska V, Castagnino P, Miki T, Wong W T and Di Fiore PP (1993). *Eps8, a substrate for the epidermal growth factor receptor kinase, enhances EGF-dependent mitogenic signals.* The Embo Journal, 12:3799–3808.

Fernández C, Baird RA and Goldberg JM (1988). *The vestibular nerve of the chinchilla. Peripheral innervation patterns in the horizontal and superior semicircular canals.* J Neurophysiol, 60(1):167–181.

Fettiplace R and Ricci AJ (2003). *Adaptation in auditory hair cells.* Curr Opin Neurobiol, 13(4):446-451.

Fettiplace R and Hackney CM (2006). *The sensory and motor roles of auditory hair cells*. Nature review. Neuroscience, 7(1):19–29.

Fettiplace R and Kim KX (2014). *The physiology of mechanoelectrical transduction channels in hearing.* Physiol Rev, 94(3):951–986.

Fettiplace R (2017). *Hair cell transduction, tuning, and synaptic transmission in the mammalian cochlea.* Compr Physiol, 7(4):1197–1227.

Fitzpatrick RC and Day BL (2004). *Probing the human vestibular system with galvanic stimulation.* Journal of Applied Physiology, 96:2301–2316.

Frittoli E, Matteoli G, Palamidessi A, Mazzini E, Maddaluno L, Disanza A, Yang C, Svitkina T, Rescigno M and Scita G (2011). *The signaling adaptor Eps8 is an essential actin capping protein for dendritic cell migration.* Immunity, 35(3):388–399.

Frolenkov GI, Belyantseva IA, Friedman TB and Griffith AJ (2004). *Genetic insights into the morphogenesis of inner ear hair cells.* Nat Rev Genet, 5:489–498.

Fuchs PA (2005). *Time and intensity coding at the hair cell's ribbon synapse*. Journal of Physiology, 566(1):7–12.

Funato Y, Terabayashi T, Suenaga N, Seiki M, Takenawa T and Miki H (2004). I*RSp53/Eps8 complex is important for positive regulation of Rac and cancer cell motility/invasiveness.* Cancer Research, 64:5237–5244.

Furness DN and Hackney CM (2006). *The structure and composition of the stereociliary bundle of vertebrate hair cells.* In: Eatock RA, Fay RR and Popper AN (eds). Vertebrate Hair Cells, 95–153. New York: Springer.

Furness DN, Johnson SL, Manor U, Ruttiger L, Tocchetti A, Offenhauser N, Olt J, Goodyear RJ, Vijayakumar S, Dai Y, Hackney CM, Franz C, Di Fiore PP, Masetto S, Jones SM, Knipper M, Holley MC, Richardson GP, Kachar B and Marcotti W (2013). *Progressive hearing loss and gradual deterioration of sensory hair bundles in the ears of mice lacking the actin-binding protein Eps8L2*. Proc Natl Acad Sci USA, 110:13898–13903.

Gacek RR (1960). *Efferent component of the vestibular nerve.* In: GL Rasmussen and WF Windle (eds). Neural Mechanisms of the Auditory and Vestibular Systems, 276–284. Springfield: Thomas.

Gale JE and Jagger DJ (2010). *Cochlear supporting cells.* In: Fuchs, P.A. (eds). The Oxford Handbook of Auditory Science: The Ear. Oxford: Oxford University Press.

Géléoc GS, Lennan GW, Richardson GP and Kros CJ (1997). *A quantitative comparison of mechanoelectrical transduction in vestibular and auditory hair cells of neonatal mice.* Proc Biol Sci, 264(1381):611–621.

Géléoc GS, Risner JR and Holt JR (2004). *Developmental acquisition of voltage-dependent conductances and sensory signaling in hair cells of the embryonic mouse inner ear.* J Neurosci, 24:11148–11159.

Giese APJ, Tang YQ, Sinha GP, Bowl MR, Goldring AC, Parker A, Freeman MJ, Brown SDM, Riazuddin S, Fettiplace R, Schafer WR, Frolenkov GI and Ahmed ZM (2017). *CIB2 interacts with TMC1 and TMC2 and is essential for mechanotransduction in auditory hair cells.* Nat Commun, 8(1):43.

Gillespie PG and Cyr JL (2004). *Myosin-1c, the hair cell's adaptation motor.* Annu Rev Physiol, 66:521–545.

Glowatzki E and Fuchs PA (2002). *Transmitter release at the hair cell ribbon synapse.* Nat Neurosci, 5:147–154.

Glowatzki E, Grant L and Fuchs P (2008). *Hair cell afferent synapses.* Current Opinion in Neurobiology, 18(4):389–395.

Goldberg JM and Fernández C (1975). *Responses of peripheral vestibular neurons to angular and linear accelerations in the squirrel monkey.* Acta Otolaryngol, 80(1–2):101–110.

Goldberg JM (2000). *Afferent diversity and the organization of central vestibular pathways.* Experimental Brain Research, 130(3):277–297.

Goodyear RJ and Richardson GP (1992). *Distribution of the 275 kD hair cell antigen and cell surface specialisations on auditory and vestibular hair bundles in the chicken inner ear.* J Comp Neurol, 325(2):243–256.

Goodyear RJ and Richardson GP (2003). *A novel antigen sensitive to calcium chelation that is associated with the tip links and kinocilial links of sensory hair bundles.* J Neurosci, 23(12):4878–4887.

Goodyear RJ, Marcotti W, Kros CJ and Richardson GP (2005). *Development and properties of stereociliary link types in hair cells of the mouse cochlea.* J Comp Neurol, 485(1):75–85.

Goodyear RJ, Jones SM, Sharifi L, Forge A and Richardson GP (2012). *Hair bundle defects and loss of function in the vestibular end organs of mice lacking the receptor-like inositol lipid phosphatase PTPRQ.* J Neurosci, 32:2762–2772.

Guinan Jr JJ (2012). *How are inner hair cells stimulated? Evidence for multiple mechanical drives.* Hear Res, 292:35–50.

Hackney CM and Furness DN (2013). *The composition and role of cross links in mechanoelectrical transduction in vertebrate sensory hair cells.* J Cell Sci, 126:1721–1731.

Hertzog M, Milanesi F, Hazelwood L, Disanza A, Liu H, Perlade E, Malabarba MG, Pasqualato S, Maiolica A, Confalonieri S, Le Clainche C, Offenhäuser N, Block J, Rottner K, Di Fiore PP, Carlier MF, Volkmann N, Hanein D and Scita G (2010). *Molecular basis for the dual function of Eps8 on actin dynamics: bundling and capping.* PloS Biology 8:e1000387.

Hilgert N, Smith RJ and Van Camp G (2009). *Function and expression pattern of nonsyndromic deafness genes.* Curr Mol Med, 9:546–564.

Holt JR, Corey DP and Eatock RA (1997). *Mechanoelectrical transduction and adaptation in hair cells of the mouse utricle, a low-frequency vestibular organ.* J Neurosci, 17(22):8739–8748.

Housley GD and Ashmore JF (1992). *Ionic currents of outer hair cells isolated from the guinea-pig cochlea.* The Journal of Physiology, 448:73–98.

Housley GD, Marcotti W, Navaratnam D and Yamoah EN (2006). *Hair cells – beyond the transducer.* Journal of Membrane Biology, 209 (2-3):89–118.

Horwitz GC, Risner-Janiczek JR, Jones SM and Holt JR (2011). *HCN channels expressed in the inner ear are necessary for normal balance function.* J Neurosci, 31(46):16814–16825.

Hurley KM, Gaboyard S, Zhong M, Price SD, Wooltorton JR, Lysakowski A and Eatock RA (2006). *M-like K^+ currents in type I hair cells and calyx afferent endings of the developing rat utricle.* J Neurosci, 26:10253–10269.

Ion A, Crosby AH, Kremer H, Kenmochi N, Van Reen M, Fenske C, Van Der Burgt I, Brunner HG, Montgomery K, Kucherlapati RS, Patton MA, Page C, Mariman E and Jeffery S (2000). *Detailed mapping, mutation analysis, and intragenic polymorphism identification in candidate Noonan syndrome genes MYL2, DCN, Eps8, and RPL6.* J. Med. Genet., 37 (11):884–886.

Iurato S, Luciano L, Pannese E and Reale E (1972). *Efferent vestibular fibers in mammals: morphological and histochemical aspects.* Prog Brain Res, 37:429–443.

Jaramillo F and Hudspeth AJ (1991). *Localization of the hair cell's transduction channels at the hair bundle's top by iontophoretic application of a channel blocker*. Neuron, (3):409–420.

Johnson SL, Marcotti W and Kros CJ (2005). *Increase in efficiency and reduction in Ca^{2+} dependence of exocytosis during development of mouse inner hair cells.* J Physiol, 563:177–191.

Johnson SL, Kennedy HJ, Holley MC, Fettiplace R and Marcotti W (2012). *The resting transducer current drives spontaneous activity in prehearing mammalian cochlear inner hair cells.* J Neurosci, 32:10479–10483.

Johnson SL, Kuhn S, Franz C, Ingham N, Furness DN, Knipper M, Steel KP, Adelman JP, Holley MC and Marcotti W (2013). *Presynaptic maturation in auditory hair cells requires a critical period of sensory-independent spiking activity.* Proc Natl Acad Sci USA, 110:8720–8725.

Jones C, Roper VC, Foucher I, Qian D, Banizs B, Petit C, Yoder B and Chen P (2008). *Ciliary proteins link basal body polarization to planar cell polarity regulation.* Nat Genet, 40:69–77.

Jones SM and Jones TA (2014). *Genetics of peripheral vestibular dysfunction: lessons from mutant mouse strains.* J Am Acad Audiol, 25:289–301.

Jones TA, Jones SM and Paggett KC (2001). *Primordial rhythmic bursting in embryonic cochlear ganglion cells.* J Neurosci, 21:8129–8135.

Jones TA, Leake PA, Snyder RL, Stakhovskaya O and Bonham B (2007). *Spontaneous discharge patterns in cochlear spiral ganglion cells before the onset of hearing in cats.* J Neurophysiol, 98:1898–1908.

Jørgensen F (1974). *The sensory epithelia of the inner ear of two turtles, Testudo graeca and Pseudemys scripta (Schoepff).* Acta Zoologica, 55:289–298.

Kawashima Y, Géléoc G, Kurima K, Labay V, Lelli A, Asai Y, Makishima T, Wu DK, Della Santina CC, Holt JR and Griffith AJ (2011). *Mechanotransduction in mouse inner ear hair cells requires transmembrane channel-like genes.* J. Clin. Invest., 121:4796–4809.

Khan S and Chang R (2013). *Anatomy of the vestibular system: a review.* NeuroRehabilitation, 32(3):437–443.

Kros CJ, Ruppersberg JP and Rüsch A (1998). *Expression of a potassium current in inner hair cells during development of hearing in mice.* Nature, 394:281–284.

Kros CJ, Marcotti W, van Netten SM, Self TJ, Libby RT, Brown SD, Richardson GP and Steel KP (2002). *Reduced climbing and increased slipping adaptation in cochlear hair cells of mice with Myo7a mutations.* Nat Neurosci, 5(1):41–47.

Kremer H, van Wijk E, Märker T, Wolfrum U, and Roepman R (2006). *Usher syndrome: molecular links of pathogenesis, proteins and pathways.* Hum. Mol. Genet., 15(2): 262–270.

Lanzetti L, Rybin V, Malabarba MG, Christoforidis S, Scita G, Zerial M and Di Fiore PP (2000). *The Eps8 protein coordinates EGF receptor signalling through Rac and trafficking through Rab5.* Nature, 408:374–377.

Lapeyre P, Guilhaume A and Cazals Y (1992). *Differences in hair bundles associated with type I and type II vestibular hair cells of the guinea pig saccule.* Acta Otolaryngol, 112(4):635–642.

Lee JD, Park MK, Lee BD, Park JY, Lee TK and Sung KB (2011). *Otolith function in patients with head trauma.* Eur Arch Otorhinolaryngol, 268(10):1427–1430.

Lefèvre G, Michel V, Weil D, Lepelletier L, Bizard E, Wolfrum U, Hardelin JP and Petit C (2008). *A core cochlear phenotype in USH1 mouse mutants implicates fibrous links of the hair bundle in its cohesion, orientation and differential growth.* Development, 135:1427–1437.

Leibovici M, Verpy E, Goodyear RJ, Zwaenepoel I, Blanchard S, Lainé S, Richardson GP and Petit C (2005). *Initial characterization of kinocilin, a protein of the hair cell kinocilium.* Hear Res, 203:144–153.

LeMasurier M and Gillespie PG (2005). *Hair-cell mechanotrasduction and coclea amplification.* Neuron, 48(3):403–415.

Levin ME and Holt JR (2012). *The function and molecular identity of inward rectifier channels in vestibular hair cells of the mouse inner ear.* J Neurophysiol, 108:175–186.

Li A, Xue J and Peterson EH (2008). *Architecture of the mouse utricle: macular organization and hair bundles heights.* J Neurophysiol, 99(2):718–733.

Lindeman HH (1969). *Studies on the morphology of the sensory regions of the vestibular apparatus.* Ergeb Anat Entwicklungsgesch, 42:1–113.

Lindeman HH (1973). *Anatomy of the otolith organs.* Adv Otorhinolaryngol, 20:405–433.

Lippe WR (1994). *Rhythmic spontaneous activity in the developing avian auditory system.* J Neurosci, 14:1486–1495.

Lysakowski A and Goldberg JM (1997). *A regional ultrastructural analysis of the cellular and synaptic architecture in the chinchilla cristae ampullares.* J Comp Neurol, 389:419–443.

Lysakowski A and Goldberg JM (2008). *Ultrastructural analysis of the cristae ampullares in the squirrel monkey (Saimiri sciureus).* Journal of Comparative Neurology, 511(1):47–64.

Maa MC, Lai JR, Lin RW and Leu TH (1999). *Enhancement of tyrosyl phosphorylation and protein expression of eps8 by v-Src.* Biochim. Biophys. Acta, 1450(3):341–351

Maa MC and Leu TH (2013). *EPS8, an adaptor protein acts as an oncoprotein in human cancer.* In: Tonissen K (eds). Carcinogenesis.

Maeda R, Kindt KS, Mo W, Morgan CP, Erickson T, Zhao H, Clemens-Grisham R, Barr-Gillespie PG and Nicolson T (2014). *Tip-link protein protocadherin 15 interacts with transmembrane channel-like proteins TMC1 and TMC2.* Proc. Natl. Acad. Sci. USA, 111:12907–12912.

Magistretti J, Spaiardi P, Johnson SL and Masetto S (2015). *Elementary properties of Ca(2+) channels and their influence on multivesicular release and phase-locking at auditory hair cell ribbon synapses.* Front Cell Neurosci, 9:123.

Manor U and Kachar B (2008). *Dynamic length regulation of sensory stereocilia.* Semin Cell Dev Biol, 19:502–510.

Manor U, Disanza A, Grati M, Andrade L, Lin H, Di Fiore PP, Scita G and Kachar B (2011). *Regulation of stereocilia length by myosin XVa and whirlin depends on the actin-regulatory protein Eps8*. Curr Biol, 21:167–172.

Marcotti W, Géléoc GS, Lennan GW and Kros CJ (1999). *Transient expression of an inwardly rectifying potassium conductance in developing inner and outer hair cells along the mouse cochlea.* Pflugers Arch, 439:113–122.

Marcotti W, Johnson SL, Holley MC and Kros CJ (2003a). *Developmental changes in the expression of potassium currents of embryonic, neonatal and mature mouse inner hair cells.* J Physiol, 548:383–400.

Marcotti W, Johnson SL, Rüsch A and Kros CJ (2003b). *Sodium and calcium currents shape action potentials in immature mouse inner hair cells.* J Physiol, 552:743–761.

Marcotti W, Johnson SL and Kros CJ (2004a). *Effects of intracellular stores and extracellular* Ca^{2+} *on* Ca^{2+}*-activated* K^{+} *currents in mature mouse inner hair cells.* J Physiol, 557:613–633.

Marcotti W, Johnson SL and Kros CJ (2004b). *A transiently expressed SK current sustains and modulates action potential activity in immature mouse inner hair cells.* J Physiol, 560:691–708.

Marcotti W and Masetto S (2010). *Hair Cells.* Encyclopedia of Life Sciences (ELS).

Marcotti W (2012). *Functional assembly of mammalian cochlear hair cells.* Exp Physiol, 97(4):438–451.

Marcotti W, Corns LF, Goodyear RJ, Rzadzinska AK, Avraham KB, Steel KP, Richardson GP and Kros CJ (2014). *The acquisition of mechano-electrical transducer current adaptation in auditory hair cells requires myosin VI.* J Physiol, 594(13):3667–3681.

Marieb EN (2001). *Human anatomy & physiology.* Benjamin Cummings.

Martini A, Castiglione A, Bovo R, Vallesi A and Gabelli C (2014). *Aging, cognitive load, dementia and hearing loss.* Audiol. Neurootol., 19(1):2–5.

Masetto S, Perin P, Malusà A, Zucca G and Valli P (2000). *Membrane properties of chick semicircular canal hair cells in situ during embryonic development.* Journal of Neurophysiology, 83(5):2740–2756.

Matòsková B, Wong WT, Nomura N, Robbins KC and Di Fiore PP (1996). *RN-tre specifically binds to the SH3 domain of eps8 with high affinity and confers growth advantage to NIH3T3 upon carboxy-terminal truncation.* Oncogene, 12:2679–2688.

Matsui JI, Oesterle EC, Stone JS and Rubel EW (2000). *Characterization of damage and regeneration in cultured avian utricles.* J Assoc Res Otolaryngol, 1(1):46–63.

Meiteles LZ and Raphael Y (1994). *Distribution of cytokeratins in the vestibular epithelium of the guinea pig.* Ann Otol Rhinol Laryngol, 103(2):149–155.

Menna E, Disanza A, Cagnoli C, Schenk U, Gelsomino G, Frittoli E, Hertzog M, Offenhauser N, Sawallisch C, Kreienkamp HJ, Gertler FB, Di Fiore PP, Scita G and Matteoli M (2009). *Eps8 regulates axonal filopodia in hippocampal neurons in response to brain-derived neurotrophic factor (BDNF).* PLoS Biol, 7(6):e1000138.

Meredith FL and Rennie JK (2016). *Channeling your inner ear potassium: K+ channels in vestibular hair cells.* Hear Res, 338:40–51.

Mescher AL (2011). *Junqueira's Basic Histology: Text and Atlas.* Lange.

Michalski N, Michel V, Bahloul A, Lefèvre G, Barral J, Yagi H, Chardenoux S, Weil D, Martin P, Hardelin JP, Sato M and Petit C (2007). *Molecular Characterization of the Ankle-Link Complex in Cochlear Hair Cells and Its Role in the Hair Bundle Functioning.* J Neurosc, 27(24):6478–6488.

Michel V, Goodyear RJ, Weil D, Marcotti W, Perfettini I, Wolfrum U, Kros CJ, Richardson GP and Petit C (2005). *Cadherin 23 is a component of the transient lateral links in the developing hair bundles of cochlear sensory cells.* Dev. Biol., 280:281–294.

Mongiovi AM, Romano PR, Panni S, Mendoza M, Wong WT, Musacchio A, Cesareni G and Di Fiore PP (1999). *A novel peptide-SH3 interactio.* EMBO J, 18(19):5300–5309.

Monzack EL and Cunningham LL (2013). *Lead roles for supporting actors: critical functions of inner ear supporting cells.* Hear Res, 303:20–29.

Moody WJ and Bosma MM (2005). *Ion channel development, spontaneous activity, and activity-dependent development in nerve and muscle cells.* Physiological Reviews, 85(3):883–941.

Morita I, Komatsuzaki A and Tatsuoka H (1997). *The morphological differences of stereocilia and cuticular plates between type-I and type-II hair cells of human vestibular sensory epithelia.* ORL J Otorhinolaryngol Relat Spec, 59(4):193–197.

Moser T, Neef A and Khimich D (2006). *Mechanisms underlying the temporal precision of sound coding at the inner hair cell ribbon synapse.* J Physiol, 576(1):55–62.

Nayak GN, Ratnayaka HSK, Goodyear RJ and Richardson GP (2007). *Development of the hair bundle and mechanotransduction.* Int J Dev Biol, 51:597–608.

Nayak G, Goodyear RJ, Legan PK, Noda M and Richardson GP (2011). *Evidence for multiple, developmentally regulated isoforms of Ptprq on hair cells of the inner ear.* Dev. Neurobiol., 71:129–141.

Nyby JG (2001). *Auditory communication among adults.* In: Willott JF (eds). The handbook of mouse auditory research from behaviour to molecular biology, 3–18. Florida: CRC Press.

Oestreicher E, Wolfgang A and Felix D (2002). *Neurotransmission of the cochlear inner hair cell synapse--implications for inner ear therapy.* Adv Otorhinolaryngol, 59:131–139.

Oda K, Shiratsuchi T, Nishimori H, Inazawa J, Yoshikawa H, Taketani Y, Nakamura Y and Tokino T (1999). *Identification of BAIAP2 (BAI-associated protein 2), a novel human homologue of hamster IRSp53, whose SH3 domain interacts with the cytoplasmic domain of BAI1*. Cytogenet Cell Genet, 84:75–82.

Offenhäuser N, Borgonovo A, Disanza A, Romano P, Ponzanelli I, Iannolo G, Di Fiore PP and Scita G (2004). *The eps8 family of proteins links growth factor stimulation to actin reorganization generating functional redundancy in the Ras/Rac pathway.* Mol Biol Cell, 15(1):91–98.

Offenhäuser N, Castelletti D, Mapelli L, Soppo BE, Regondi MC, Rossi P, D'Angelo E, Frassoni C, Amadeo A, Tocchetti A, Pozzi B, Disanza A, Guarnieri D, Betsholtz C, Scita G, Heberlein U and Di Fiore PP (2006). *Increased ethanol resistance and consumption in Eps8 knockout mice correlates with altered actin dynamics*. Cell, 127:213–226.

Oliver D, Klöcker N, Schuck J, Baukrowitz T, Ruppersberg JP and Fakler B (2000). *Gating of Ca^{2+}-activated K^+ channels controls fast inhibitory synaptic transmission at auditory outer hair cells.* Neuron, 26:595–601.

Oliver D, Knipper M, Derst C and Fakler B (2003). *Resting potential and submembrane calcium concentration of inner hair cells in the isolated mouse cochlea are set by KCNQ-type potassium channels*. J Neurosci, 23:2141–2149.

Pack AK and Slepecky NB (1995). *Cytoskeletal and calcium-binding proteins in the mammalian organ of Corti: cell type-specific proteins displaying longitudinal and radial gradients.* Hear Res, 91(1–2):119–135.

Palmer AR and Russell IJ (1986). *Phase-locking in the cochlear nerve of the guinea-pig and its relation to the receptor potential of inner hair-cells.* Hear Res, 24:1–15.

Pan Z, Selyanko AA, Hadley JK, Brown DA, Dixon JE and McKinnon D (2001). *Alternative splicing of KCNQ2 potassium channel transcripts contributes to the functional diversity of M-currents.* J Physiol, 531(2): 347–358.

Peng AW, Belyantseva IA, Hsu PD, Friedman TB, Heller S (2009). *Twinfilin 2 regulates actin filament lengths in cochlear stereocilia.* J Neurosci, 29:15083–15088.

Petit C and Richardson GP (2009). *Linking genes underlying deafness to hair-bundle development and function.* Nat Neurosci, 12:703–710.

Pickles JO (2008). *An Introduction to the Physiology of Hearing*. Academic Press.

Platzer J, Engel J, Schrott-Fischer A, Stephan K, Bova S, Chen H, Zheng H and Striessnig J (2000). *Congenital deafness and sinoatrial node dysfunction in mice lacking class D L-type Ca^{2+} channels.* Cell, 102:89–97.

Poppi LA, Tabatabaee H, Drury HR, Jobling P, Callister RJ, Migliaccio AA, Jordan PM, Holt JC, Rabbitt RD, Lim R, Brichta AM (2017). *ACh-induced hyperpolarization and decreased resistance in mammalian type II vestibular hair cells.* J Neurophysiol. doi: 10.1152/jn.00030.2017.

Pujol R, Lavigne-Rebillard M and Lenoir M (1998). *Development of sensory and neural structures in the mammalian cochlea.* In: Rubel EW, Popper AN and Fay RR (eds). Development of the Auditory System, 146–192. New York: Springer.

Pujol R and Puel JL (1999). *Excitotoxicity, synaptic repair, and functional recovery in the mammalian cochlea: a review of recent findings.* Ann NY Acad Sci, 884:249–254.

Purves D, Augustine GJ, Fitzpatrick D, Hall WC, LaMantia AS, McNamara JO and White LE (2007). *Neuroscience*. Sinauer Associates.

Raybould NP, Jagger DJ and Housley GD (2001). *Positional analysis of guinea pig inner hair cell membrane conductances: implications for regulation of the membrane filter*. Journal of the Association for Research in Otolaryngology, 2:362–376.

Raphael Y and Altschuler RA (1991). *Reorganization of cytoskeletal and junctional proteins during cochlear hair cell degeneration.* Cell Motil Cytoskeleton, 18(3):215–227.

Raphael Y and Altschuler RA (2003). *Structure and innervation of the cochlea.* Brain Research Bulletin, 60:397–422.

Rennie KJ and Correia MJ (1994). *Potassium currents in mammalian and avian isolated type I semicircular canal hair cells.* J Neurophysiol, 71:317–329.

Revenu C, Athman R, Robine S, and Louvard D (2004). *The co-workers of actin filaments: from cell structures to signals.* Nat. Rev. Mol. Cell Biol., 5:635–646.

Robertson D and Paki B (2002). *Role of L-type Ca^{2+} channels in transmitter release from mammalian inner hair cells. II. Single-neuron activity.* J Neurophysiol, 87:2734-2740.

Roux I, Hosie S, Johnson SL, Bahloul A, Cayet N, Nouaille S, Kros CJ, Petit C and Safieddine S (2009). *Myosin VI is required for the proper maturation and function of inner hair cell ribbon synapses.* Hum Mol Genet, 18:4615–4628.

Runge-Samuelson CL and Friedland DR (2010). *Cochlear Anatomy and Central Auditory Pathways*. In: Niparko JK (ed). Cummings Otolaryngology Head and Neck Surgery.

Rüsch A and Eatock RA (1996). *A delayed rectifier conductance in type I hair cells of the mouse utricle*. J Neurophysiol, 76:995–1004.

Rüttiger L, Sausbier M, Zimmermann U, Winter H, Braig C, Engel J, Knirsch M, Arntz C, Langer P, Hirt B, Müller M, Köpschall I, Pfister M, Münkner S, Rohbock K, Pfaff I, Rüsch A, Ruth P and Knipper M (2004). *Deletion of the Ca2+-activated potassium (BK) alphasubunitbut not the BK beta1-subunit leads to progressive hearing loss.* Proc. Natl. Acad. Sci. USA, 101:12922–12927.

Rzadzinska A, Schneider M, Noben-Trauth K, Bartles JR and Kachar B (2005). *Balanced levels of Espin are critical for stereociliary growth and length maintenance.* Cell Motil Cytoskeleton, 62:157–165.

Schneider ME, Belyantseva IA, Azevedo RB and Kachar B (2002). *Rapid renewal of auditory hair bundles.* Nature, 418(837):838.

Schrott-Fischer A, Kammen-Jolly K, Scholtz A, Rask-Andersen H, Glueckert R and Eybalin M. (2007). *Efferent neurotransmitters in the human cochlea and vestibule.* Acta Otolaryngol, 127(1):13–19.

Schwander M, Kachar B and Müller U (2010). *Review series: The cell biology of hearing.* J Cell Biol, 190(1):9–20.

Schweizer FE, Savin D, Luu C, Sultemeier DR and Hoffman LF (2009). *Distribution of high-conductance calcium-activated potassium channels in rat vestibular epithelia.* J. Comp. Neurol., 517:134–145.

Selyanko AA, Delmas P, Hadley JK, Tatulian L, Wood IC, Mistry M, London B and Brown DA (2002). *Dominant-negative subunits reveal potassium channel families that contribute to M-like potassium currents.* J Neurosci, 22: RC212.

Seoane A and Llorens J (2005). *Extruding auditory hair cells in rats exposed to subchronic 3,3'-iminodipropionitrile.* Environ Toxicol Pharmacol, 19(3):571–574.

Shin JB, Longo-Guess CM, Gagnon LH, Saylor KW, Dumont RA, Spinelli KJ, Pagana JM, Wilmarth PA, David LL, Gillespie PG and Johnson KR (2010). *The R109H variant of fascin-2, a developmentally regulated actin crosslinker in hair-cell stereocilia, underlies early-onset hearing loss of DBA/2J mice.* J Neurosci, 30:9683–9694.

Shnerson A, Devigne C and Pujol R (1982). *Age-related changes in the C57BL/6J mouse cochlea. II. Ultrastructural findings.* Developmental Brain Research, 2:77–88.

Sterling P and Matthews G (2005). *Structure and function of ribbon synapses.* Trends in Neuroscience, 28(1):20–29.

Strassmaier M and Gillespie PG (2002). *The hair cell's transduction channel.* Current Opinion in Neurobiology, 12(4): 380–386.

Street VA, Kallman JC, Strombom PD, Bramhall NF and Phillips JO (2008). *Vestibular function in families with inherited autosomal dominant hearing loss.* J Vestib Res, 18:51–58.

Tocchetti A, Confalonieri S, Scita G, Di Fiore PP and Betsholtz C (2003). *In silico analysis of the EPS8 gene family: genomic organization, expression profile, and protein structure.* Genomics, 81(2):234–244.

Tilney LG, Tilney MS and DeRosier DJ (1992). *Actin filaments, stereocilia, and hair cells: how cells count and measure.* Annu. Rev. Cell Biol., 8:257–274.

Tritsch NX and BerglesDE (2010). *Developmental regulation of spontaneous activity in the Mammalian cochlea.* J Neurosci, 30:1539-1550.

Trussell LO (2002). *Transmission at the hair cell synapse.* Nat Neurosci, 5:85–86.

Vaggi F, Disanza A, Milanesi F, Di Fiore PP, Menna E, Matteoli M, Gov NS, Scita G and Ciliberto A (2011). *The Eps8/IRSp53/VASP network differentially controls actin capping and bundling in filopodia formation.* PLoS Comput Biol 7(7):e1002088.

Verpy E, Leibovici M, Michalski N, Goodyear RJ, Houdon C, Weil D, Richardson GP and Petit C (2011). *Stereocilin connects outer hair cell stereocilia to one another and to the tectorial membrane.* J. Comp. Neurol., 519:194–210.

Wang H, Patel V, Miyazaki H, Gutkind JS and Yeudall WA (2009). *Role for EPS8 in squamous carcinogenesis.* Carcinogenesis, 30(1):165–174.

Wang HC and Bergles DE (2015). *Spontaneous activity in the developing auditory system.* Cell Tissue Res, 361(1):65–75.

Wangemann P, Itza EM, Albrecht B, Wu T, Jabba SV, Maganti RJ, Lee JH, Evrett LA, Wall SM, Royaux IE, Green ED, Marcus DC (2004). *Loss of KCNJ10 protein expression abolishes endocochlear potential and causes deafness in Pendred syndrome mouse model.* BMC Med, 2:30–44.

Watanuki K, Stupp HF and Meyer zum Gottesberge A (1971). *Distribution pattern of the type I and type II sensory cells on the maculae sacculi and utriculi in the guinea pig.* Pract Otorhinolaryngol, 33(5):304–311.

Welsch T, Endlich K, Giese T, Büchler MW, Schmidt J (2007). *Eps8 is increased in pancreatic cancer and required for dynamic actin-based cell protrusions and intercellular cytoskeletal organization.* Cancer Lett, 255(2):205–218.

Wersäll J (1956). *Studies on the structure and innervation of the sensory epithelium of the cristae ampullaris in the guinea pig. A light and electron microscopic investigation.* Acta Otolaryngol Suppl, 126:1–185.

Wersäll J and Bagger-Sjöbäck D (1974). *Morphology of the vestibular sense organ.* In: Kornuber HH (eds). Handbook of sensory physiology, 123–170. New York: Spring.

Wong WT, Carlomagno F, Druck T, Barletta C, Croce CM, Huebner K, Kraus MH and Di Fiore PP. (1994). *Evolutionary conservation of the EPS8 gene and its mapping to human chromosome 12q23-q24.* Oncogene, 9:3057–3061.

Xiong W, Grillet N, Elledge HM, Wagner TFJ, Zhao B, Johnson KR, Kazmierczak P and Müller U (2012). *TMHS is an integral component of the mechanotransduction machinery of cochlear hair cells.* Cell, 151:1283–1295.

Zampini V, Rüttiger L, Johnson SL, Franz C, Furness DN, Waldhaus J, Xiong H, Hackney CM, Holley MC, Offenhauser N, Di Fiore PP, Knipper M, Masetto S and Marcotti W (2011). *Eps8 regulates hair bundle length and functional maturation of mammalian auditory hair cells.* PLoS Biol, 9:e1001048.

Zenner HP, Zimmermann U and Gitter AH (1990). *Cell potential and motility of isolated mammalian vestibular sensory cells.* Hear Res, 50:289–293.

Zhao B, Wu Z, Grillet N, Yan L, Xiong W, Harkins-Perry S and Müller U (2014). *TMIE is an essential component of the mechanotransduction machinery of cochlear hair cells.* Neuron, 84:954–967.

Zheng L, Sekerková G, Vranich K, Tilney LG, Mugnaini E and Bartles JR (2000). *The deaf jerker mouse has a mutation in the gene encoding the espin actin-bundling proteins of hair cell stereocilia and lacks espins.* Cell, 102:377–385.

Zwaenepoel I, Naba A, Da Cunha MM, Del Maestro L, Formstecher E, Louvard D and Arpin M (2012). *Ezrin regulates microvillus morphogenesis by promoting distinct activities of Eps8 proteins.* Mol Biol Cell, 23(6):1080–1094.